FIELD INTERACTIONS IN THE PERIPHERAL AUDITORY NEURAL SYSTEM WITH REFERENCE TO COCHLEAR IMPLANTS

by

Robert Jönsson

Submitted in partial fulfillment of the requirements of the degree
Philosophiae Doctor (Biosystems)
in the
Faculty of Engineering, Built Environment and Information Technology
UNIVERSITY OF PRETORIA

December 2010

SUMMARY

Field interactions in the peripheral auditory neural system with reference to cochlear implants

by

Robert Jönsson

Promotor	:	Prof T Hanekom
Co-promotor	:	Prof JJ Hanekom
Department	:	Electrical, Electronic and Computer Engineering
Degree	:	Philosophiae Doctor (Biosystems)

SUMMARY

This study investigates the effect of field interactions on neural excitation profiles within the electrically stimulated auditory system on two levels: interneural by studying the ephaptic excitatory effect of neurons on one another and extraneural by studying the effect of inhomogeneities in the neural volume on excitation profiles. The investigation contributes to the tool base available for computational neuromodelling.

Ephaptic stimulation of a neuron refers to excitation of a neuron by the extracellular environment induced by other neurons. It is usually assumed that neurons communicate only through anatomical specializations such as gap junctions or synapses, but since a large extracellular potential from active neurons, arising during the propagation of action potentials, can trigger an action potential in another subthreshold neuron, ephaptic stimulation could be significant and should therefore be taken into account when dealing with neuron interaction. The objective of the study was to quantify the influence of ephaptic excitation on nerve stimulation utilizing models with increasing anatomical, morphological and morphometrical detail and determine whether it is a necessary factor in neuromodelling.

An initial, simple model of ephaptic excitation suggested a possible significant effect on electric hearing. The results show that the contribution of ephaptic excitation is most significant close to threshold and continues to be significant up to at least 6–7 dB above threshold. Cochlear implant subjects normally have a small dynamic range (average of 7 dB), indicating that the ephaptic effect might be important in models of the implanted cochlea.

The model was extended to include more details including neural membrane noise, the three-dimensional geometry and conductive properties of the cochlear volume and variation in stimulating pulse shape. It was shown that the ephaptic effect is still significant in the presence of these amendments and is affected by all of the mentioned parameters. It was also shown that ephaptic excitation significantly contributes to cross-turn stimulation which in turn has implications for pitch perception in cochlear implant subjects. Ephaptic excitation of ectopic neural populations was proposed as a possible mechanism that could produce pitch confusions suggesting that interpretation of psychoacoustic and neural response data from literature may be aided when the ephaptic effect is taken into account.

The effect of heterogeneity, caused by the structure of the neural tissue, on potential distributions within the neural population was investigated by means of finite element modelling. It was demonstrated that the presence of fibres in the medium has a significant effect on the extracellular potential distribution at small distances from the point sources in that it decreased the potential. This in turn affects the excitation profile within the neural population.

The results of this study show that the significance of the ephaptic effect at stimulus intensities close to threshold can be demonstrated by a very simple deterministic model. However, further quantification of the effect shows that factors such as anatomical, morphological and morphometrical details, membrane noise and stimulus waveform should be included when modelling the responsiveness of auditory nerve fibres close to threshold.

KEY WORDS

Ephaptic excitation, Hodgkin-Huxley model, cochlear implant, spread of neural excitation, computational model, auditory neuron

OPSOMMING

Veldinteraksies in die perifere ouditiewe neurale stelsel met verwysing na kogleêre inplantings

deur

Robert Jönsson

Promotor	:	Prof T Hanekom
Mede-promotor	:	Prof JJ Hanekom
Departement	:	Elektriese, Elektroniese en Rekenaar-Ingenieurswese
Graad	:	Philosophiae Doctor (Biosisteme)

OPSOMMING

Hierdie studie ondersoek die effek van veldinteraksies op neurale prikkelingsprofiele binne die elektriesgestimuleerde ouditiewe stelsel op twee vlakke: interneuraal deur die efaptiese effek van neurone op mekaar te bestudeer en ekstraneuraal deur die effek van nie-homogeniteite in die neurale volume op prikkelingspatrone te bestudeer. Die ondersoek dra by tot die gereedskapsbasis wat beskikbaar is vir numeriese neuromodellering.

Efaptiese stimulasie van 'n neuron verwys na prikkeling van 'n neuron deur die ekstrasellulêre omgewing wat deur ander neurone geïnduseer word. Daar word gewoonlik aanvaar dat neurone net deur anatomiese spesialisasies soos spleetintervlakke of sinapse kommunikeer, maar omdat 'n groot ekstrasellulêre potensiaal wat ontstaan as gevolg van voortplanting van aksiepotensiale op 'n aantal aktiewe neurone 'n aksiepotensiaal in 'n ander subdrempel-neuron kan veroorsaak, kan efaptiese stimulasie beduidend wees en behoort dit dus in berekening gebring te word wanneer neurale interaksie ter sprake is. Die doel van die studie was om die invloed van die efaptiese effek op senuweestimulasie te kwantifiseer deur modelle te gebruik met toenemende anatomiese, morfologiese en morfometriese detail en daardeur te bepaal of dit 'n noodsaaklike faktor in neuromodellering is.

'n Aanvanklike, eenvoudige model van efaptiese prikkeling het gedui op 'n potensieel beduidende effek op elektriese gehoor. Die resultate het getoon dat die bydrae van efaptiese prikkeling die grootste effek het naby drempel en dat dit aanhou om 'n beduidende effek te hê tot minstens 6 tot 7 dB bo drempel. Kogleêre inplanting-subjekte het gewoonlik 'n klein dinamiese bereik (gemiddeld 7 dB), wat daarop dui dat die efaptiese effek belangrik kan wees in modelle van die geïnplanteerde koglea.

Die model is uitgebrei om meer besonderhede in te sluit soos neurale membraanruis, die drie-dimensionele geometrie en geleidingseienskappe van die kogleêre volume en variasie in die stimulasiegolfvorm. Daar is getoon dat die efaptiese effek met in agneming van die veranderinge ook beduidend is en deur al die genoemde parameters beïnvloed word. Daar is veder getoon dat efaptiese stimulasie 'n beduidende bydrae tot kruisdraaistimulasie lewer wat weer implikasies het vir toonhoogtepersepsie in kogleêre inplanting-subjekte. Efaptiese prikkeling van ektopiese neurale populasies is voorgestel as 'n moontlike meganisme wat toonhoogteverwarrings kan veroorsaak wat impliseer dat die interpretasie van psigoakoestiese- en neurale reponsdata in die literatuur aangehelp kan word indien efaptiese prikkeling in berekening gebring word.

Die effek van 'n heterogene medium, wat deur die struktuur van die neurale weefsel veroorsaak word, op potensiaalverspreidings binne die neurale populasie is ondersoek deur eindige element modellering. Daar is gedemonstreer dat die teenwoordigheid van neurone in die medium 'n beduidende effek op die ekstrasellulêre potensiaalverspreiding op klein afstande vanaf die bron het deurdat dit 'n verlaging in die potensiaal tot gevolg het. Dit affekteer die prikkelingspatrone binne die neurale populasie.

Die resultate van hierdie studie toon dat die beduidendheid van die efaptiese effek naby drempel gedemonstreer kan word deur 'n eenvoudige deterministiese model. Verdere kwantifisering van die effek dui egter daarop dat faktore soos anatomiese, morfologiese en morfometriese details, membraanruis en stimulusgolfvorm ingesluit behoort te word wanneer die prikkelbaarheid van ouditiewe neurone naby drempel gemodelleer word.

SLEUTELWOORDE

Efaptiese prikkeling, Hodgkin-Huxley model, kogleêre inplanting, verspreiding van neurale prikkeling, numeriese model, ouditiewe neuron

Acknowledgements

First of all, I would like to thank my supervisor for helping and guiding me through this project.

My sincerest thanks to my colleagues and everyone else who has been there for me whenever I have had problems or questions about anything from administration to technical assistance.

Also, I would like to thank my family whom I could always count on and for having confidence in me.

I owe my deepest gratitude to my friends for their support and encouragement through conversations, phone calls and emails, which have motivated me and kept my mental state on a level that would almost qualify as sanity.

Lastly, and above all, I would like to thank my beloved wife for her endless support and extraordinary patience with me despite all my whining.

Contents

List of abbreviations

3D	:	Three dimensional	(p. 59)
AP	:	Action potential	(p. 28)
BM	:	Basilar membrane	(p. 39)
CN	:	Central node	(p. 29)
EE	:	Ephaptic excitation	(p. 41)
FE	:	Finite element	(p. 77)
HH	:	Hodgkin-Huxley	(p. 30)
IC	:	Inferior colliculus	(p. 39)
PN	:	Peripheral node	(p. 29)

Chapter 1

INTRODUCTION

1.1 PROBLEM STATEMENT

1.1.1 Context of the problem

The objective of this study is to investigate the effect of electrical potential field interactions caused by the morphology of the auditory nerve and its constituting fibres, on neural excitation profiles in cochlear implants. The study will aim to quantify the amount of detail with regard to morphology that is required to make accurate predictions of spread of neural excitation. The three primary research questions that will be addressed are:

1. To what extent does ephaptic interaction between auditory fibres affect neural excitation patterns?

2. To what extent does the structure of the auditory nerve affect neural excitation patterns?

3. Does a compound neural model, that reflects the composition of the auditory nerve with regard to fibre type and location as well as ephaptic interactions, provide a better estimate of neural excitation than that provided by single fibre models?

1.1.2 Context of problem and research gap

The cochlear implant is an electronic device that provides a perception of sound to a profoundly deaf person. The most common cause of deafness is the loss of hair cells in the cochlea preventing the sound information from reaching the central nervous system (Loizou, 1998). By electrically stimulating the auditory fibres, the cochlear implant bypasses all the mechanisms in the external and middle ear. The cochlear implant typically consists of the following parts: a microphone, a speech processor and a transmitter, which are attached externally to the deaf person, and a receiver and an electrode array, which are surgically implanted. The electrode array is placed along the length of the cochlea so that different auditory nerve fibres can be stimulated at different places, based on the tonotopic principle, i.e. the frequency sensitivity of the fibres is a function of the location along the length of the cochlea in that the fibres toward the base are more sensitive for high frequencies and those toward the apex more for lower frequencies.

The auditory nerve fibres must be stimulated to elicit a sound sensation for the deaf person. The stimulation process is, however, governed by a number of complex physical, anatomical and physiological factors (Finley et al., 1990). Nerve morphology is one of these factors and it is important for three reasons. First, the human auditory nerve consists of 30 000 fibres and there is a wide variation between the fibres (Gleich and Wilson, 1993; Glueckert et al., 2005). This presents a relevant problem in single-fibre modelling where the morphology of a typical fibre is chosen (see for example Frijns et al., 2001; Rattay et al., 2001a).

Second, from animal studies it is known that long-term deafness changes the morphology of nerves, e.g. demyelination and degeneration of the peripheral dendrites, demyelination and shrinkage of the soma and demyelination of the central axon (Cartee et al., 2000). This has implications for stimulation strategies since the morphological changes stated above affect temporal characteristics and site of excitation of fibres.

The third reason is that several modelling studies have shown that small variations in nerve fibre morphology can have a significant influence on the behaviour of a spike (Rattay et al., 2001a; Frijns et al., 1996). Frijns et al. (1996) showed that narrowing the peripheral axon from 3 μm to 2 μm increased the calculated excitation thresholds with approximately 2 dB and in Rattay's model a small variation of the length of the

last peripheral internode made the difference to whether a spike would propagate or not. The action potential was also stopped if the number of soma layers was reduced from three to two or by enlargement of the soma surface. Furthermore, modellers have remained focused on animal models to investigate and predict auditory nerve function (Rattay et al. 2001a) even though animal nerve morphology is essentially different than that of human nerves, e.g. in structure and myelination. Rattay et al. (2001a) demonstrated that characteristic differences between man and cat auditory nerve fibres cause significant differences in spiking behaviour.

There is also a need for further research of the interaction of electrical fields in the cochlea. Results from experiments made by Stickney et al. (2006) suggest that there is a relationship between electrical field interactions and speech recognition performance in cochlear implant patients. They concluded that electrical field interaction accounted for as much as 70% of the variance in speech recognition scores. These field interactions, arising when electric fields add together from simultaneous electrode stimulation, can disrupt the stimulus waveform prior to neural activation. Ways of controlling and limiting field interactions include electrode configuration and electrode positioning (Rattay et al., 2001a Stickney et al., 2006; Finley et al., 1990; Briaire et al., 2006).

According to Finley et al. (1990) significant field interaction effects may appear in the case of cross-turn stimulation because of the myelinated neural fibres filling the core of the modiolus. The phenomenon of cross-turn stimulation is a consequence of the anatomy of the cochlea and results from excitation of modiolar parts of nerve fibres, originating from apical cochlear turns instead of the turn where the stimulus source is. Cross-turn stimulation could also result from ephaptic excitation. Ephaptic excitation of a nerve fibre occurs through the extracellular environment induced by other fibres. It is usually assumed that fibres communicate only through anatomical specializations such as gap junctions or synapses (Holt and Koch, 1999), but since a propagating action potential can give rise to an extracellular potential, which can trigger an action potential in a neighbouring fibre, ephaptic excitation could be significant and should be investigated when dealing with neural interaction.

Finally, current cochlear models assume a uniform potential distribution throughout the neural population located at a specific position along the length of the cochlea. They thereby ignore the possibility that the structure of the nerve tissue could affect

potential distributions within the nerve fibre population causing the fibres at a specific location to be subjected to dissimilar potential distributions. This heterogeneity may influence thresholds and the ephaptic behaviour of nerve fibres.

In summary, there is a need for further research in field interactions and nerve morphology to improve current models of electrical excitation of auditory nerve fibres. The outcome of this study could advance existing models by contributing information about the level of details needed for accurate predictions of neural excitation and provide insights for the development of future cochlear implants.

1.2 RESEARCH OBJECTIVE

The objective of this study is to investigate the effect of electrical potential field interactions that are affected by the structure and anatomy of the auditory nerve fibres on neural excitation profiles in cochlear implants. The study can be broken down into three topics.

Normally only gap junctions and synapses are considered when dealing with nerve communication and ephaptic interaction is disregarded. The first topic will be to investigate to what extent ephaptic interaction between auditory fibres does affect neural excitation patterns. This is relevant in cochlear implants because of mass synchronous discharge of auditory fibres producing elevated extracellular currents. It will be investigated whether or not the ephaptic effect is significant enough to be included in neural models and if it could help to decrease the discrepancy between predicted and measured data.

The second topic is to investigate to what extent the structure of the auditory nerve affects neural excitation patterns. Increasing anatomical details, such as neural composition and geometry, will be added and it will be investigated how these additional details affect the ephaptic influence. This topic also involves the development of a compound model. This model will contain the composition of the auditory nerve with regard to both fibre type and location as well as taking ephaptic interactions into account.

The third topic is to investigate how the heterogeneity caused by the structure of

the nerve tissue affects potential distributions within the nerve fibre population. This topic involves the development of a FEM model.

1.3 APPROACH

The approach that will be followed can be broken down into two primary research activities that deal with the three research questions as stated above. The investigation of interactions between auditory fibres based on ephaptic excitation and on the structure of the auditory nerve will be developed separately following slightly different approaches. The investigation of ephaptic neural interaction will start with a simple single fibre model (Chapter 3) which will consequently be developed with increasing anatomical detail in Chapter 4. A FEM model is implemented in Chapter 5 based on the morphology of the single fibre model presented in Chapter 4. To investigate the effect of the structure a compound neural model based on the composition and anatomy of the auditory nerve is developed in Chapter 4.

1.3.1 Investigation of ephaptic interaction among auditory fibres

Ephaptic interaction among auditory fibres in the electrically stimulated human cochlea will be investigated by developing a model of this phenomenon. The development of the model will comprise of the following steps:

1. Implementation of an existing nerve fibre model and modification of the model to reflect human auditory nerve fibre properties. Both the original and a simplified version of the neural model presented by Rattay et al. (2001) and described above, will be used to simulate propagating action potentials in a number of auditory fibres that are stimulated by an external electrode.

2. Definition and implementation of the equations and parameters that govern ephaptic interactions. The resulting membrane currents from the active fibres (i.e. the fibres excited by the electrode stimulus) will subsequently be used as

stimulating currents for a nearby passive or target fibre (i.e. an inactive fibre that can be ephaptically excited).

3. Derivation of the parameters that define the structure of the auditory nerve that will affect ephaptic interaction. This includes the composition and anatomy of the auditory nerve. The influence of the spatial orientation of the active fibres relative to the target fibre, stimulus intensity and neural density on ephaptic excitation will then be investigated.

4. Integration of the ephaptic model into the existing volume conduction-nerve fibre model of the human cochlea to facilitate assessment of the influence of ephaptic excitation on neural excitation profiles.

5. Implementation of FEM models of segments of the central axon, based on neural morphology presented by Rattay et al. (2001) for an FEM approach to investigating ephaptic interaction in a bundle of central axons.

It is not possible to separate ephaptic effects from synaptic effects in psychoacoustic data, so published results on ephaptic excitation are scarce. The single fibre model will therefore be verified by applying the effects of ephaptic excitation on existing modelled excitation profiles. The resulting profiles will then be compared to experimentally determine mammalian neural excitation profiles, e.g. those measured in the cat (Moore et al., 2002). This is carried out in Chapter 3.

The model will be used to quantify the influence of ephaptic excitation on nerve stimulation and determine whether it is a necessary factor in neuromodelling.

1.3.2 Investigation of the effect of the structure of the auditory nerve on neural excitation patterns

The effect of the structure of the auditory nerve on neural excitation patterns will be investigated using a volume conductor model of the auditory nerve that includes much anatomical detail. The development of the model comprises the following steps:

1. Assessment of the composition and anatomy of the auditory nerve inside the cochlea to define model parameters in this regard.

2. Development of the model geometry.

3. Definition of loading and boundary conditions.

4. Integration of the model with the current volume conduction-nerve fibre model of the human cochlea.

Since many existing models have turned out to be very sensitive to changes in nerve fibre morphology, the model will be used to investigate how different morphologies affect neural excitation patterns and to what extent increasing the morphological details affect the results.

1.4 RESEARCH CONTRIBUTION

This study aims to quantify the influence morphological details have on neural excitation patterns and the results are relevant for improving existing models of the cochlea and auditory nerve fibres. Furthermore, the notion of ephaptic interaction is a poorly known and documented and often disregarded phenomenon and the results presented by this study therefore provide important information to expand field interaction research in general and, more specifically, cochlear implant research. Current neural models do not take ephaptic interaction into account and the findings from this study may help to explain some of the discrepancy between measured and predicted data. It could furthermore prove to be an important factor in the development of future neural models.

1.5 OVERVIEW OF THE STUDY

In Figure 1.1 an overview of what is covered in this study is shown.

Related issues not covered by the study include:

1. Electrically evoked compound action potentials (ECAPs)

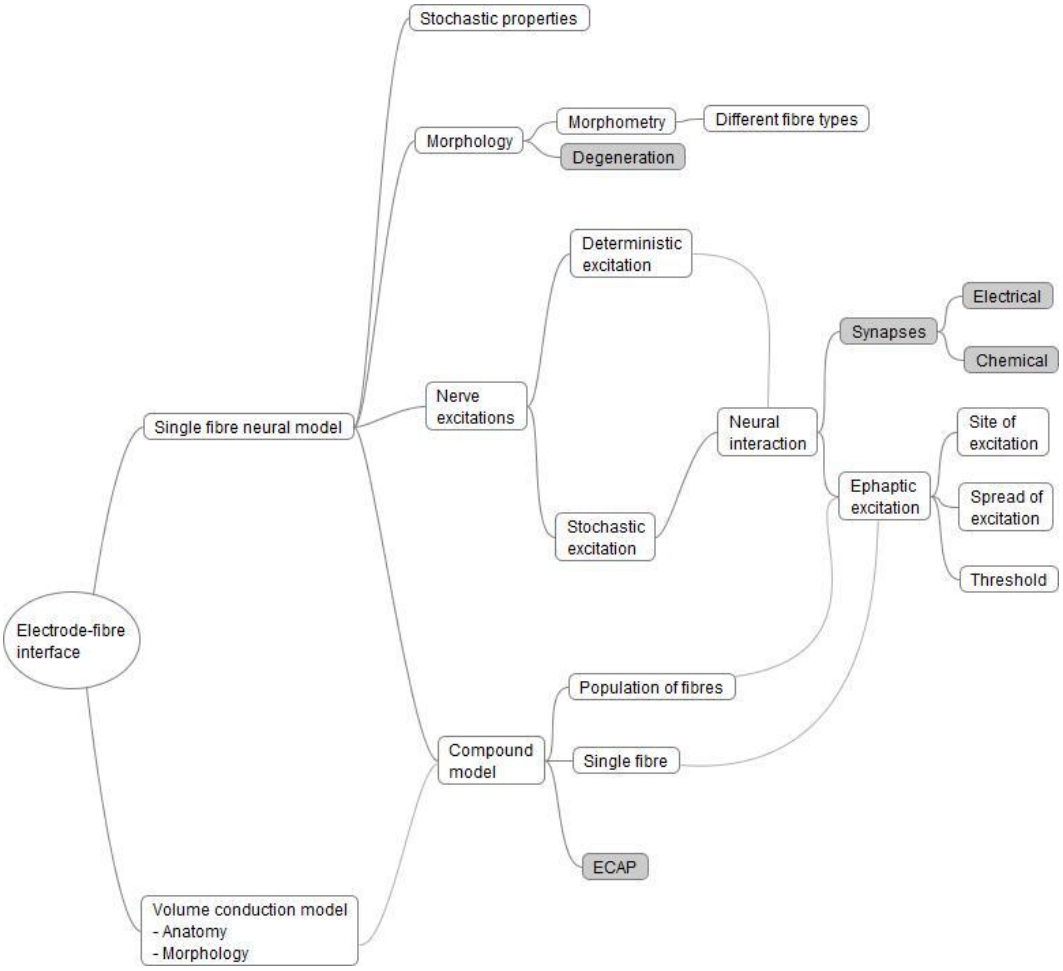

Figure 1.1: Overview of the study. The figure shows issues covered by this study. Issues that are related but not covered are indicated by grey boxes.

2. Electric and chemical synapses.

3. Degeneration of fibres.

The thesis is divided into the following chapters:

In Chapter 2 the background information and argument to understand the research is presented.

In Chapter 3 a simplified version of the single fibre model presented by Rattay et al. (2001) is developed and used to quantify the influence of ephaptic excitation on nerve stimulation.

In Chapter 4 a compound model, consisting of a volume conduction model and the full single fibre model presented by Rattay et al. (2001), is created to determine the influence of a stochastic neural model in combination with the 3D geometry of the cochlea on ephaptic excitation. Furthermore, the influence of pulse shape on ephaptic excitation is investigated.

In Chapter 5 a FEM model is implemented. The ephaptic effect in a bundle of central axons is investigated.

In Chapter 6 a general discussion and conclusion of the study is presented as well as suggestions for future research.

Chapter 2

BACKGROUND REVIEW

Hearing loss is generally divided into two broad categories: conductive and sensorineural hearing loss. Conductive hearing loss refers a mechanical deficit of transferring the sound vibrations from the environment in the outer and middle ear to the inner ear, while sensorineural hearing loss refers to the problem of converting vibrations to an electrical signal that the nerves and the brain can perceive. A cochlear implant is a prosthetic device that is implanted in the inner ear and can restore hearing for people with sensorineural hearing loss by means of electrical stimulation of the auditory nerve fibres. The prosthesis can be divided into an internal and external part. Externally there is a microphone that senses sound, a speech processor that transforms the microphone output into stimuli for the electrodes, and an external transmitter that transmits the information via a radio-frequency signal. Internally there is an implanted receiver that decodes the information and a stimulator to generate stimuli for the implanted electrode array along the cochlea. The number of people that have been implanted with cochlear implants has increased exponentially during the last twenty years and has now exceeded 120 000 worldwide (Wardrop et al., 2005; Wilson et al., 2008).

The most common cause of hearing loss is damage to the sensory hair cells (Hinojosa, 1983, as cited in Loizou, 1998). There can be several factors causing the damage, e.g. genetic defects, infectious diseases (e.g. rubella and meningitis), overexposure to loud sounds, certain drugs (e.g. kanamycin, streptomycin and cisplatin) and aging (Wilson et al., 2008). Since deafness is caused by the loss of hair cells rather than

auditory neurons, a cochlear implant can bypass the normal hearing mechanism and directly stimulate localized populations of auditory nerve fibres with the implanted electrode array in the cochlea. The stimulation process is governed by a number of physical, anatomical and physiological factors, e.g. the configuration and placement of electrodes, the amplitude, shape and type of the stimulating current, the impedance of the cochlear tissue, the location and anatomy of surviving nerve fibres and the deterministic and stochastic characteristics of stimulated neural membranes (Finley et al., 1990). To develop improved cochlear implants it is important to understand how all the mechanisms in the auditory system function.

2.1 FIELD INTERACTIONS

Field interactions arise when electric fields from different sources add together. In cochlear implants, field interactions from simultaneous electrode stimulation can disrupt the stimulus waveform prior to neural activation and this alteration of the stimulus is subsequently represented in the neural firing pattern (Stickney et al., 2006).

2.1.1 General excitation

Neural excitation occurs normally through synapses, which are specialised junctions through which information is transferred from a presynaptic to a postsynaptic neuron. Synapses are either chemical or electrical and they differ both in mechanism of information transfer and morphological organization (Hormuzdi et al., 2004). Electrical synapses are formed through gap junctions where ions flow from the presynaptic neuron to the postsynaptic neuron. The more common chemical synapses transfer the information through neurotransmitters, which are released from vesicles in the presynaptic neuron when a propagating action potential reaches the terminal. The neurotransmitters then dock at receptor molecules in the membrane of the postsynaptic neuron and the docking causes the neuron to activate.

There are, however, events that cannot be explained with synaptic excitation. Groups of neurons have been observed in the hippocampus with synchronous excitation in the absence of a synaptic function (Krnjevic, 1986). Furthermore, studies on macaque

monkeys show that neurons that have lost their connections to degenerated sensory cells may still send electrical signals to the cochlear nuclei (Kimura et al., 1987). Ephaptic excitation has been proposed as a possible mechanism that could explanation these phenomena.

2.1.2 Ephaptic excitation

Ephaptic stimulation of a neuron refers to excitation of a neuron by the extracellular environment induced by other neurons. It is usually assumed that neurons communicate only through anatomical specializations such as gap junctions or chemical synapses (Holt and Koch, 1999), but since a large extracellular potential from one neuron, arising during the propagation of an action potential, can trigger an action potential in another neuron, ephaptic stimulation could be significant and should therefore be taken into account when dealing with neuron interaction.

It has been known for a long time that electrical fields generated by active neurons can have an effect on neighbouring passive neurons (Yim et al., 1986) and several studies have been done on both natural ephaptic excitation and artificially induced ephaptic excitation. Ephaptic interactions can occur naturally in networks with a high neuron density and can have important consequences. For example, ephaptic interactions among closely spaced neurons in the cerebral cortex and hippocampus can cause epileptic seizures (McCormick and Contreras, 2001). Another example of ephaptic interaction is the underlying mechanism in the development of ocular neuromyotonia (Koop and Graf, 2006). Ocular neuromyotonia is a rare disorder characterized by involuntary contractions of one or several ocular motor muscles, which are the muscles that control the movement of the eyelids and eyeballs.

Holt and Koch (1999) reports on two demonstrated cases of electrical ephaptic effects (in human) in normal operations. The first case is ephaptic activity between the Mauthner cell and its inhibitory afferents, where an unusually resistive extracellular space can enhance the ephaptic effects (Korn and Faber, 1980; Faber and Korn, 1989). The second case involves activity between basket cells and Purkinje cells in the cerebellum, where tight junctions around the synapses increase ephaptic influence (Korn and Axelrad, 1980).

The hippocampus has a structure that should be highly favourable for ephaptic interactions because of the close packing of cells and the lack of glia in the pyramidal cell layers (Yim et al., 1986). Several studies on rats' hippocampal cells have shown significant effects of field potentials in response to electrical stimulation (Dalkara et al., 1986; Turner and Richardson, 1991; Yim et al., 1986).

Turner and Richardson (1991) studied the rat hippocampus in vitro and found that extracellular fields in apical dendrites of pyramidal cells may depolarize the dendritic membrane during synchronous orthodromic activation and suggested that ephaptic interaction at the dendritic level could contribute to depolarization and discharge of pyramidal cells during naturally occurring spontaneous activity.

Yim et al. (1986) recorded transmembrane potentials generated by antidromically evoked electrical fields in CA1 hippocampal neurons of rats. The antidromic fields, combined with subthreshold stimulus pulses, increased the firing probability of cells that was not activated by the stimulus. The ephaptic excitation differed from synaptic excitation in that it had shorter latency, greater jitter of spike latency compared to the antidromic spikes and was unable to follow pulse trains at low frequencies (2 Hz). The results showed larger excitatory effects in neurons that had a high threshold for antidromic activation and a significant excitatory effect with antidromic fields as small as 1 mV was detected, indicating a functional relevance in promoting synchronized firing of CA1 neurons. Taylor et al. (1984, as cited in Yim et al., 1986) showed that CA3 neurons in situ can be excited ephaptically.

Dalkara et al. (1986) showed that antidromically evoked population spikes in the CA3 region of the hippocampus of rats can be chemically modulated by various excitatory and inhibitory agents, which can either promote or prevent ephaptic synchronization of the activation in pyramidal cells.

In cochlear implants neural responses to electric stimuli are frequently 100% entrained or time-locked to the stimulus at stimulus rates below 400 Hz and sometimes up to 800 Hz (Javel and Shepherd, 2000). This implies a mass synchronous discharge of auditory neurons, which could produce significantly elevated extracellular currents. These currents could in turn produce ephaptic excitation of neighbouring neurons, which would not normally be excited by the stimulus alone.

Studies on the macaque monkey suggest that neurons that have lost their connections

to degenerated sensory cells may still send electrical signals to the cochlear nuclei through the ephapses of their neurites in the Rosenthal's canal (Kimura et al., 1987). They identified four types of cells (type I cells with myelinated somas and myelinated axons; type II cells with unmyelinated somas and unmyelinated axons; a third type with myelinated somas and unmyelinated axons; and a fourth type with unmyelinated somas and myelinated peripheral processes) and suggested that nerve fibres of different types communicate with each other. Type I neurons had direct contact with each other in the first segment of the peripheral processes and furthermore formed ephapses with type II peripheral processes. Moreover, type II neurons formed ephapses with each other and the third type of neurons.

In the human cochlea large ganglion cells form clusters surrounded by Schwann cell layers. Contact between cell membranes has been observed in places where adjacent cells lacked a Schwann cell covering and it has been speculated whether these contact areas constitute ephaptic transmission pathways (Tylstedt and Rask-Andersen, 2001). Three types of membrane specializations in the ganglion cell were observed: symmetrical, asymmetrical and asymmetrical subplasmalemmal.

Holt and Koch (1999) estimated the extracellular potentials associated with an action potential in a cortical pyramidal cell using a detailed compartmental model of a layer V adult cat neocortical cell published by Mainen and Sejnowski (1996). The model included the full complexity of the dendritic geometry and the only modification made was that the current injection through an electrode was replaced by time-invariant synaptic input. They investigated the extracellular potential around cell bodies because the action potential around the somas can be especially large with a maximum of 3 to 5 mV, whereas an axon in normal tissue has an extracellular potential of only a few μV, since the currents involved in the action potential are small. The axon hillock and initial segment of the cell has a high density of sodium channels and the soma and dendrites a low density. The maximum conductance if all sodium channels are open is 30.000 pS/μm^2 in the axon hillock in comparison with only 20 pS/μm^2 in the soma and dendrites.

They found that within a radius of 10 to 20 μm of the axon hillock extracellular potentials were about 1 mV in amplitude and at the membrane of the axon hillock they could be as large as 5 mV. Besides the large amplitude, another implication for ephaptic interaction could be that the potential is more confined in space than a

potential from an axon so that it has a large amplitude over a small region (50 μm).

They concluded that ephaptic interactions near cell bodies can depolarize a passive fibre to evoke an action potential if the fibre is close to threshold and if there are active channels at the location of depolarization. Furthermore, they found that there are qualitative differences between two axons interacting and ephaptic interactions between a cell body and a nearby axon. The extracellular potential around a cell body is more spatially confined than the extracellular potential along an axon. Therefore the relevant segment of the passive fibre is small and the intracellular medium is approximately isopotential which results in the transmembrane potential being approximately equal to the negative extracellular potential. For two axons interacting however, the temporal derivative of the membrane potential is approximately proportional to the extracellular potential spatial differences.

2.2 NEURAL MODELS

Although it has been speculated about whether ephapses can constitute ephaptic transmission pathways (Tylstedt and Rask-Andersen, 2001), the ephaptic effect is disregarded in neural models. This study intends to investigate the ephaptic effect, as a contributor to electrical field interactions, in auditory nerve fibres by means of computational modelling. In general, in order to develop improved cochlear implants all mechanisms in the auditory system involved in the stimulation process must be investigated and better understood and computational models are an important part of this field of research.

2.2.1 Single fibre vs. neural populations

Temporal characteristics are used to describe the excitation behaviour of neurons and can be investigated either by studies on single fibres or studies on fibre populations. Single fibre studies on cats and guinea pigs (Van den Honert and Stypulkowski, 1984; 1987a; 1987b; Javel et al., 1987; Javel, 1990; Dynes and Delgutte, 1992; Shepherd and Javel, 1997; 1999; Javel and Shepherd, 2000) help in understanding responses to electrical stimulation in single fibres. Since single fibre experiments cannot be carried

out on humans, measurements on firing action potentials in populations of human nerve fibres have been performed instead (Shannon, 1985; Abbas et al., 1999; Miller et al., 2000). Electrically evoked compound action potentials (ECAPs) are the total potentials in a population of fibres and recordings of ECAPs have become widespread since the introduction of neural response telemetry (NRT) and neural response imaging (NRI) (Briaire and Frijns, 2005). Different computational models simulating ECAP responses have been developed. Miller et al. (1999a) developed an empirical model of ECAP responses based on single fibre cat data. The amplitude of the ECAP gives an indication of the number of excited neurons in a population (Miller et al., 1999a). Briaire and Frijns (2005) presented another model that tested the unitary response concept, i.e. the concept that every fibre produces the same contribution to the ECAP. They concluded that the compound action potential, as measured by the cochlear implant system, does not necessarily reflect the propagated action potential along the auditory nerve. Fibres in the centre of excitation area have a different contribution than those around the edges. ECAPs are not included in this study but in Chapter 3 a compound model is utilized where action potentials in clusters of nerve fibres are predicted.

2.2.2 Animal-based models

Excitation can be seen as a function of the potential distribution along the length of the nerve fibre and potentials that reach a threshold value evoke an action potential which propagates along the fibre. Volume conduction cochlear models are used to predict the potential distribution throughout the cochlea and along the auditory nerve fibres as a result of intracochlear electrical stimulation. Single-fibre models predict neural excitation as an effect of the potential distributions. Many models use a purely resistive volume to model the nerve bundle and peripheral axons and neglect capacitive effects based on findings by Spelman et al. (1982) which showed that potentials are frequency-independent (Finley et al., 1990; Frijns et al., 2001; Rattay et al., 2001b). Some models only employ a passive membrane (e.g. Rubinstein, 1993 and Finley, 1990) while others have implemented membrane kinetics (e.g. Rattay, 2001 and Briaire and Frijns, 2005) which predicts the propagation of the action potential.

Finley et al. (1990) based their passive nerve fibre model upon activating functions (Rattay, 1989) for most of their computations whereas Rubinstein (1991) provided

an analytical expression for spatial extent of activation by determining and solving Green's function for his passive membrane cable model. Using activating functions for investigating neuronal responsiveness provides a powerful tool in terms of shortening the simulations time. But there are limitations to this method in that it only takes initial sites of activation into account and leaves out numerous morphological aspects of the nerve fibre. Furthermore, since the ionic currents are left out, passive membrane models can not be used for investigation of ephaptic excitation.

In order to account for ephaptic effects, the kinetics of the membrane must be included in the model. In vitro experiments performed on nerve fibres from squid (Hodgkin and Huxley, 1952), toad (Frankenhæuser and Huxley, 1964) and rabbit (Chiu, Ritchie, Rogart and Stagg, 1979) have formed the basis for models describing membrane current dynamics.

The empirically developed Hodgkin and Huxley model describes the changes in the neural membrane potential in the squid giant axon. This model has been widely used and has formed the basis for other models, e.g. the Frankenhæuser and Huxley model and the Fitzhugh-Nagumo model. The Fitzhugh-Nagumo model is a two-dimensional simplification of the Hodgkin and Huxley model (Wei et al., 2009). The Frankenhæuser and Huxley model is similar to the Hodgkin-Huxley model but with two important differences; an extra delayed ionic current is added to the total membrane current and ionic permeabilities are used instead of membrane conductances (Rattay and Aberham, 1993).

Schwarz and Eikhof (1987) performed a full Hodgkin-Huxley analysis for large rat myelinated nerve fibres at body temperature. This was used by Frijns and ten Kate (1994), and Frijns et al., (1994) presented a model based upon voltage-clamp measurements in rat and cat motor nerve fibres at mammalian body temperature performed by Schwarz and Eikhof (1987) and Frijns et al., (1995). Frijns et al., (2000) presented a generalized version of this model coupled with a rotationally symmetric volume conduction model of the second turn of the guinea pig cochlea using the boundary-element method. This model was later modified with human morphometry (Briaire and Frijns, 2005; Briaire and Frijns, 2006).

Rattay and Aberham, (1993) and Rattay et al. (2001) compared results of simulations based on the above mentioned membrane models and found that the heated Hodgkin-

Huxley model with an increased ion channel density gives the best fit to the observed temporal behaviour of auditory nerve fibres in that it is the only model that fulfils all of the following criteria; (i) it is able to produce multiple spiking at low frequency sinusoidal stimulation; (ii) it has a sufficiently long chronaxie of 340 μs, which corresponds well with Parkins and Colombo (1987) who reported a chronaxie of 350 μs in squirrel monkeys; (iii) if a stimulating pulse is too weak to generate an action potential (AP), the model can make use of a second weak pulse applied shortly after the first one to give rise to an AP (Rattay et al., 2001).

Based on this result Rattay et al. (2001) used the heated Hodgkin-Huxley model to govern the kinetics in the nodes of Ranvier in a compartmental model of the human auditory nerve fibre. The model has the form of a cable model consisting of connected electric circuits based on the geometry of the neuron. They differed between a short and long dendritic fibre to account for the variation of position of the soma in the human auditory nerve fibre. The model was used to investigate site of excitation, speed of AP propagation, the vanishing of an AP at the soma under some conditions, influence of the electrode position and consequences of dendritic degeneration.

Although computational models based on animal physiology are an important part of cochlear implant research, there are several anatomical and morphological factors that must be taken into account before translating the results from animals to humans. With regards to the volume conductor, Shin-ichi et al. (1990) measured the dimensions of the scala tympani in both human and cat and found that the cross-sectional area of human scala tympani undergoes a significant reduction over the first 1.5 mm from the round window, whereas the cross-sectional area of the cat scala tympani increases over the first 1.0 mm and is actually larger than the human scala tympani in this region. However, throughout the rest of the measured cochlea, the cat scala tympani has a smaller cross-sectional area than that of human. Nadol (1988) investigated the cochlea and auditory nerve of guinea pig, rat, cat, monkey and man, and reported on major differences among species, e.g. the length and width of the basilar membrane, the number of inner and outer hair cells, and the length of hairs on both inner and outer hair cells. In the spiral ganglion, he found significant differences in the number of spiral ganglion cells, the number of cochlear nerve fibres, the percentage of spiral ganglion cells which are myelinated, and the presence of synapses on spiral ganglion cells. Rattay et al. (2001) demonstrated with their single-fibre model some characteristic differences between man and cat concerning cochlear nerve geometry and the degree

of insulation by myelin, which especially at the soma cause significant differences in spiking behaviour. Furthermore, cochlear implant users have an electrode array implanted whereas many animal experiments are performed with a single electrode. Animals used in experiments are also frequently acutely deafened while humans usually lose their hearing over long time.

2.2.3 Human-based models

Although several of the above mentioned models are based on human morphometric data and are used to model the human cochlea and human auditory nerve fibres, the dynamics of the ionic currents are still those of animals, such as rat, guinea-pig and squid. Smit (2008) presented a model simulating a human type I peripheral auditory nerve fibre based on a modified Hodgkin-Huxley model using recorded ionic membrane current data from human myelinated peripheral nerve fibres. The model successfully described and predicted action potential dynamics at the nodes of Ranvier as well as temporal characteristics in a human fibre. However, the model includes the ion channel protein KCNQ2 which makes it unsuitable to represent ionic membrane currents in somas and dendrites. The model was therefore not used in this study.

2.2.4 Verification of models using experimental studies

Experimental studies are used to validate results from computational models and for an investigation of ephaptic excitation by means of neural modelling, it is important that the model representing the nodal kinetics is evaluated and verified by comparing it to measured data. In addition to the above mentioned model evaluations by Rattay and Aberham, (1993) and Rattay et al. (2001), Cartee (2000) examined several of the existing models describing neural membrane ionic currents and determined their adequacy for modelling the summation and refraction properties of auditory neurons in response to electrical stimulation. To evaluate the models, the physiological time constants used for comparison were recorded using intrameatal electrical stimulation in cats. Cartee found that none of the examined models was clearly superior for modelling both the refraction and summation properties of the auditory neuron. Instead both the choice of a membrane model and the temperature used to evaluate the model are

important.

Ephaptic effects are normally not implemented in neural models and are likely to influence the spread of excitation predicted by models when included. If model predictions show that the ephaptic influence has a significant effect on the spread of excitation, it could be inferred that ephaptic effects should be included in neuromodelling.

2.3 NERVE MORPHOLOGY

Several modelling studies have shown that small variations in nerve fibre morphology can have a significant influence on the behaviour of a spike (Rattay et al., 2001a; Frijns et al., 1996). There is a wide variation between fibres (Gleich and Wilson, 1993; Glueckert et al., 2005) and still a lack of knowledge on morphometry of human nerve fibres, especially concerning the sequence of internodal lengths, and length and shape of the pre- and postsomatic region (Rattay et al., 2001a). For these reasons there is a need for further research in nerve morphology and its effects and models that compare different morphologies. There are between 30,000 and 40,000 nerve fibres in the cochlea of a normal hearing adult (Tylstedt, 2003). They innervate hair cells in the Organ of Corti and then run along the osseus spiral lamina and continue inside the modiolus, a spongy bony canal around which the cochlea twists. The cell bodies of the spiral ganglion cells are situated in the Rosenthal's canal that spirals around the modiolus. Spiral ganglion cells are usually divided into two types: large type I cells constituting 95% of the cell population and small type II cells constituting 5% (Kellerhals et al., 1967; Spoendlin, 1972, 1978; Kiang et al., 1984).

The type I cells have a somatic diameter of 25-30 μm, an average diameter of the central axons of 2.5 μm and the peripheral processes about half that size (Tylstedt, 2003; Ota and Kimura, 1980; Spoendlin and Schrott, 1988, 1989; Rosbe et al., 1996). Liberman and Oliver (1984) reported mean peripheral axon diameters of 1.44 μm for high spontaneous rate and 1.19 μm for low spontaneous rate neurons and mean central axon diameters of 2.54 μm for high spontaneous rate and 2.31 μm for low spontaneous rate neurons. The lengths of the dendrites vary depending on the location of the fibre. In the lower basal turn dendrites are about 1.4 mm long, in the second turn about 1.1 mm and in the apex about 0.8 - 1.0 mm (Smit, 2008). The type I cells are mostly

bipolar but pseudomonopolar varieties exist (Tylstedt, 2003; Kiang et al., 1984).

Type II cells have an average somatic diameter of 15 μm. They are usually bipolar or pseudo-unipolar, but multipolar cells have been observed (Tylstedt, 2003). They have thinner neurites than type I cells. In humans there are roughly as many myelinated as unmyelinated type II cells (Rusznák, 2009).

For both large and small spiral ganglion cells, the cell bodies are mostly unmyelinated, although a small percentage has multiple sheaths but no compact myelin (Tylstedt, 2003; Ota and Kimura, 1980). The functional significance of the lack of myelin sheaths around the soma is most likely a slower conduction rate of the afferent signals in the auditory nerve (Tylstedt, 2003; Ota and Kimura, 1980). The type I cells tend to form clusters where they frequently share sheathing from Schwann cells. This leads to close physical contact between cell bodies and can create ephapses, i.e. places where the membranes of two or more neurons are in direct contact (Tylstedt and Rask-Andersen, 2001). The dendrites have about 23 myelin layers, i.e. about 0.25 μm thick, while the axons have between 60 and 83 myelin layers, i.e. a myelin thickness between 0.7 and 1.0 μm (Spoendlin and Schrott, 1989).

2.3.1 Fibre densities

The number of myelinated axons per millimetre length of the cochlear duct varies considerably from base to apex. It is minimal with 300 fibres per millimetre at the basal end of the cochlea, reaches a maximum in the lower second turn with 1400 fibres per millimetre and decreases again towards the cochlear apex to about 400 fibres per millimetre. This corresponds to an average of 15 nerve fibres per inner hair cell in the lower second turn and 3-4 nerve fibres per inner hair cell at the base and apex (Spoendlin and Schrott, 1989). This leads to an average interneural distance of 7×10^{-5} cm in the lower second turn of the cochlea and 3.3×10^{-4} cm at the basal end.

As mentioned above, spiral ganglion cells are usually divided into large type I cells and small type II cells. However, studies on both animals and humans show that these types can be further divided into subtypes. Kimura et al. (1987) studied spiral ganglion cells in Rosenthal's canal of the macaque monkey by means of electron microscopy and found four types of cells. Type I cells showed myelinated somas with

myelinated axons and type II cells showed unmyelinated somas and unmyelinated axons. A third type showed myelinated somas with unmyelinated axons and the fourth type showed unmyelinated somas and myelinated peripheral processes.

Rosbe et al, (1996) studied human spiral ganglion cells and suggested three types of cells: large, intermediate and small, where the large and intermediate cells were subtypes of the classic Type I spiral ganglion cell and the small cell was consistent with the classic Type II ganglion cell. Only independent morphologic variables, i.e. cell diameter, nuclear diameter and axon diameter, were used. The maximal cross-sectional area of the cell body was less than 200 μm^2 for small cells, approximately 400-650 μm^2 for intermediate cells, and 550-900 μm^2 for large cells. They also provided information about how much of the total spiral ganglion cell population each type constituted; large cells comprised 49% of the total population, intermediate cells 38% and small cells 13%. This information, combined with the above mentioned neural densities, determines the density of each type throughout the cochlea. Large and intermediate cells had similar axon diameter (approximately 2-5 μm) whereas small cells had diameters of approximately 1-2 μm. This suggests that large and intermediate cells are subtypes of the type I spiral ganglion cell. When putting these results into the classically described type I and type II categories the following measurements can be concluded: the cross-sectional area of the cell bodies of type I cells is 400-900 μm^2 and the axon diameter 2-5 μm; and the cross-sectional area of the cell bodies of type II cells is less than 200 μm^2 and the axon diameter 1-2 μm.

The maximum cross-sectional area for a large cell body (900 μm^2) yields a diameter of 34 μm. This corresponds well with the single fibre model presented by Rattay et al., (2001), where the soma diameter was set to 30 μm.

2.4 PERCEPTUAL MEASURES

2.4.1 Threshold

In this study, the threshold for a deterministic model will be defined as the stimulus level at which an action potential is evoked in a fibre and for a stochastic model as the stimulus level that results in a 50% firing probability. Since the ephaptic effect

has been neglected in neural models so far, it is expected to decrease the calculated threshold when added to a model since less current from an electrode is required. Lower thresholds should be of general interest for cochlear implant developers since power consumption would be reduced. Mechanisms that could account for variations in threshold are therefore important to study. Threshold depends on several different factors, e.g. electrode configuration and location (Ranck Jr., 1975; Tehovnik, 1996; Smit, 2008), pulse shape (van Wieringen et al., 2005) and nerve morphology (Van den Honert and Stypulkowski, 1984). Degenerated fibres have lower threshold than normal fibres (Van den Honert and Stypulkowski, 1984) and this could mean that the ephaptic effect constitutes a larger part of the total stimulus on degenerated fibres than it does on non-degenerated fibres because of a lower electrode stimulus.

For cochlear implants, thresholds differ among electrode configurations. When the single electrodes in an array have a reference in a remote electrode (usually placed in the temporalis muscle or on the outside of the case for the receiver/stimulator (Wilson et al., 2008)), monopolar stimulation is effected. When stimuli are presented between closely-space electrodes within the array, the arrangement is called bipolar stimulation. Monopolar stimulation yields lower thresholds compared to bipolar stimulation. Studies on cats show 7.0 to 8.0 dB lower thresholds for monopolar stimulation while studies on guinea-pigs show 5.7 dB lower thresholds for monopolar stimulation (Smit, 2008). Monopolar configuration is preferable because while it performs just as well as bipolar configuration, it requires substantially less current and battery power. Therefore, all implant systems in current widespread use utilize monopolar stimulation (Wilson et al., 2008) and all simulations performed in this study only use monopolar configuration. Results from studies on polarity of monopolar stimulation differ between cats and guinea-pigs. Cathodic monopolar stimulation in cats yields lower thresholds compared to anodic stimulation (Van den Honert and Stypulkowski, 1987b; Miller et al., 1998; 1999b; 2001a). However, in guinea-pigs anodic stimulation yields lower thresholds (Miller et al., 1998). These diverging results have not been explained but it was speculated by the authors that the significant differences in the anatomy of cat and guinea pig cochleae could lead to significantly different current paths and, hence, activating functions (Miller et al., 1998).

Single fibre and ECAP studies on cats and guinea-pigs show that monophasic stimulation yields lower thresholds compared to biphasic stimulation (Miller et al., 1995; 1999b; 2001b). However, electrode polarization can cause damage in the neural tis-

sue and since monophasic current pulses are not charge-balanced they are for safety reasons not used with human subjects (van Wieringen et al., 2005). To diminish tissue damage, charge-balanced biphasic pulses should be used, since the second pulse actively discharges the polarization produced by the first one even though this means that the effective strength of the first phase is reduced by the second one due to integration of the externally applied current by the neural membrane. If monophasic pulses are used, the electrode should be discharged between pulses (Tehovnik, 1996). Once a particular threshold for neuronal damage is surpassed, tissue damage increases as a function of charge per phase. To decrease the charge per phase, shorter pulse durations may be used. By limiting the pulse duration to the chronaxie, most of the applied charge will go to evoke a response from the neuron, while duration significantly greater than the chronaxie will not improve the neural responses but contribute to tissue damage (Tehovnik, 1996). A possible solution to the problem is pseudomonophasic stimulation, i.e. increasing the duration of the second phase of a biphasic stimulation, which also decreases the threshold (Miller et al., 2001b). Van Wieringen et al., (2005) reports on a 3.0 - 6.0 dB decrease in threshold when biphasic pulses are replaced with pseudomonophasic pulses.

Longer pulse durations decrease thresholds; anodic stimulation more so than cathodic stimulation (Smit, 2008). Extremely long-duration pulses (e.g. 2-10 ms) generate multiple action potentials per single pulse and such pulses are known to increase the refractory period of neurons (Tehovnik, 1996). Since both shape and duration of a pulse can decrease threshold, these factors then also indirectly affects the influence of the ephaptic effect, since a lower electrode stimulus is needed. The effects of different pulse shapes are investigated in Chapter 4 and 5.

Both the electric field and the extracellular potential decrease when the distance between electrode and fibre increases. In an isotropic medium the electric field is inversely proportional to the square of the distance from the source, while - as known from Ohm's law - the extracellular potential is inversely proportional to the distance. Threshold current injected through an electrode is proportional to the square of the distance between the neuron and the electrode (Ranck Jr., 1975; Tehovnik, 1996). The proportionality constant depends on the size of the axon and whether it is myelinated or not and can therefore vary a lot from neuron to neuron. For a cathodic pulse with a duration of 0.2 ms it was found to vary between 100 and 4000 μA/mm^2. Furthermore, the proportionality constant has a negative correlation to the conduction velocity of

the axon, i.e. the greater the constant the lower the conduction velocity (Tehovnik, 1996). Rattay (2008) simulated a muscle fibre using a one-dimensional cable model that can be extended to an auditory nerve fibre model. By means of activating function analysis they found that while threshold for stimulation at the fibre end is proportional to the square of the distance, the current-distance relation for excitation at a central location on the fibre changes to cubic.

Threshold currents can be limited by placing the electrodes closer to the modiolus (Hanekom, 2001; Briaire and Frijns, 2006). The shape of the electrode can also decrease the threshold for neurons located near the electrode contact. The current density is defined as the current divided by the surface area of a sphere. At a far field, the current density needed to evoke an action potential from a neuron is dependent only of the current and the distance between the electrode and neuron. This means that the effective current spread at far field is independent of the surface area of the electrode. For neurons located near the electrode contact, however, lower threshold currents are needed for electrode contacts with smaller surface area. Since current density in a near field is calculated by dividing the current with the surface area of the electrode contact, smaller electrode contacts yield higher current densities. So, in order to excite high-threshold neurons using low currents, small electrode contacts should be used (Tehovnik, 1996). In this study modelled electrodes were implemented in the volume conduction model in Chapter 4. For the other models, point sources were utilized.

The neural membrane integrates the stimulus current and to indicate the integration properties of a membrane a strength-duration curve can be used. This curve describes the relationship between the threshold amplitude and the duration of a stimulus. The longer the duration the lower the threshold until it asymptotically reaches a limit. This limit is known as rheobase and is the minimum stimulus with infinite duration that will evoke an action potential. When the membrane acts as a perfect integrator the strength-duration curve will have the shape of a hyperbolic function. For a leaky integrator the curve takes the shape of an exponential function. The duration of a stimulus twice the size of rheobase is called chronaxie time and this duration can be used to indicate the integration properties of a membrane. The shorter the chronaxie time, the steeper the slope of the curve, which means the curve approaches a hyperbolic curve. The stimulus wave form and the distance from the source affect the chronaxie (Smit, 2008).

2.4.2 Frequency resolution

Another disadvantage with high threshold currents is that they can indirectly decrease resolution in frequency mapping by means of coarser spatial specificity. The cochlea of a normal hearing person is tonotopically organized so that high frequency sound stimulates neurons near the base while low frequency sound stimulates neurons at the apex. Intracochlear electrodes are located to mimic this tonotopy so that electrodes near the base are stimulated for high frequency signals etc. However, present placements of electrodes in the scala tympani do not support more than 4 to 8 effective sites of stimulation and cochlear implants use between 12 and 22 intracochlear electrodes, so the number of electrodes exceeds the number of effective channels for practically all subjects and for all current devices (Wilson et al., 2008). A plausible explanation for this limitation is that the electric fields from different intracochlear electrode contacts overlap at the sites of neural excitation.

Electrode configuration affects the spread of activation. In general, a bipolar configuration produces a localized spread of activation and a monopolar configuration produces a greater spread of activation because of its greater current spread. The monopolar configuration does, however, reduce the required current levels for auditory sensations, but the broader electric fields are problematic when electrodes are stimulated simultaneously since they have a greater probability of overlapping and interacting prior to reaching the fibres within the modiolus (Stickney et al., 2006). This can distort the stimulus and affect the perception of speech. Improving the spatial resolution of electrical stimulation should lead to restriction of the number of nerve fibres excited by one electrode and thus to a more natural perception (Kral et al., 1998).

Another way to increase the spatial specificity is to decrease the distance between electrode and target tissue. Even medial electrodes result in a large distance and two possible solutions to decrease the distance have been proposed. The first one involves promoting the growth of neurites from the ganglion cells toward the electrodes in the scala tympani with controlled delivery of neurotrophic drugs into the perilymph. The second one is to implant an array of electrodes directly within the auditory nerve (an intramodiolar implant), through an opening made in the basal part of the cochlea (Wilson et al., 2008). That would mean that the electrodes would be placed adjacent to axons of the auditory nerve. According to a study by Middlebrooks et al (2008), intraneural stimulation has several advantages compared to a conventional intrascalar

cochlear implant, such as providing access to fibres serving a broader frequency range, activation of more tonotopically restricted fibre populations, lower thresholds, and reduced interference between simultaneously stimulated channels. Due to the high neural density in the modiolus, the ephaptic effect would have a larger influence. Both of the mentioned propositions however need further study and validation (see Wilson et al., 2008 for more details).

A mismatch between electrode assigned frequencies and perceived pitch can also occur by cross-turn stimulation, i.e. stimulation of a fibre or a population of fibres in another turn of the cochlea due to the three-dimensional cochlear geometry. An ephaptic effect could be a significant contribution to this ectopic excitation. Ectopic excitations by the stimulus alone have been reported in the literature (Briaire and Frijns, 2000; Frijns et al., 2001). However, the ephaptic effect occurs in addition to the stimulus and although no direct experimental assessment of this has been made, several studies could be interpreted as indirect evidence for the ephaptic effect in that ectopic excitation can be expected to add unrelated pitch information. Henry et al. (2000), Throckmorton et al. (1999) and Busby et al. (1994) reported that one or more electrodes are frequently indiscriminable with regard to pitch. Busby et al. (1994), Shannon (1983) and Nelson et al. (1995) showed that reversals in place-pitch ordering on some electrodes in some subjects occur. Nelson et al. (1995) described instances of better electrode ranking in the apical half of the electrode array than in the basal half and vice-versa. Finally, Mens et al. (1995) reported that one of their subjects experienced complex pitch sensations on three of his apical electrodes. In each of theses cases an ectopic region of excitation could be the source of the observed pitch results.

In the next chapter a first model of ephaptic excitation is implemented.

Chapter 3

A FIRST MODEL OF EPHAPTIC EXCITATION

Jönsson, R., Hanekom T., Hanekom J.J., 2008. Initial results from a model of ephaptic excitation in the electrically excited peripheral auditory nervous system, Hearing Research, 237, 49-56.

3.1 OBJECTIVE

This chapter reports on a study performed to investigate the occurrence and effect of ephaptic excitation in electrical stimulation of the auditory system. The objective of the study was to quantify the influence of ephaptic excitation on nerve stimulation and determine whether it was a necessary factor in neuromodelling.

The approach that was taken is the following: A simplified version of the neural model presented by Rattay et al. (2001) was used to simulate propagating action potentials in a number of auditory neurons that are stimulated by an external electrode. The resulting membrane currents from the active neurons (i.e. the neurons excited by the electrode stimulus) were subsequently used as stimulating currents for a nearby passive or target neuron (i.e. an inactive neuron that could be ephaptically excited). The influence of the spatial orientation of the active neurons relative to the target neuron, stimulus intensity and neural density on ephaptic excitation was investigated.

3.2 BACKGROUND

Rattay's model (Rattay et al., 2001) simulates a neuron in a human and a propagating action potential. This model consists of connected electric circuits and it takes the geometry of the neuron into account. The neuron consists of six peripheral nodes, one presomatic region, the soma, one postsomatic region and fifteen central nodes. Between each central node and each peripheral node there are myelinated regions called internodes. Each region of the neuron is called a subunit and in the model each subunit is usually represented by one compartment. A compartment is simulated by an electric circuit and Figure 3.1 shows part of the electric network. A compartment consists of a membrane capacitance, a membrane conductance and an axoplasmatic resistance to each neighbouring circuit.

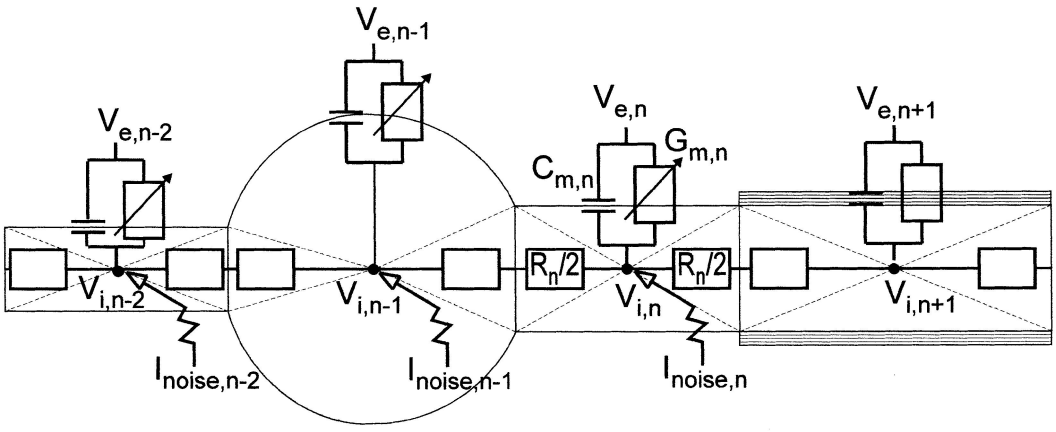

Figure 3.1: Part of electric network used in Rattay's model. The figure describes the presomatic and postsomatic compartment, the soma, and the first central internode. Figure taken from Rattay et al. (2001).

Kirchhoff's current law at the n-th compartment results to

$$C_{m,n} \cdot \frac{d(V_{i,n} - V_{e,n})}{dt} + I_{ion,n} + \frac{V_{i,n} - V_{i,n-1}}{R_n/2 + R_{n-1}/2} + \frac{V_{i,n} - V_{i,n+1}}{R_n/2 + R_{n+1}/2} = 0 \qquad (3.1)$$

This is rewritten as a first order ordinary differential equation for the potential

$$\frac{dV_n}{dt} = \Big\{ - I_{ion,n} + \frac{1}{R_{n,n-1}} \left(V_{n-1} - V_n + V_{e,n-1} - V_{e,n}\right) + \frac{1}{R_{n,n+1}} \left(V_{n+1} - V_n + V_{e,n+1} - V_{e,n}\right) \Big\} / C_{m,n} \tag{3.2}$$

where

$$\frac{1}{R_{n,n+1}} = \frac{1}{R_n/2 + R_{n+1}/2} \tag{3.3}$$

and

$$\frac{1}{R_n} = \frac{\text{Area}}{\rho \cdot \Delta x_n} = \frac{\pi \cdot d_n^2}{4} \cdot \frac{1}{\rho \cdot \Delta x_n} \tag{3.4}$$

where d_n is the diameter of the node, ρ is the specific resistance and Δx is the internodal distance. The neuron is stimulated by an electrode placed at a distance r from the first peripheral node. The electrode induces a step current which induces an external potential $V_{e,n}$, which in turn triggers an action potential. The external potential for the n-th node is given by

$$V_{e,n} = \frac{\rho \cdot I_{st}}{4\pi r} = \frac{\rho \cdot I_{st}}{4\pi\sqrt{x^2 + z^2}} \tag{3.5}$$

where the distance r now is rewritten in Cartesian coordinates. The membrane capacitance is inversely proportional to the number of layers of myelin N. Therefore the membrane capacitance is given by

$$C_{m,n} = \frac{\pi \cdot d_n \cdot L_n \cdot c_{m,n}}{N} \tag{3.6}$$

where L_n is the length of the node. The ionic current I_{ion} consists of two components: $I_{ion} = I_{ion,HH} + I_{noise}$. $I_{ion,HH}$ is the ionic current determined by the Hodgkin-Huxley equations

$$I_{ion,HH} = \left[g_{Na} m^3 h \left(V - V_{Na}\right) + g_K n^4 \left(V - V_K\right) + g_L \left(V - V_L\right)\right] \cdot \pi d L \tag{3.7}$$

and I_{noise} is represents ion channel current fluctuations in the active compartments. The Hodgkin-Huxley equations describe changes in the neural membrane potential. Equation (3.7) describes the dynamics of ionic currents consisting of the sum of the sodium current, potassium current and a term labelled leakage current which accounts for all other ions such as chloride and bicarbonate. The currents are given as

$$\begin{aligned} I_{Na} &= g_{Na} m^3 h \left(V - V_{Na}\right) \\ I_K &= g_K n^4 \left(V - V_K\right) \\ I_L &= g_L \left(V - V_L\right) \end{aligned} \tag{3.8}$$

where the m, n and h are the gating variables given by

$$\begin{aligned} \frac{\mathrm{d}m}{\mathrm{d}t} &= \left[-\left(\alpha_m + \beta_m\right) \cdot m + \alpha_m\right] \cdot \kappa \\ \frac{\mathrm{d}n}{\mathrm{d}t} &= \left[-\left(\alpha_n + \beta_n\right) \cdot n + \alpha_n\right] \cdot \kappa \\ \frac{\mathrm{d}h}{\mathrm{d}t} &= \left[-\left(\alpha_h + \beta_h\right) \cdot h + \alpha_h\right] \cdot \kappa \end{aligned} \tag{3.9}$$

where κ is a thermic coefficient and the coefficients α_i and β_i are voltage dependent and given by

$$\begin{aligned} \alpha_m &= \frac{0.1 \cdot \left(25 - V_m\right)}{\exp\left[\left(25 - V_m\right)/10\right] - 1} \\ \beta_m &= 4 \cdot \exp\left(-V_m/18\right) \\ \alpha_h &= 0.07 \cdot \exp\left(-V_m/20\right) \\ \beta_h &= \frac{1}{\exp\left[\left(30 - V_m\right)/10\right] + 1} \end{aligned} \tag{3.10}$$

The Hodgkin-Huxley equations are used since they give the best fit to the observed temporal behaviour of auditory nerves (Rattay et al., 2001). For a detailed overview of the model, see Addendum A. The model used in this chapter differs from the original Hodgkin-Huxley system in two ways: temperature and ion channel density. The original model data in the Hodgkin-Huxley system are based on low temperature experiments at a temperature of 6.3°C. At other temperatures the gating processes are multiplied with the thermic coefficient κ, where

$$\kappa = 3^{(T-6.3)/10} \tag{3.11}$$

where T is the temperature in °C. In the simulations made in this project the temperature of 29°C is assumed, resulting in the value $\kappa \approx 12$. Furthermore, for all of the compartments, except for the soma, the sodium, potassium, and leakage conduc-

tances are multiplied by the factor 10 to simulate 10-fold channel density (Rattay et al., 2001).

Figure 3.2 shows the behaviour of the state variables during the firing of an AP. When depolarization occurs, the sodium channels open and sodium ions flow into the cell. As sodium ions flood in, the membrane potential reverses such that the interior becomes positive relative to the outside. The positive potential then causes potassium channels to open resulting in an outflow of potassium ions. When the potential falls the sodium channels close.

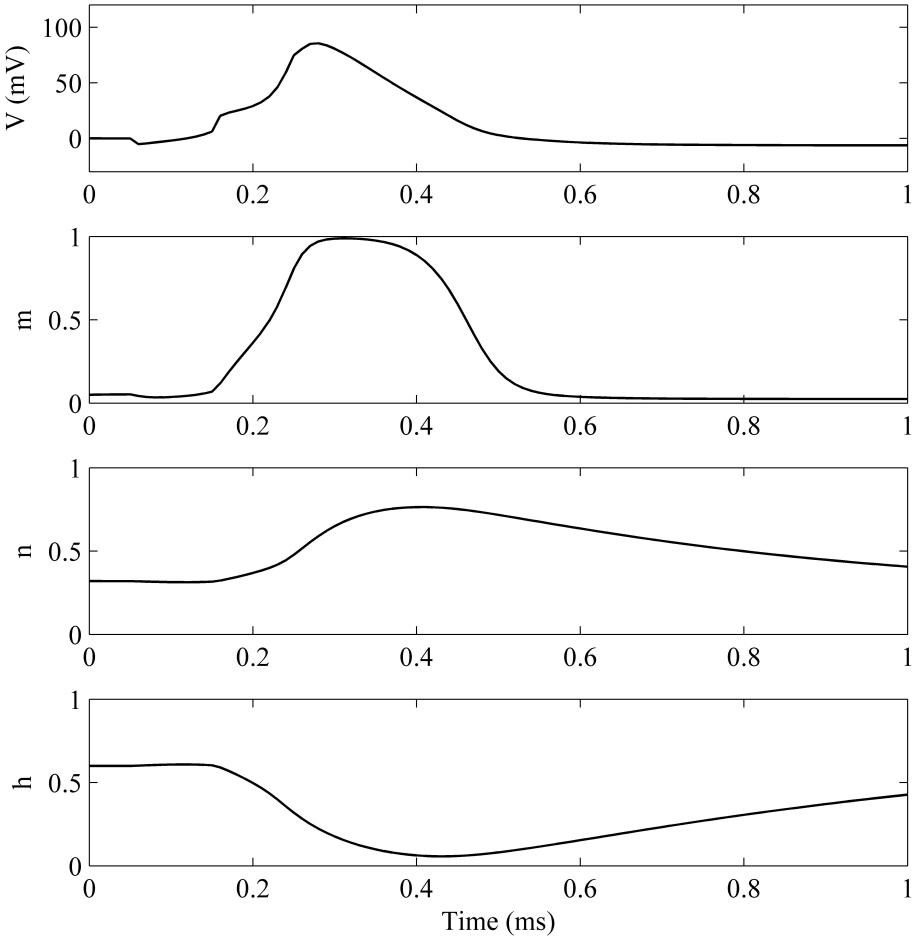

Figure 3.2: Action potential and the gating variables in the heated HH system.

Figure A.1 on page 128 shows an AP and the state variables with the original param-

eters in the HH model used to calculate the ionic currents in a Rattay fibre. When compared to Figure 3.2 the opening and closing of the state variables are much slower in the non-heated model than in the heated one, resulting in a longer AP.

3.2.1 Detail description of the model

Rattay's model (Rattay et al., 2001) was implemented to simulate a neuron in a human and a propagating action potential with a few simplifications. The first assumption is that there is no noise. This means that the ionic current is given by equation (3.7). The presomatic region is modelled as one compartment with the length 100 μm. This is another simplification of Rattay's model, which uses three compartments for the presomatic region. The last assumption is that the nodal resistance of axoplasma is neglected.

In Table 3.1 the parameters used for modelling the neuron are shown.

Table 3.1: Parameters for neuron. The presomatic region is divided into three regions, each with a length of 0.0033 cm.

	Length (cm)	Diameter (cm)	Myelin layers
Peripheral nodes	0.00025	0.00011	40
Presomatic region	0.01	0.00011	40
Soma	0.003	0.0033	3
Postsomatic region	0.0005	0.00022	80
Central nodes	0.00025	0.00022	80

The standard parameter values for the Hodgkin-Huxley model are used

$$
\begin{aligned}
g_{Na} &= 120\ \mathrm{k\Omega^{-1}cm^{-2}} \\
V_{Na} &= 115\ \mathrm{mV} \\
g_K &= 36\ \mathrm{k\Omega^{-1}cm^{-2}} \\
V_K &= -12\ \mathrm{mV} \\
g_L &= 0.3\ \mathrm{k\Omega^{-1}cm^{-2}} \\
V_L &= 10.6\ \mathrm{mV} \\
\rho &= 0.3\ \mathrm{k\Omega\ cm} \\
c_m &= 1\ \mu\mathrm{F\ cm^{-2}}
\end{aligned}
$$

3.3 STIMULI AND GEOMETRY OF MODEL AND STIMULUS

A Cartesian coordinate system was used to describe the geometry of the model. The x-axis is placed along the neuron with the first peripheral node at $x = 0$ and the z-axis gives the distance between the active neuron and the target neuron (see Figure 3.3). The electrode was placed right above the first peripheral node of the active neuron at a distance of 100 μm. The electrode is assumed to be a point source stimulating the active neuron with a cathodic pulse chosen arbitrarily as -33 μA and with a duration of 1 ms. The nerve fibres are placed in an infinite, homogeneous, isotropic and resistive medium with a resistivity of 0.3 kΩ cm.

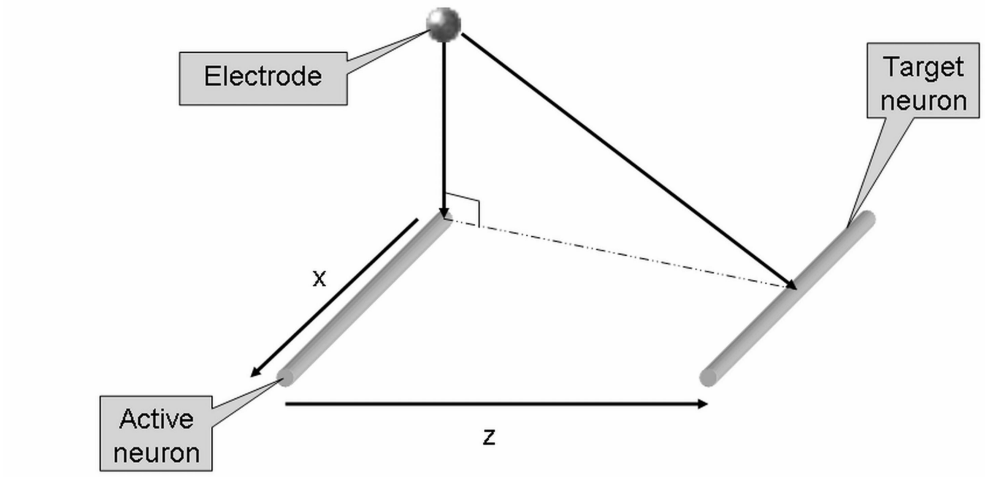

Figure 3.3: Model setup. An electrode is placed above the first peripheral node of the active nerve fibre. A target neuron is placed at a distance z from the active neuron.

3.4 MODELLING OF EPHAPTIC EXCITATION

3.4.1 Detection of ephaptic excitation

To detect whether ephaptic excitation occurred in the target neuron, the transmembrane potential in the axon was observed. Once the potential exceeded a threshold value (90 mV) in the 7th central node, it was concluded that a propagating action potential had occurred, i.e. the target neuron was excited (Reilly et al., 1985).

Two main conditions for ephaptic excitation were modelled: ephaptic excitation with coincidental spatial location, which is a simplified representation of a nerve bundle, and ephaptic excitation with separation of the neural elements, which is similar to the orientation of the peripheral neural processes.

3.4.2 Ephaptic excitation with coincidental spatial location of active neurons

3.4.2.1 Excluding electrode stimulus

Simulations were first preformed excluding the effect of the stimulus at the target neurons to obtain an indication of the extent of ephaptic excitation. The lowest number of active neurons necessary for triggering an ephaptic action potential in a target neuron at a specific location using only the ionic currents as stimulus was determined. The active neurons are assumed to be bundled together so they all have the same position in space (see Figure 3.3). This makes the stimulating currents for the passive neuron proportional to the number of active neurons. Furthermore, it is assumed that the passive neuron is positioned parallel to the active neurons. Hence, in Cartesian coordinates, the displacement of the passive neuron relative to the active ones can be described using only one spatial coordinate. When calculating the extracellular potential, the ionic currents of all the compartments must be included.

The extracellular potential for the n-th node, $V_{e,n}$, is calculated by

$$V_{e,n} = \frac{\rho}{4\pi} \sum_{i=1}^{26} \frac{I_{ion,i}}{\sqrt{(x_i - x_n)^2 + z^2}} \tag{3.12}$$

where $I_{ion,i}$ is the ionic current given by the HH system for the i-th node in the active neuron and z is the distance between the active and the passive neurons. Results were obtained by calculating the number of active neurons that would ephaptically excite a target neuron at a specific distance from the active neurons.

3.4.2.2 Including electrode stimulus

In this simulation the stimulating current from the electrode was included in the stimulus of the passive neuron. This is, of course, a more realistic application of the model since the effect of the stimulus cannot be separated from that of the active neurons. The extracellular potential for the n-th node in the passive neuron, $V_{e,n}$, was calculated by

$$V_{e,n} = \frac{\rho}{4\pi} \sum_{i=1}^{26} \frac{I_{ion,i}}{\sqrt{(x_i - x_n)^2 + z^2}} + \frac{\rho}{4\pi} \frac{I_{electrode}}{\sqrt{(x_i - x_n)^2 + z_{electrode}^2}} \tag{3.13}$$

where $I_{electrode}$ is the stimulating current from the electrode and $z_{electrode}$ is the distance between the electrode and the passive neuron.

This simulation was carried out in the same way as the previous one by adding active neurons until the potential in the ephaptically stimulated neuron exceeded a threshold value, i.e. a propagating action potential was detected.

3.4.3 Ephaptic excitation with spatial separation of the active neurons

The simulations described above assumed all active neurons to be bundled together in a fixed location. In the following simulations the model was extended by spatially separating the active neurons (Figure 3.4).

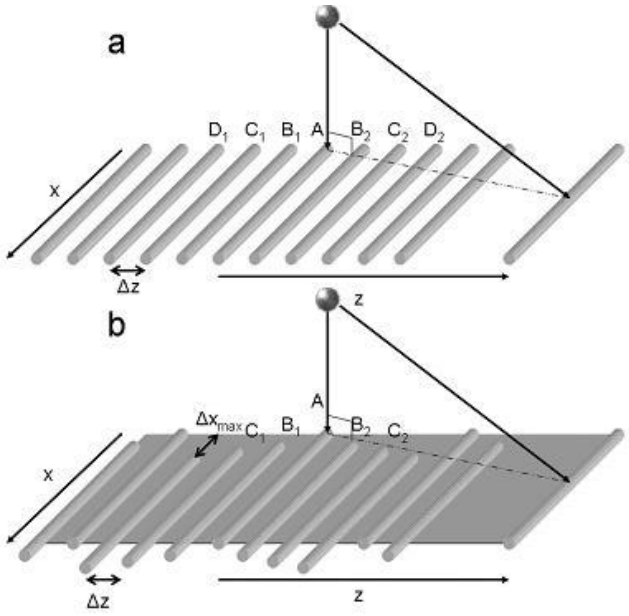

Figure 3.4: Variation of location in one dimension (a) and variation of location in two dimensions (b).

3.4.3.1 Variation of location in one dimension

The effect of a one-dimensional displacement of active neurons relative to one another was investigated by separating the active neurons by a small distance Δz. After having added the first neuron (A in Figure 3.4a), active neurons were added in pairs, one pair at a time, i.e. (B1,B2), (C1,C2), (D1,D2) etc. in Figure 5a, at an interneuron distance Δz on either side of the previous active neuron pair until ephaptic excitation occurred. The number of myelinated axons per millimetre length of the cochlear duct varies considerably from base to apex. It is minimal with 300 fibres per millimetre

at the basal end of the cochlea, reaches a maximum in the lower second turn with 1400 fibres per millimetre and decreases again towards the cochlear apex to about 400 fibres per millimetre. This corresponds to an average of 15 nerve fibres per inner hair cell in the lower second turn and 3-4 nerve fibres per inner hair cell at the base and apex (Spoendlin and Schrott, 1989). This leads to an average interneural distance of 7×10^{-5} cm in the lower second turn of the cochlea and 3.3×10^{-4} cm at the basal end. Results were calculated for conditions both excluding and including the electrode stimulus, and for the three interneural distances, i.e. 7×10^{-5} cm, 1×10^{-4} cm and 3.3×10^{-4} cm, corresponding to a high, middle and low neuron density.

The electrode position is held constant at 100 μm above the active neuron at $z = 0$, but since the active neurons are now spatially separated, the stimulating current must increase with increasing spatial spread of the active neurons. The stimulation current is a cathodic pulse with amplitude $I_n = 4\pi\rho^{-1}rV_{e,t}$, where $V_{e,t}$ is the potential threshold value calculated for the specific stimulus and r is the distance between the active neuron on the boundary of the excited region and the electrode.

3.4.3.2 Variation of location in two dimensions

The effect of two-dimensional displacement of active neurons relative to one another was investigated by separating the active neurons both along the x-axis and the z-axis. Different variations in neural distribution along the x-axis were evaluated to determine a worst-case neural distribution, i.e. a neural distribution that would minimize ephaptic excitation. The worst case-distribution among the ones tested was provided by a regular distribution of the neurons along the x-axis (see Figure 3.4b). Neurons were again added in pairs, one at each side of the active neuron region, i.e. (B1,B2), (C1,C2), etc. according to Figure 3.4b, displaced along the x-axis by $8/3 \times 10^{-2}$ cm relative to the previous pair until the maximum displacement was reached ($\Delta x_{max} = 8 \times 10^{-2}$ cm). The neuron distribution was thus symmetrical about the neuron at $z = 0$. The value 8×10^{-2} cm corresponds to the difference between Rattay's long dendritic model and short dendritic model (Rattay, 2001). Note that the active neurons are still located in the same plane.

3.5 VERIFICATION OF MODEL RESULTS

Estimates of the effect of ephaptic excitation were applied to modelled neural excitation profiles (Hanekom, 2001) and these profiles were then compared to neural excitation profiles measured in the inferior colliculus (IC) of the cat (Moore et al., 2002).

Limitations with IC data from cat include an under representation of low frequencies and an over representation of high frequencies in the frequency mapping as well as anatomical differences between human and cat cochleae. However, since IC data is a direct measurement of neural excitation profiles (as opposed to behavioural measurements that include central processing) and only low to midrange frequencies are relevant for the comparison, measurements in the IC of cat were chosen to verify the model results.

To convert the results from depth into the IC to length along the basilar membrane (BM), two frequency-position functions (Brown et al., 1997) were combined: one for frequency as a function of proportional distance across the IC and one for frequency as a function of proportional position along the BM. To use the function the measured data were normalized and a 20% shift along the depth of the IC was implemented corresponding to the offset in the frequency-position function. Finally, absolute threshold was defined at 0 dB to express results as intensity above threshold.

The function for IC is given by

$$f = A\left(10^{Bx} - C\right) \tag{3.14}$$

where x is the proportional distance across the IC. The function for cochlea is given by

$$f = D\left(10^{Ey} - F\right) \tag{3.15}$$

where y is the proportional distance along the BM. The following parameters were used (taken from Brown et al. (1997)):

$$A = 2444$$
$$B = 1.4$$
$$C = 2.1$$
$$D = 456$$
$$E = 2.1$$
$$F = 0.8$$

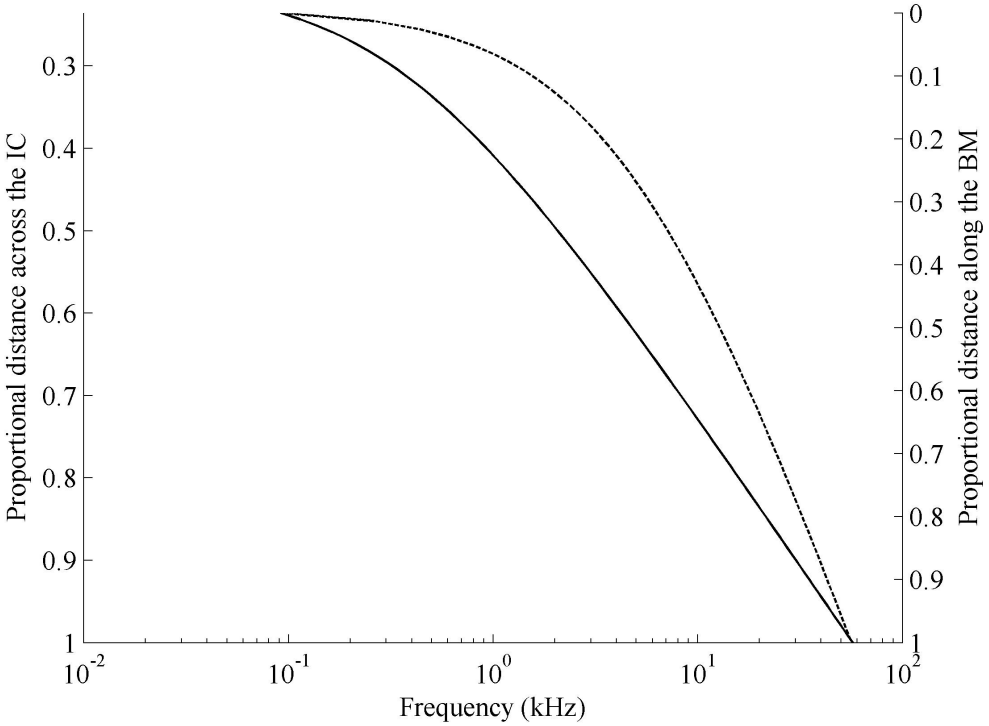

Figure 3.5: Greenwood functions for the frequency organisation of both the IC (dashed line) and the basilar membrane (solid line). Figure re-created from Brown et al. (1997).

In order to translate the measured data from the results of Moore et al. (2002), a function that maps the proportional distance across the IC on to the proportional distance along the BM. By equating the two above Greenwood functions the resulting

equation becomes

$$D\left(10^{Ey}-F\right)=A\left(10^{Bx}-C\right)\Leftrightarrow 10^{Ey}-F=\frac{A}{D}\left(10^{Bx}-C\right)$$
$$\Leftrightarrow 10^{Ey}=\frac{A}{D}\left(10^{Bx}-C\right)+F\Leftrightarrow Ey=\log_{10}\left[\frac{A}{D}\left(10^{Bx}-C\right)+F\right]$$

So the proportional distance along BM as a function of the proportional distance across the IC is

$$y\left(x\right)=\frac{1}{E}\log_{10}\left[\frac{A}{D}\left(10^{Bx}-C\right)+F\right]$$

Since the proportional distance along BM can not be negative, there is a lower boundary on the domain:

$$y\left(x\right)\geq 0\Leftrightarrow\frac{A}{D}\left(10^{Bx}-C\right)+F\geq 1\Leftrightarrow x\geq\frac{1}{B}\log_{10}\left[\frac{D}{A}\left(1-F\right)+C\right]$$

So using this function, the excitation profiles presented by Moore et al. (2002) were translated to excitation profiles of the cochlea and used to verify the results presented through this simulation.

The ephaptic effect was added to the model data (M_d) from Hanekom (2001) by

$$M_{d,EE}=M_d+M_d\cdot EE_{\%} \tag{3.16}$$

where the M_d is the normalised modelled data, i.e. divided by the length of BM, and $EE_{\%}$ is given by

$$EE_{\%}=\frac{z-S}{S} \tag{3.17}$$

where z is the distance from the first excited fibre to the target fibre and S is the spread calculated by

$$S=\frac{n-1}{2}\cdot\Delta z \tag{3.18}$$

where n is the number of active fibres and Δz is the distance between fibres.

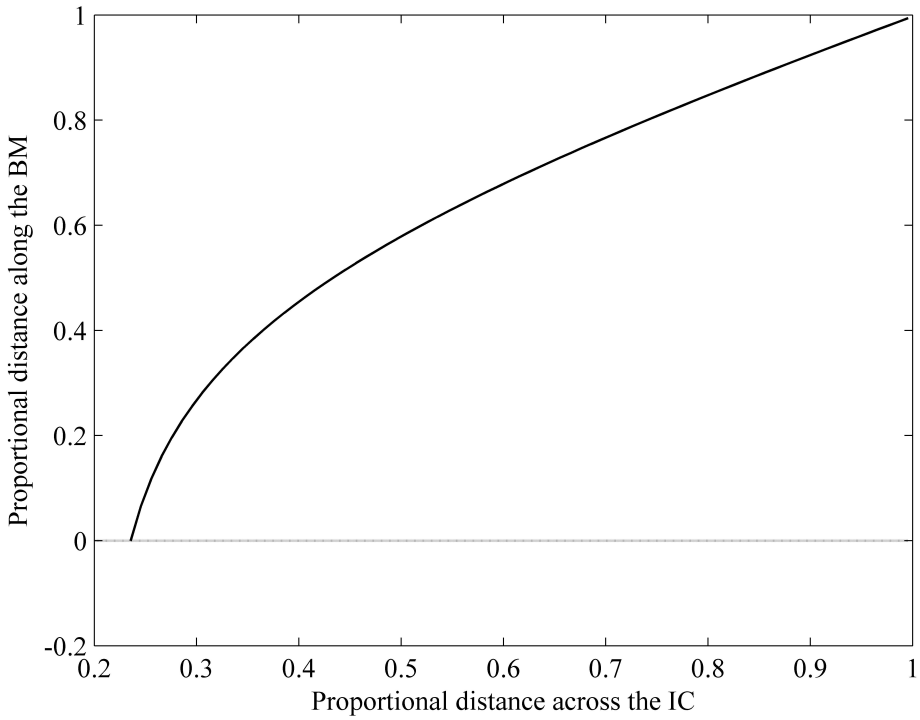

Figure 3.6: Proportional distance along the BM as a function of the proportional distance across the IC within the valid domain.

3.6 RESULTS

3.6.1 Ephaptic excitation with coincidental spatial location of active neurons

A first remark is that results for the case where the active neurons occupy a coincidental spatial location (i.e. all the active neurons are aligned in all dimensions) were generated for a constant stimulus intensity, i.e. the stimulus intensity did not increase with the number of excited neurons since spread of excitation and stimulus intensity are independent of one another in this case. The dashed graph in Figure 3.7 shows the result of ephaptic excitation excluding the electrode stimulus. When the active neurons are bundled together and the stimulus is neglected, the number of neurons required to effect ephaptic excitation increases exponentially with increasing distance between the active and target neurons. Ephaptic excitation can only be induced at small distances, e.g. at 0.02 cm more than 8000 active neurons are necessary to cause ephaptic excitation.

The solid graph in Figure 3.7 shows the result of ephaptic excitation including the electrode stimulus. The results suggest that the electrode stimulus significantly influences excitation of the passive neuron at smaller active to target neuron separations, i.e. spread of excitation as a result of the electrode stimulus completely outweighs ephaptic excitation at small active-passive interneuron separations (up to approximately 160 μm). As the interneuron separation increases above 160 μm ephaptic excitation starts to contribute to the spread of excitation. At a separation of approximately 300 μm, spread of excitation approaches the curve predicted for ephaptic excitation excluding the stimulus. The implication is that the effect of the stimulus (at a specific stimulus intensity) is at some stage outweighed by ephaptic excitation (approximately 300 μm in this case). Since the active neurons are spatially coincidental, no noise is present, the medium is infinite, homogeneous and resistive and the time course of the action potentials are identical, the problem reduces to a threshold-dependent one. By calculating the threshold at which ephaptic excitation occurs and then calculating the location of that threshold as a function of the number of active neurons, the same results as in Figure 3.7 were obtained, i.e. in this special case the neural model need only be solved to determine the threshold for the specific stimulation setup.

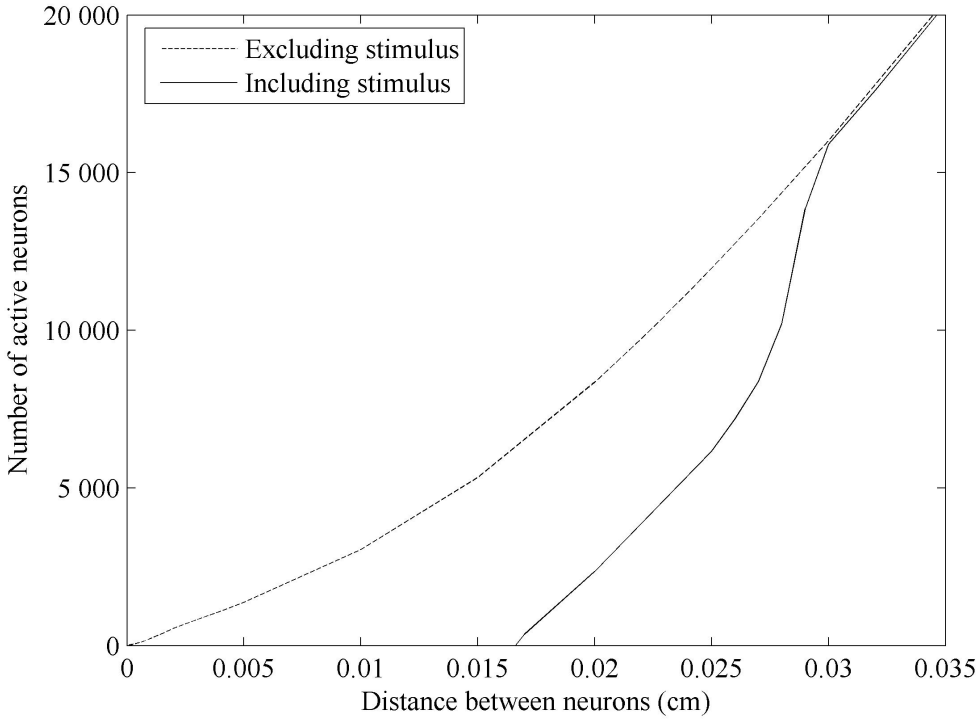

Figure 3.7: The dashed line shows the lowest number of active neurons needed for ephaptic excitation when only the ionic currents from the active neurons are used as stimulus. The solid line shows the result when the electrode currents are included.

3.6.2 Variation of location in one dimension

Figure 3.8 shows the results of the separation of the active neurons in one dimension for different interneural distances both including and excluding the stimulus. When the stimulus is excluded, ephaptic excitation only occurs for high and medium neuron densities when the active neuron region borders the target neuron. This leads to a linear relationship since the neuron distribution along the z-axis is linear. When the stimulus is included, the ephaptic excitation is significant for small active to target neuron distances but decreases as the distance increases. This is true for all the modelled neural densities. It was not possible to elicit ephaptic excitation for the low neural density when the stimulus was excluded. Figure 3.8 also shows that the two graphs representing ephaptic excitation including and excluding the stimulus converge at high stimulus intensities for medium and high neural densities. It is, however, not possible to compare the extent of ephaptic excitation from the graph in Figure 3.8 directly, since the spread of the active neuron region for a specific number of active neurons is dependent on neural density. For this reason, and to present the data in a way that is interpretable in the context of cochlear implants, the contribution of ephaptic excitation to spread of excitation was calculated as a function of stimulus intensity. Spread of ephaptic excitation was normalized with respect to the spread of excitation generated by the stimulus alone. These values were then plotted as percentages versus stimulus intensity in decibels above threshold (Figure 3.9). Threshold was calculated as the lowest stimulus current that could excite a single neuron in the model. This value was used as the 0 dB reference in Figure 3.9.

Figure 3.9 shows that relative spread of ephaptic excitation decreases with increasing stimulus intensity and at approximately 8 dB a margin of 1 dB in the stimulus spread corresponds to less than 1% contribution by the ephaptic spread and can be negligible. The contribution of ephaptic excitation to spread of excitation is significant close to threshold with maximum contributions of approximately 340% for high neural densities and approximately 240% for low neural densities. However, as the stimulus intensity increases the contribution rapidly decreases and except for stimulus intensities very close to threshold, the relative contribution of spread of ephaptic excitation appears to be independent of neural density.

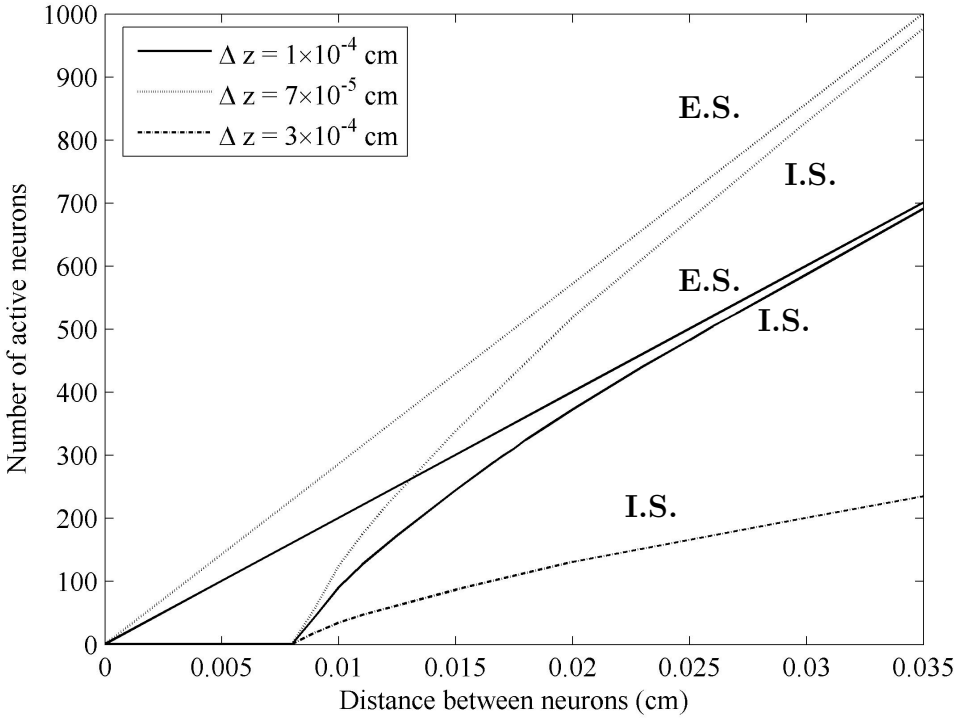

Figure 3.8: Variation of location in one dimension for different interneural distances with both excluding (E.S.) and including stimulus (I.S.). For low neural density it was not possible to elicit ephaptic excitation when excluding stimulus.

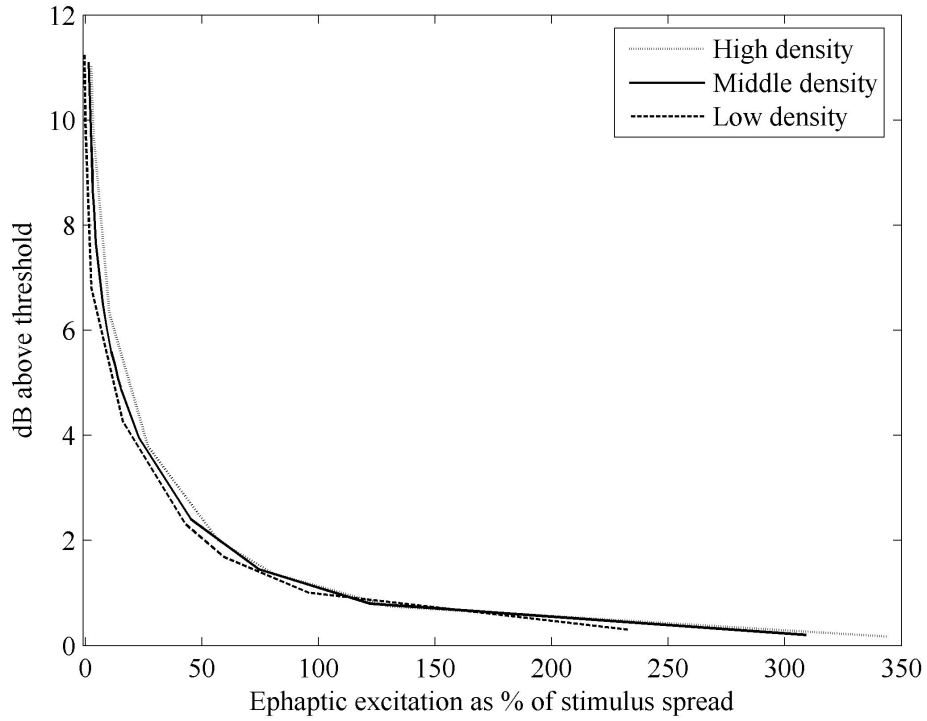

Figure 3.9: Contribution of ephaptic excitation towards spread of stimulus excitation spread versus the intensity above threshold for high, middle and low neural densities for separation of location in one dimension.

3.6.3 Variation of location in two dimensions

Figure 3.10 shows the results of the separation of the active neurons in two dimensions including the stimulus for different interneural distances.

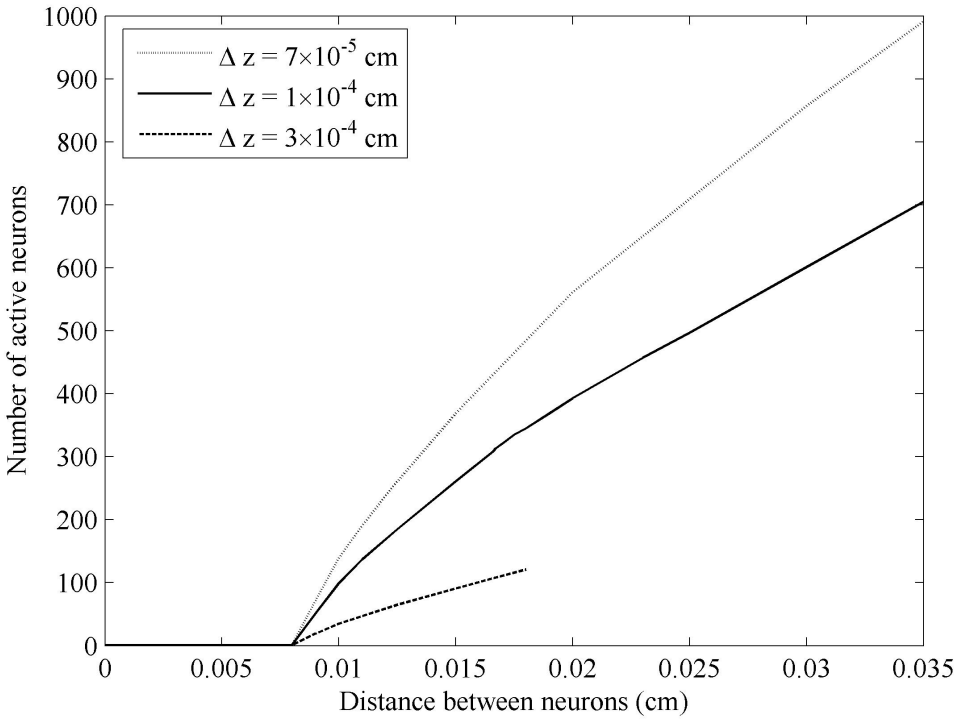

Figure 3.10: Variation of location in two dimensions for different interneural distances.

Ephaptic excitation can logically only occur outside the active neuron region and for the low neural density case ephaptic excitation ceases at 0.018 cm.

Ephaptic excitation decreases as the stimulus intensity increases. The contribution of ephaptic excitation to spread of stimulus excitation is again significant close to threshold with maximum contributions of approximately 270% for high neural densities and approximately 235% for low neural densities. As for one-dimensional separation, the contribution rapidly decreases for high stimulus intensities and there is not much difference between the different densities.

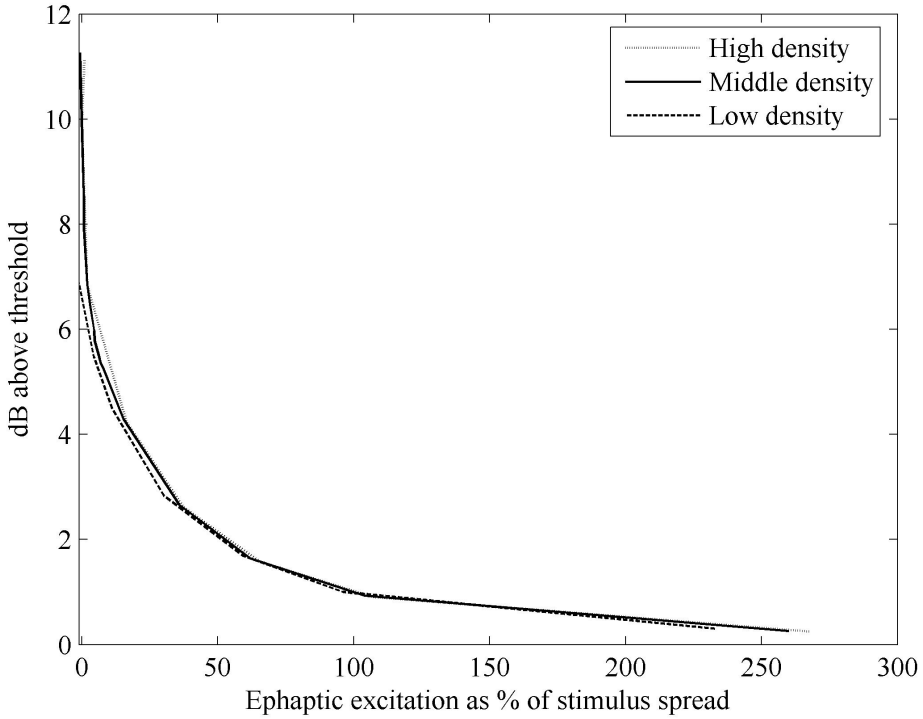

Figure 3.11: Contribution of ephaptic excitation towards spread of stimulus excitation spread versus the intensity above threshold for high, middle and low neural densities for separation of location in two dimensions.

3.6.4 Comparison with electrophysiological data

Estimates of the effect of ephaptic excitation applied to modelled neural excitation profiles (Hanekom, 2001) were compared to translated neural excitation profiles measured in the cat (Moore et al., 2002). Figure 3.12 shows the translated measured data from the cat, modelled data (Hanekom, 2005) and the ephaptic effect added to the modelled data.

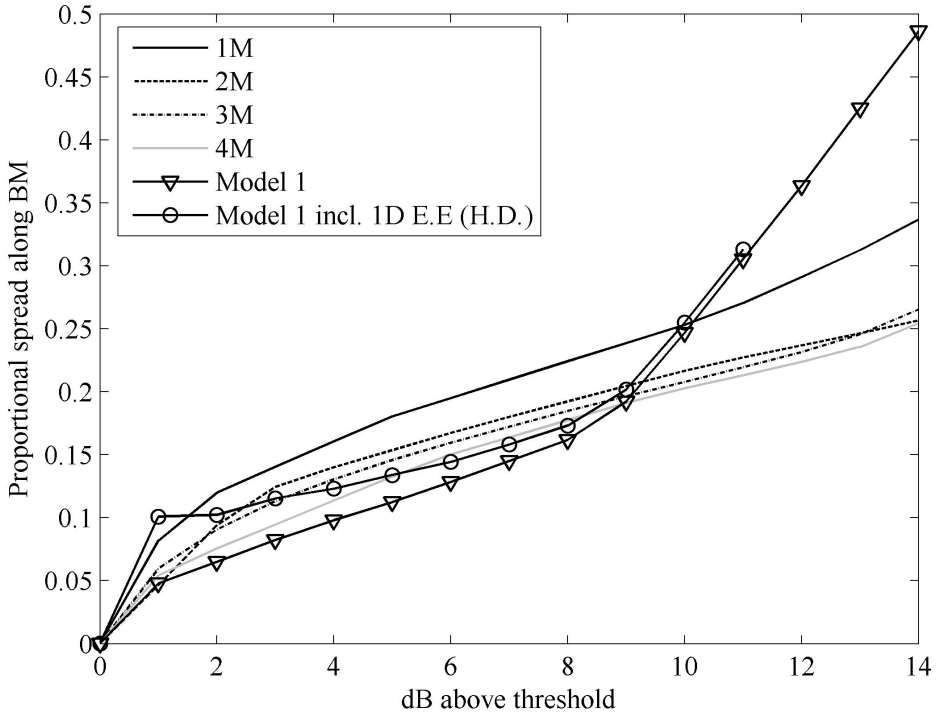

Figure 3.12: Results of measured data, modelled data excluding ephaptic effect and modelled data including ephaptic effect (E.E.) from the variation of location in one dimension and high neural density (H.D.). 1M and 2M are apical electrodes and 3M and 4M are basal electrodes.

Measured data have a larger spread of excitation than modelled data when the stimulus is close to threshold. When adding the ephaptic effect to the modelled data, the spread increases close to threshold.

3.7 DISCUSSION

There is a significant qualitative difference between the results of the coincidental location and the separation of location of the active nerve fibres. This can be ascribed to the factors described below. When the fibres are bundled together a constant stimulus current is used, while the current increases with an increase in spread of the active fibres when they are spatially separated. Also, when the fibres are bundled together there is no spatial constraint to the number of active neurons, which leads to the large numbers of active neurons in Figure 3.7. This is also the reason why excitation by the electrode stimulus is at some stage outweighed by ephaptic excitation in these results while the electrode stimulus dictates spread of excitation at high stimulus intensities (i.e. large numbers of active neurons) when the active neurons are spatially separated.

The model for separation of location in one and two dimensions predicts similar qualitative results but the relative contribution of spread of ephaptic excitation is slightly higher for one-dimensional separation and fewer active neurons are necessary to trigger the target neuron ephaptically. For low neural densities in the case of two-dimensional separation, ephaptic excitation is limited to stimulus intensities close to threshold, i.e. there is an insufficient number of neurons in the excited region at higher stimulus intensities to cause ephaptic excitation.

At threshold the model predicts that the relative contribution of ephaptic excitation for high densities will be more than three times the spread of excitation, and the relative contribution of ephaptic excitation for low densities more than twice the spread of excitation (Figures 3.9 and 3.11). This is an artefact of the model caused by the different interneural distances: at threshold the maximum distance at which ephaptic excitation occurs is independent of neural density (Figure 3.8), thus causing a larger relative contribution when the neural density is included in the normalization process (Figure 3.9). However, the contribution of ephaptic excitation seems to be important up to at least 6 to 7 dB above threshold (Figure 3.9). Cochlear implant patients normally have a small dynamic range (average of 7 dB), indicating that the ephaptic effect might be important in models of the implanted cochlea. To decrease the ephaptic effect for cochlear implants, more localized stimulation by the electrode is needed for low intensities.

In the model all active neurons were assumed to be either bundled together in a fixed location or located in a plane. Results obtained for the planar orientation of the fibres could be used to estimate the extent of ephaptic excitation for the peripheral part of the fibres along the basilar membrane. The spiral ganglion is three-dimensional and consists of bundles of neurons. As a first approximation the model using coincidental location of the neurons could be used to estimate the effect of ephaptic excitation in the localized parts of the fibre bundles in the spiral ganglion. However, a combination of the coincidental and separated locations of active neurons could provide a more accurate description of the spiral ganglion. Also, by placing the active neurons in a three-dimensional location, the cross-sectional neural density would be higher than in our planar experiments, which could lead to a larger spread of ephaptic excitation.

When adding the ephaptic effect to the modelled data in Figure 3.12, spread of excitation increased. The estimate of the extent of ephaptic excitation could be improved if the following aspects are considered and implemented. Firstly, the model used to predict the ephaptic effect was simple. The fibres were in a plane and placed in an infinite, homogeneous, isotropic and resistive medium. If the model is expanded to include the three-dimensional geometry of the volume conductor as well as material inhomogeneities, the estimate of ephaptic excitation could improve. Secondly, the measured data came from a cat cochlea while the modelled data came from a human cochlea model. The maximum neural density used in our model is 1400 fibres per millimetre while the neural density in the cat spiral ganglion is about 5000 fibres per millimetre (Keithley and Schreiber, 1987). Furthermore, the anatomy of the human cochlea and especially the basal turn is essentially different from that of other species (Frijns et al., 2001). In the cat the basal turn of the cochlea is wider compared to that of a human cochlea (Shin-ichi et al., 1990). This would generally lead to an increase in the current spread along the length of the basilar membrane because of a decrease in the local impedance of the scala tympani. A larger spread of current corresponds to a wider spread of excitation. The spread of excitation could thus be somewhat under-estimated by the model since it is based on human anatomy. This would especially be the case for the results measured with the 4M electrode (Figure 3.12), which shows a basal electrode. The apical electrodes in the measured data (1M and 2M) would correspond best to the modelled data, since these electrodes are a bit removed from the basal part of the cochlea. Results for regions outside the basal region should be comparable since the anatomy is similar for cats and humans in this area of the cochlea.

3.8 CONCLUSION

In conclusion, it was shown with a very simple model that ephaptic excitation could be important at stimulus intensities close to threshold. Limitations of our model include an assumed ideal volume conductor, a point source electrode and planar fibre location. Future research work in this field should focus on the development of a model that includes a more realistic description of the volume conductor (i.e. the cochlea with the implanted electrodes). The results obtained from such a model should be compared with physiological results measured in animals or psychoacoustic results measured in human subjects, e.g. forward masking data that provide an indication of the spread of neural excitation.

Chapter 4

A MODEL WITH ANATOMICAL DETAIL

Jönsson, R., Hanekom T., Hanekom J.J., 2010. Evidence for an ectopic excitation mechanism in cochlear implants, *submitted for publication*

4.1 OBJECTIVE

The main objective of this chapter is to expand on the study on ephaptic excitation presented in the previous chapter by escalating the detail of the model. The study showed that ephaptic excitation could influence neural excitation close to threshold. However, the effects of membrane noise, three-dimensional geometry and conductive properties of the cochlear volume and pulse shape have not been considered. This study investigates the effect of inclusion of the mentioned alterations to the model on ephaptic excitation and consequently evaluates the necessity thereof in neuromodelling. The influence of ephaptic stimulation on channel interaction in cochlear implants is also discussed.

4.2 BACKGROUND

The previous chapter employed a deterministic neural model, which showed that ephaptic excitation could have an important influence at stimulus intensities close to threshold. Membrane noise, which is an integral part of the normal sensory process (Zeng et al., 2000), has been shown to improve hearing in both sound detection at threshold and at suprathreshold discrimination of sound by means of stochastic resonance. It is a nonlinear phenomenon where the addition of an appropriate amount of noise enhances signal detection (Behnam et al., 2003). Membrane noise is typically in the order of 0.49 mV in a peripheral human node (Rattay et al., 2001). Since the previous chapter employed a deterministic neural model, it is at this stage unknown whether the ephaptic effect is significant in the presence of membrane noise. An increased sensitivity to stimuli caused by stochastic resonance could affect the contribution of ephaptic excitation to thresholds and spatial extent of neural excitation since the ratio of ionic currents from the excited neurons to the electrode current could change.

Neural excitation thresholds are also influenced by stimulation pulse shape. Van Wieringen et al. (2005) reported that thresholds for alternating monophasic stimuli were 5-8 dB lower than for biphasic waveforms. Furthermore, dynamic ranges of pseudomonophasic pulse shapes were greater than those of biphasic pulse shapes (van Wieringen et al., 2005). It is possible that the degree of ephaptic excitation could be dependent on stimulation pulse shape since i) ephaptic currents will add to, and thus alter, stimulus currents depending on stimulus parameters such as leading phase polarity and phase duration and ii) neural excitation profiles, which could influence ephaptic excitation, are dependent on stimulation pulse shape (van Wieringen et al., 2005).

4.3 METHODS

4.3.1 Construction of model

Two models of ephaptic excitation were employed in this study to investigate ephaptic interactions. The first was similar to the model described in Chapter 3 where the volume conductor was described as an infinite homogeneous, isotropic, resistive medium containing straight single fibres in various arrangements relative to one another. However, the neural model in this study also contains a membrane noise component. The second model introduces anatomical detail to the volume conductor. The compound model consists of a volume conduction model of a cochlea containing an electrode array (Hanekom, 2001) integrated with a stochastic single auditory nerve fibre model (Rattay et al., 2001). It thus took the morphology of the fibres, geometry and conductive properties of the cochlea and membrane noise into account. Both models were used to simulate propagating action potentials in a number of auditory neurons that are stimulated by an external electrode. The resulting membrane currents from the active neurons (i.e. the neurons excited by the electrode stimulus) were used as stimulating currents for the ectopic target neuron (i.e. an inactive neuron that could be ephaptically excited). The compound model was subsequently employed to predict responses to two different pulse shapes. The results were analyzed to determine whether it is necessary to include the ephaptic effect in neuromodelling, and if so, under which conditions.

4.3.1.1 Neural model

The neural model used in this chapter is a compartmental cable model consisting of connected electric circuits based on the geometry of a human auditory neuron and was presented by Rattay et al. (2001). Each circuit models a compartment consisting of a membrane capacitance and conductance and an axoplasmatic resistance to each neighbouring compartment. The neuron consists of six peripheral nodes, a presomatic region, a soma, a postsomatic region and 15 central nodes. Between each peripheral node and each central node there are myelinated internodes. The internodes in the peripheral axon each have 40 shielding layers of myelin and the ones in the central axon each have 80 layers. Though the human soma is unmyelinated, it is assumed

to have three layers of insulating membranes in this model to aid propagation of the action potential across the soma.

Just as for the neural model used in Chapter 3, the dynamics of the ion channels are governed by the heated Hodgkin-Huxley (HH) equations, i.e. the gating processes were multiplied by a factor 12 producing a heated system of 29° C. The sodium, potassium and leakage conductances are multiplied by a factor 10 to simulate a 10-fold channel density. For additional details refer to Rattay et al. (2001).

4.3.1.2 Calibration of noise parameters

A noise term is added to the ionic currents governed by the HH equations to simulate randomness in excitation behaviour of the nerve fibres. The noise used in the neural model consists of a random variable which is added to the ionic current and is proportional to the square root of the number of sodium channels in a compartment (Rattay et al., 2001). It is expressed as

$$I_{noise} = \text{GAUSS} \cdot k_{noise} \cdot \sqrt{A_n \cdot g_{Na}} \tag{4.1}$$

where GAUSS is a Gaussian noise current term that changes value every 10 μs, k_{noise} is a scaling factor, A_n is the membrane area of the nth compartment in cm^2 and g_{Na} is the maximum sodium conductance density with the value 1200 mS cm^{-2}.

To calibrate the scaling factor (k_{noise}), I_{noise} was fitted to the probability function presented by Bruce et al. (1999). The threshold given by Bruce et al. (1999) was 49.1 dB (re 1μA) and the distance between electrode and fibre generating the same threshold was found to be 0.083 cm. This value lies within the range of distances reported in literature (Shin-ichi et al., 1990) that show distances between electrode and dendrite ranging from approximately 0.01 cm for an electrode in the middle turn to 0.2 cm for an electrode close to the round window. Simulations were carried out with a varying scaling factor and Figure 4.1 shows an approximate fit to the discharge probability presented by Bruce et al. (1999) with $k_{noise} = 0.0036$ μA mS$^{-1/2}$.

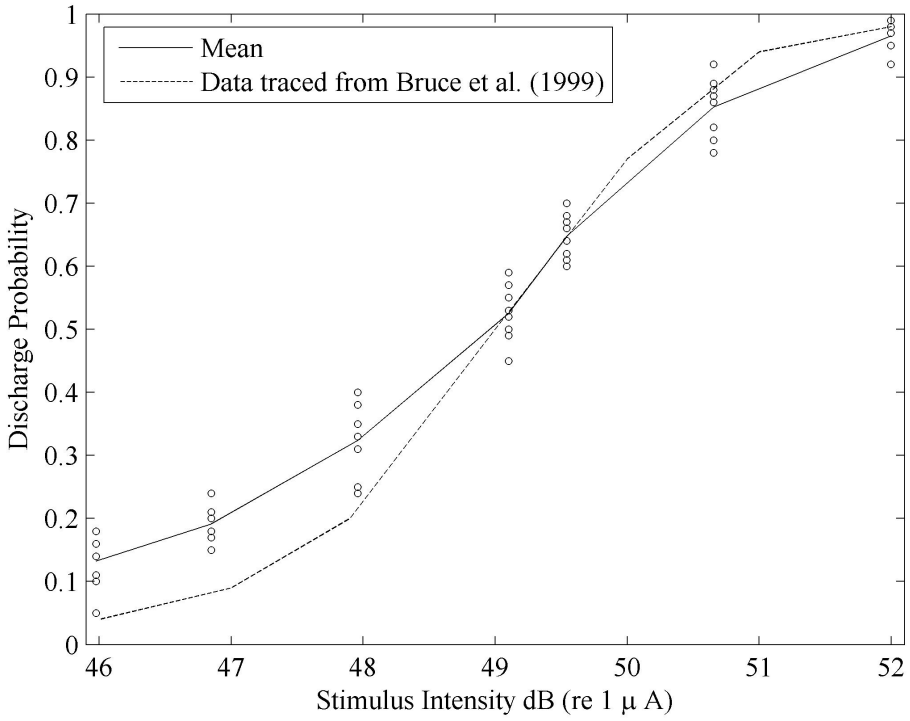

Figure 4.1: Discharge probability as a result of the calibrated noise parameters $k_{noise} = 0.0036$ μA mS$^{-1/2}$ and standard deviation 1. Each open circle represents 100 iterations and the solid line is the average of a total of 800 simulations. The dashed line shows the discharge probability presented by Bruce et al. (1999).

4.3.1.3 Volume conduction model

To determine the effect of the three-dimensional geometry of the cochlea on ephaptic excitation a three-dimensional volume conduction model containing two turns of the human cochlea (Hanekom, 2001) was used to calculate potential distributions through the cochlear tissue. The materials in the model are purely resistive. For material properties, see Hanekom (2001). The model incorporates the effect of neighbouring canals and conduction along the fluid-filled canals of the cochlea and is designed to allow for two possible electrode array locations relative to the modiolus: medial and lateral. Only the medial electrode location was used in this study since its location corresponds to most modern cochlear implant electrode arrays. The model contained 111 segments, each spaced about 6.54 degrees apart around the modiolus, allowing for 111 clusters of nerve fibres. An electrode array containing 22 possible electrode contacts distributed along the length of the scalae was modelled. These were numbered from the base of the modelled cochlea to the apex.

The input to the volume conduction model was the stimulation current from a modelled electrode inside the scala tympani as well as small currents along each cluster of nerve fibres, simulating excited nodes of Ranvier. The output of the volume conduction model was the potential distributions at the nerve fibres as a result of both the electrode stimulus and the modelled excited nodes.

4.3.1.4 Compound model

To integrate the volume conduction and nerve fibre models, the potential distribution through the neural tissue in the volume conduction model was used as input to clusters of modelled nerve fibres. The location of the modelled nodes of Ranvier in the volume conduction model corresponded to the location of the nodes in the nerve fibre model. Each cluster of nerve fibres consisted of a number of single nerve fibres of which the constitution and morphology are described below.

The modelled voltage values between a specific electrode and all nodes of every fibre from the volume conduction model as well as voltage values between excited neurons and target fibre were then scaled to correspond with the stimulus and ionic currents of the nodes of Ranvier in the neural model.

The first output from the compound model was thus the superimposed potential distribution at the nerve fibres resulting from both the electrode stimulus and the electrical activity from the primary excited nerve fibres, i.e. the nerve fibres that provide the source for ephaptic excitation. The second output, which is also the final output from the model, was the resultant neural excitation pattern reflecting the activity of both stimulus and ephaptically excited neurons.

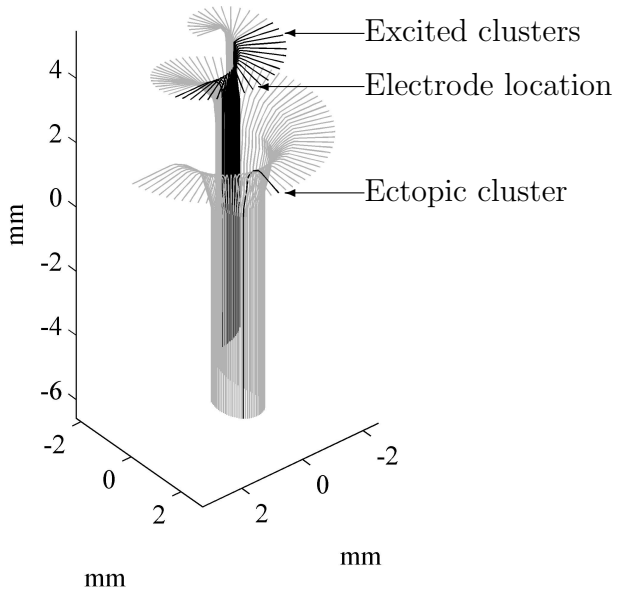

Figure 4.2: Excitation in an ectopic neural cluster in the basal turn by means of ephaptic contribution from excited neurons in the middle turn. The figure shows all the modelled fibre clusters (light grey), the ectopic cluster (dark grey) and the excited fibre clusters contributing to ephaptic excitation (black).

The number of myelinated axons per millimeter length of the cochlear duct varies considerably from base to apex. In this model a density of 300 fibres per millimeter in the basal turn and 1400 fibres per millimeter in the middle turn was used. Rosbe et al. (1996) suggested three types of spiral ganglion cells: large, intermediate and small, where the large and intermediate cells were subtypes of the classic Type I spiral ganglion cell and the small cell was consistent with the classic Type II ganglion cell. Only morphologic variables, i.e. soma diameter and axon diameter, were used. The maximal cross-sectional area of the cell body was less than 200 μm^2 for small cells,

Table 4.1: Morphological parameters.

		Basal turn	Middle turn	Upper middle turn
Large	Soma diameter (μm)	25	28	27
	Axon diameter(μm)	2.4	3.0	3.2
Intermediate	Soma diameter (μm)	22	24	24
	Axon diameter(μm)	2.5	2.6	2.8
Small	Soma diameter (μm)	14	14	15
	Axon diameter(μm)	1.8	1.8	2.3

approximately 400-650 μm^2 for intermediate cells, and 550-900 μm^2 for large cells. The values chosen for this model are shown in Table 4.1.

The axon diameter for large and intermediate cells (approximately 2-5 μm) is similar but the axon diameter of small cells (approximately 1-2 μm) is distinctly smaller than that of both intermediate and large cells. This suggests that large and intermediate cells are subtypes of the Type I spiral ganglion cell. According to Rosbe et al. (1996) large cells comprised 49% of the total population, intermediate cells 38% and small cells 13%. Each cluster of nerve fibres in the volume conduction model was modelled using this composition of nerve fibres together with the density mentioned above. As an example, a cluster of fibres in the middle turn consisted of 137 large cells, 106 intermediate cells and 36 small cells.

4.3.2 Setup for prediction of ephaptic excitation

4.3.2.1 Simulation of ephaptic response in a two-dimensional model using a neural model incorporating a noise term

The objective was to determine whether ephaptic excitation is significant in the presence of membrane noise. Simulations were performed to predict ephaptic excitation of a single straight fibre with coincidental location of active neurons to correspond with the model setup presented in Chapter 3. Results were calculated as the number of active fibres required to excite a target fibre at a specific distance from the active fibres. The same pulse was used as in the calibration of the scaling factor k_{noise} in Figure 4.1, i.e. a cathodic/anodic biphasic pulse with amplitude 49.1 dB re 1μA (or

285.1 μA) and phase duration 100 μs. Since noise was included, the model was no longer deterministic and a 50% firing rate was chosen as the excitation threshold of the target fibre. The electrode was located 0.080 cm above the dendritic terminal to correspond with the set up for calibrating the noise parameter.

4.3.2.2 Simulation of ephaptic response using a three-dimensional cochlear geometry

The objective was to investigate the ephaptic response using the compound model, i.e. to determine the effect of the three-dimensional geometry of the cochlea on ephaptic excitation. Both the deterministic and stochastic neural models were used in these simulations to determine whether trends in the results are as a result of the stochasticity in the neural model or as a result of the three-dimensional orientation of the fibres relative to one another in the compound model.

Excited fibres in the middle turn were chosen as the source of ephaptic contribution because of the higher neuron density, which should yield the largest ephaptic effect. Simulations were then performed to investigate excitation in a neural cluster in the basal turn by means of ephaptic contribution from excited neural clusters in the middle turn (see Figure 4.2).

A medially located electrode neighbouring middle-turn neuron cluster 83 (at approximately 18 mm along the length of the basilar membrane) was chosen to inject the stimulus current. The cluster in the basal turn with the locally lowest threshold (and thus the highest probability of ectopic excitation) was cluster 26 (at approximately 6 mm along the length of the basilar membrane).

In the range of excitation, simulations were performed at cluster level, i.e. a single cluster resolution of ectopic contribution was implemented as opposed to a single fibre resolution in the two-dimensional model described above. Simulations were carried out for two different pulses; one biphasic cathodic/anodic pulse with phase duration 100 μs and one monophasic anodic pulse with duration 200 μs. Because of the inclusion of the noise term in the neural model, simulations were performed over a stimulus interval. The interval ranged from 72 to 75.8 dB (re 1 μA) for the biphasic pulse and 65.1 to 73.3 dB (re 1 μA) for the monophasic pulse, i.e. from low to high probability

of excitation of cluster 26. That means that ephaptic excitation could be investigated in the vicinity of the threshold stimulus intensity. Since spatial extent of excitation is a function of stimulus intensity, the neuron clusters involved in contributing to the source of ephaptic excitation had to be determined as a function of stimulus intensity. The spatial spread of the neural clusters comprising the source of ephaptic excitation is shown in Figure 4.3.

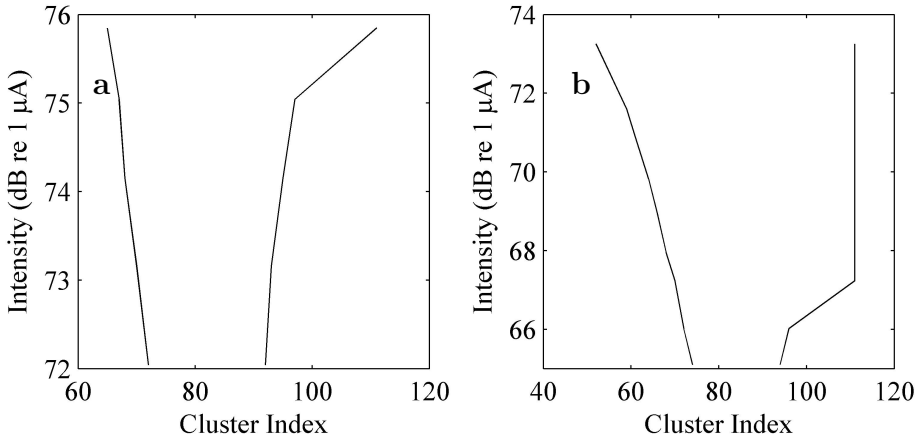

Figure 4.3: Range of excitation for biphasic pulse (a) and monophasic pulse (b). For the monophasic pulse the range reaches the limit of the model (i.e. cluster 111) at approximately 67 dB (re 1 μA).

When calculating the extracellular potential at the target fibre, the ionic currents from every compartment in each active fibre within the range of excitation is included and added to the stimulus. The scaled voltages from the volume conduction model described above corresponding to the active fibres were added to the effect of the stimulus. The capacitive current is negligible because of the small surface area of the nodes and the myelination of the internodes. The scaling was carried out by dividing the applied stimulus used in the neural model with the volume of the source and multiplying with the current density used in the volume conduction model. The current density was 1 A mm^{-3} and the volumes of the modelled electrode and nodes of Ranvier were 4.2995×10^{-2} mm^3 and 1.666528×10^{-10} mm^3 respectively. So, by multiplying with the calculated ionic currents for the nodal voltages and a pulse for the stimulus, the extracellular potential at the target neuron was obtained.

4.3.2.3 Simulation of ephaptic response to different pulse shapes

As mentioned above, biphasic and monophasic pulses were used to investigate the effect of pulse shape on ephaptic excitation in the three-dimensional compound model and the stimulus intervals over which the simulations were carried out were chosen to range from a low to high probability of excitation. For both including and excluding the ephaptic effect, 500 simulations for each stimulus value for both the biphasic and monophasic pulses were performed.

4.3.3 Verification of model

Two tests were performed to verify the compound model by investigating the decay of the electric potential in the compound model and comparing it with the analytical decay.

4.3.3.1 Decay along the basilar membrane

The first test investigated the decay of the stimulus along the basilar membrane. In the compound model the electrode is located close to cluster 85 and the potential at the first peripheral node (PN) in each cluster, from cluster 85 and onwards, was simulated. The stimulating current was set to $I_{St} = 2.376$ mA and it was scaled and multiplied to the voltage vectors (V_V) from the volume conduction model as explained above.

$$V_e = \frac{I_{St}}{0.042995} \cdot V_V \tag{4.2}$$

The analytical result was calculated for the same distances and a point source close to the first PN in cluster 85 by

$$V_e = \frac{\rho \cdot I_{St}}{4\pi\sqrt{x^2 + z^2}} \tag{4.3}$$

where $\rho = 0.3$ kΩ cm is the extracellular resistivity (from Rattay et al. (2001)), z is the vertical distance from point source to the first PN in cluster 85 and x is the horizontal distance along the basilar membrane measured from cluster 85. The point source was set at the distance $z = 0.315$ cm and the results are shown in Figure 4.4 where the decay is expressed in dB/mm. The intensity I is calculated by

$$I = 20 \cdot \log_{10}\left(\frac{V_e}{V_{e,0}}\right) \tag{4.4}$$

where $V_{e,0} = 1$ mV.

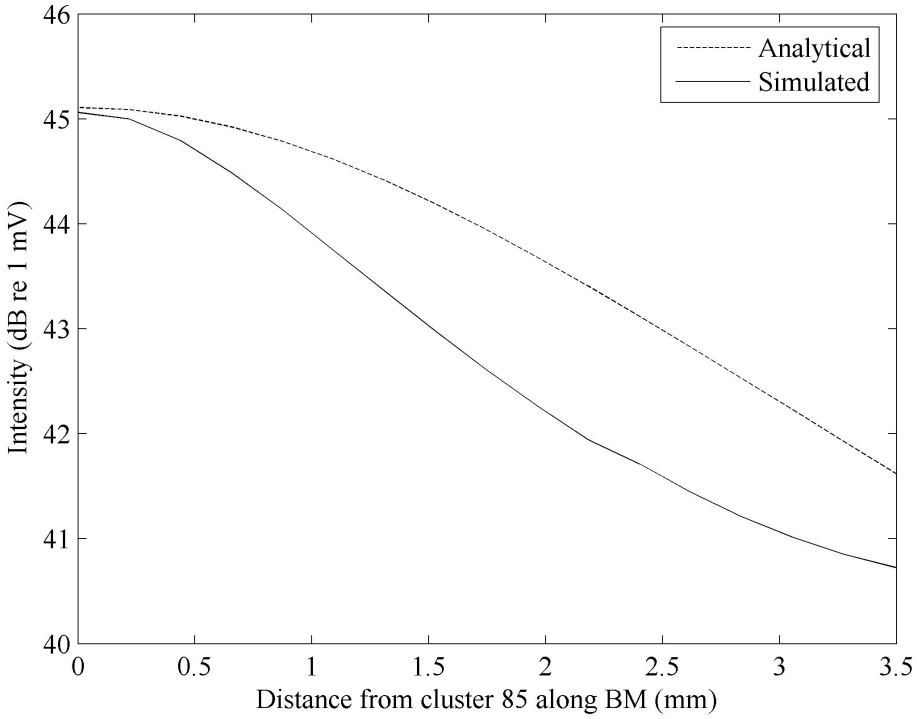

Figure 4.4: The intensity as a function of distance of a stimulus along the basilar membrane for both the compound model and an analytical decay in a medium with constant resistivity.

The simulated intensity has a steeper decay than the analytical, which thereby is larger. For smaller values of the vertical distance (z) between point source and first PN of cluster 85, the analytical solution would be even larger. The average decay over the interval was found to be approximately 1.00 dB/mm for the analytical result and 1.24 dB/mm for the simulated result. Bruce et al. (1999) used a decay of 0.5

dB/mm for monopolar stimulation and Kral et al. (1998) reported on a decay of 3.1 dB/mm for monopolar stimulation so the average decay in Figure 4.4 corresponds with reported decay constants.

4.3.3.2 Cross-turn decay

The second test investigated the decay of the potential caused by ionic currents in an excited fibre. The ionic currents for an excited fibre in cluster 85 were calculated and the resulting potential at the first PN in the ectopic bundle was simulated in order to see each excited node's contribution to the first PN in the ectopic bundle. As in the first test, the current was scaled (but with a different scaling factor) and multiplied with the voltage vectors to get the potential.

$$V_e = \frac{I_{Ion}}{1.666528 \times 10^{-10}} \cdot V_V \tag{4.5}$$

For the analytical electric potential a constant resistivity was assumed (the same as in the first test) and the potential was calculated by

$$V_e = \frac{\rho \cdot I_{Ion}}{4\pi r} \tag{4.6}$$

where r is a vector containing the distances between the first PN in the ectopic fibre and all nodes in the excited fibre. The results are again depicted in dB (re 1 mV) and are shown in Figure 4.5.

The negative intensity in Figure 4.5 is a direct result of the low electric potential at the target fibre caused by excited nodes (the largest value is about 55 nV) and that the intensities are relative to 1 mV.

The decay of the analytic solution is 2.06 dB/mm. The shape of the simulated result is probably an artefact of the mesh resolution of the volume conduction model and because of the shape of the simulated result, two average decays were calculated (from the inclinations of the two straight lines plotted in Figure 4.5). The cross-turn decay in the compound model is between 2.56 and 4.09 dB/mm

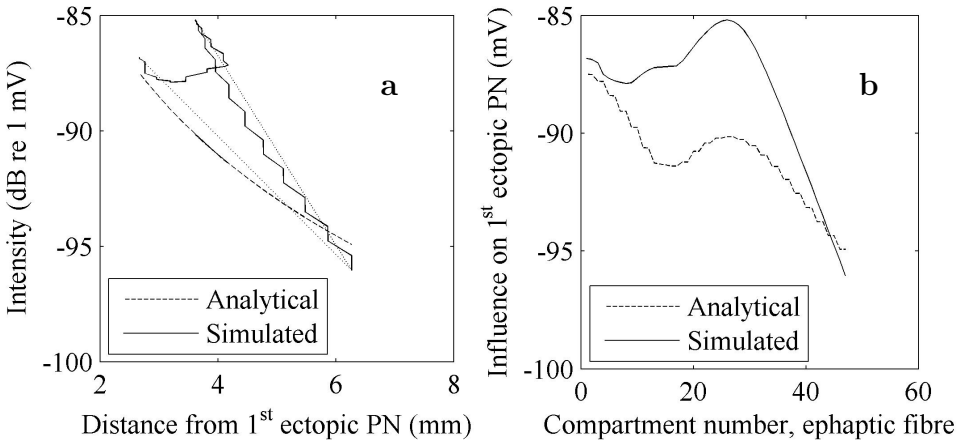

Figure 4.5: Effects of ionic currents on the 1st ectopic PN. Figure (a) shows the intensity as a function of distance and figure (b) the intensity as a function of compartment number of the single fibre model.

As expected does the simulated potential not fall on a perfectly decaying graph since the medium in a cross-turn stimulation is not homogeneous and thus does not have a constant resistivity. However, the difference between the simulated and analytical results in both tests is small and it is therefore concluded that the model has been verified.

4.4 RESULTS

4.4.1 Influence of inclusion of a noise term in the neural model

Figure 4.6 shows the number of active neurons required to ephaptically excite a target neuron at a specific distance from the active neurons' location. A 50% firing efficiency was defined to decide the number of fibres needed for the results of the stochastic neural model.

The figure also shows the results, including and excluding the stimulus, of a deterministic model (M2). When the stimulus is excluded the difference in the results predicted by the deterministic and stochastic models is small, but when the stimulus is included

the difference is more pronounced. At smaller distances to the target neuron (approximately 221.1 μm for the deterministic model and 250 μm for the stochastic model) the electrode stimulus significantly influences excitation of the passive neuron. Above these distances ephaptic excitation starts to contribute to the spread of excitation and its effect on the stochastic model is more pronounced. Since the stochastic model allows for a larger fibre separation, the results suggest that noise has a significant effect on threshold and it could sensitize the target neuron to enhance ephaptic excitation. At small distances the graphs excluding the stimulus show exponential growth which is in correspondence with the results presented in the previous chapter.

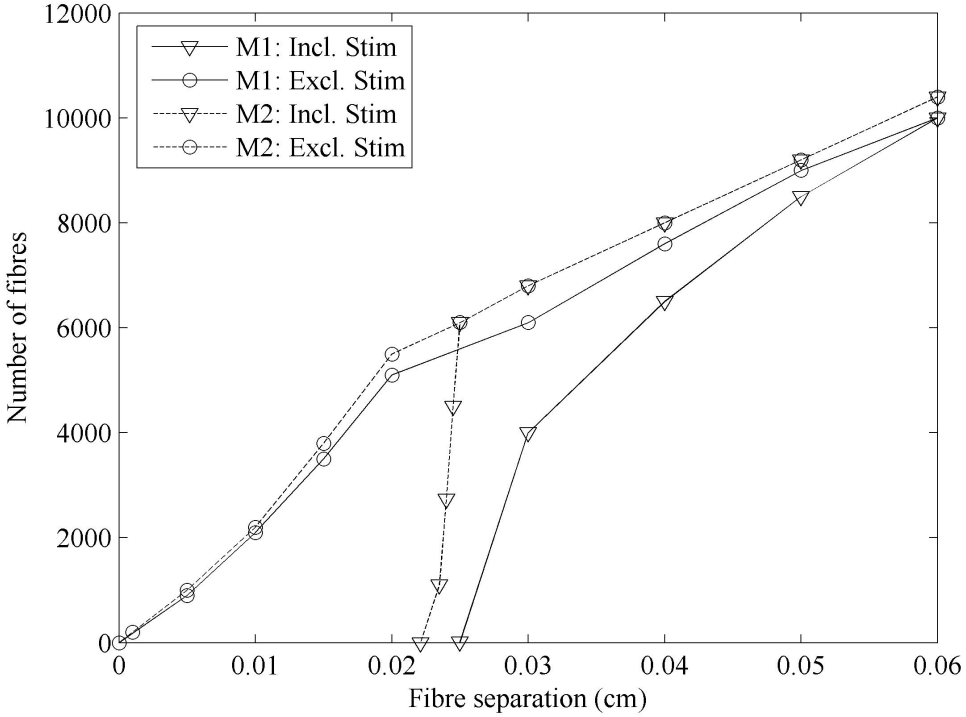

Figure 4.6: M1 is the result of the stochastic neural model and M2 the deterministic model. The influence of noise is significant when the stimulus is included.

4.4.2 Influence of three-dimensional model geometry and pulse shape

When the neural model is integrated with a volume conduction model to form a three-dimensional compound model of ephaptic excitation, the neurons do not coincide in

space as is the case for the two-dimensional model. The neurons are distributed along the length of the cochlea in a three-dimensional fashion. Results are calculated as the probability of ephaptic excitation of an ectopic fibre in the basal turn, caused by excited fibres in the middle turn of the cochlea.

Figures 4.7a and b show the probability of excitation caused by a biphasic pulse using the deterministic and stochastic models respectively. It is evident that the ephaptic contribution also has a significant effect when including a three-dimensional geometry. A comparison between the results predicted by the deterministic model and the stochastic model further suggest that the ephaptic effect is increased by the inclusion of noise in the neural model. When the ephaptic effect is included the threshold is decreased by 0.3 dB in the deterministic model while the 50% discharge probability in the stochastic model is decreased by approximately 1.64 dB.

Figures 4.8a and b show the probability of excitation caused by a monophasic pulse using the deterministic and stochastic models respectively. Both models predict that the ephaptic contribution increases the probability of excitation even more than for the biphasic pulse. The ephaptic effect decreases the threshold in the deterministic model by 3.59 dB and the 50% discharge probability in the stochastic model by approximately 3.57.

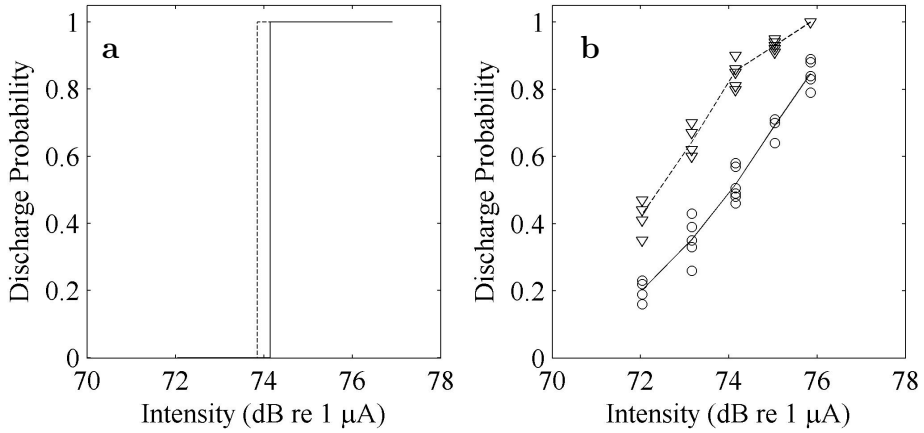

Figure 4.7: Probability of ectopic excitation for a biphasic pulse. Figure (a) shows the result of a deterministic model where the dashed line includes the ephaptic contribution and the solid line excludes it. Figure (b) includes noise for the same intensity interval. Each triangle represents 100 simulations when the ephaptic contribution is included. Each circle represents 100 simulations when the ephaptic contribution is excluded. The dashed and solid lines are the mean averages of 500 simulations per stimulus.

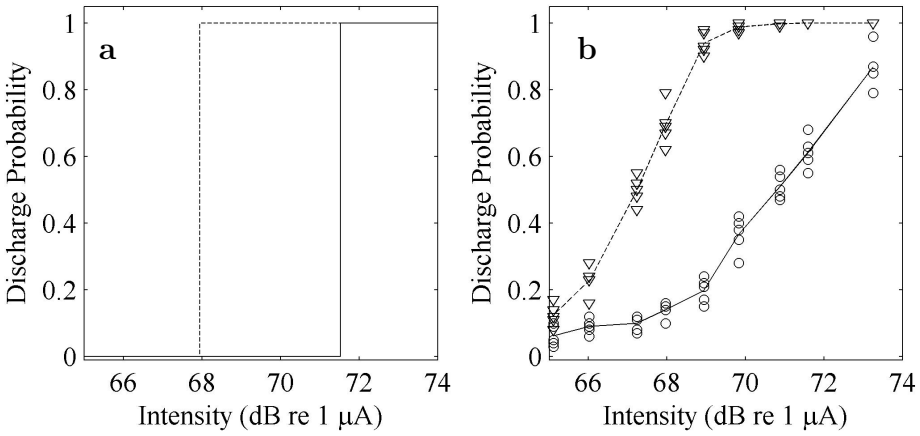

Figure 4.8: Probability of ectopic excitation for a monophasic pulse. Figure (a) shows the result of a deterministic model where the dashed line includes the ephaptic contribution and the solid line excludes it. Figure (b) includes noise for the same intensity interval. Each triangle represents 100 simulations when the ephaptic contribution is included. Each circle represents 100 simulations when the ephaptic contribution is excluded. The dashed and solid lines are the mean averages of 500 simulations per stimulus.

There are significantly qualitative differences between the ephaptic influence on the probability of excitation in the biphasic stimulus case and the monophasic stimulus case. First, noise has a large impact on threshold for a biphasic pulse, while it seems to have less impact for a monophasic pulse. The ephaptic effect has a large influence for both pulses but is most significant for a monophasic pulse. An explanation could be that threshold is lower for this pulse which means that the ephaptic currents constitute a larger part of the total stimulus. Furthermore, the spread of excitation is wider which means that more fibres contribute in the monophasic case compared to the biphasic case (see Figure 4.3).

4.4.2.1 Degeneration and statistical analysis

Simulations were performed with different neural survival rates in order to determine the significance of ephaptic excitation in neural degeneration. Simulations were carried out for 60%, 65%, 70%, 75%, 90% and 100% survival rate for a biphasic stimulus with amplitude 4550 μA. For each case, five simulations were carried out with 100 iterations per simulation (see Table 4.2).

T-tests were then performed with the non-ephaptic result and each degenerated dataset. All t-tests were one-tailed since adding the ephaptic currents to the second dataset shifted the direction of the mean values. Furthermore, the type of the tests was type 3, i.e. a two sample test for unequal variance.

Table 4.2: Discharge probabilities for stimulus 4550 μA for different neural survival rates. Each probability is a result of 100 iterations. The column to the left shows the discharge probability excluding the ephaptic effect. The top row (columns 2-7) states the neural survival. One-tailed t-tests of type 3 were carried out for the dataset excluding EE and each of the degenerated datasets.

No EE	100%	90%	75%	70%	65%	60%
0,43	0,67	0,54	0,51	0,44	0,41	0,45
0,26	0,62	0,56	0,49	0,38	0,5	0,36
0,35	0,6	0,58	0,44	0,41	0,41	0,39
0,33	0,7	0,55	0,42	0,39	0,35	0,28
0,39	0,62	0,55	0,53	0,48	0,33	0,41

The resulting P-values are plotted against the neural survival rates in Figure 4.9. For P-values above 0.05, the assumption is that the two datasets are not significantly different. The figure shows that the P-value is 0.05 at approximately 70% neural survival.

Another possible consequence of the ephaptic effect is that it could influence the time and/or site of excitation of the target fibre which could, in turn, influence response properties (van den Honert and Stypulkowski, 1987; Cartee et al., 2006), such as the refractory time and the summation time (Cartee, 2006). The tree-dimensional model was used to investigate this phenomenon. Two nodes of Ranvier were chosen in the target fibre: the second peripheral node (PN) and the second central node (CN). The time of excitation of these nodes were predicted for both pulse shapes and Figure 4.10 shows the difference in latency between excitation with and without ephaptic excitation. In the figure, Δt_P and Δt_C are the differences between the ephaptic and non-ephaptic time of excitation the second PN and the second CN respectively, i.e. $\Delta t_i = t_{EE,i} - t_i$.

The difference in latency is at most 1.3 ms for the biphasic pulse and -0.36 ms for the monophasic pulse and occurs for both pulses at threshold. For higher stimuli the difference approaches zero. Latency decreases with increasing stimulus (Rubinstein, 1995; Miller et al., 1999) and it is surprising that the result for the biphasic pulse close

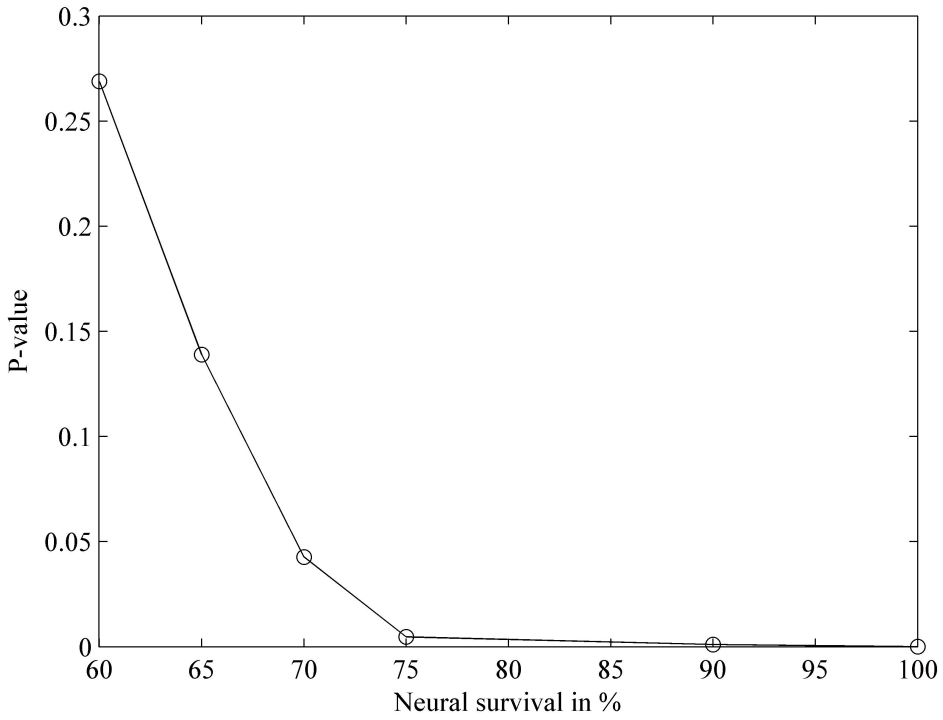

Figure 4.9: Neural survival vs. P-values. At approximately 70% neural survival the P-value is 0.05.

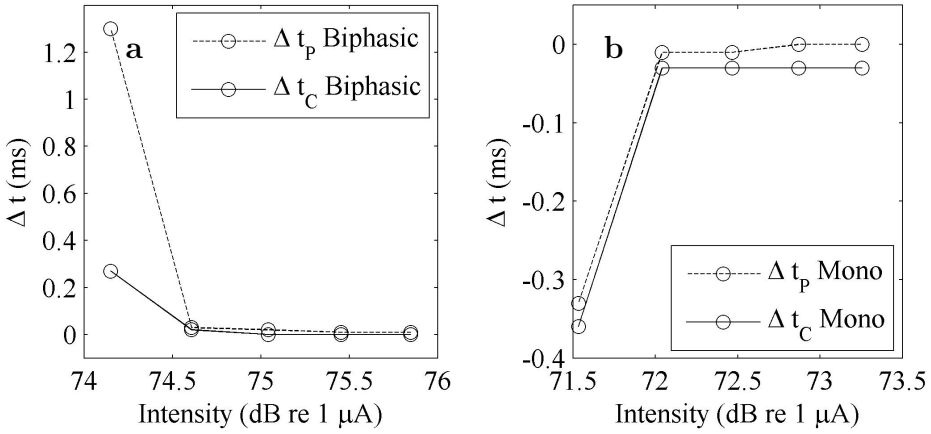

Figure 4.10: Difference in time of excitation for second PN and second CN for biphasic (a) and monophasic pulse (b).

to threshold is positive indicating that the latency is larger when the ephaptic effect is included. The results for the monophasic pulse at threshold are as expected negative. The shift in latency is only significant at threshold and for larger intensities it is either zero or close to zero.

4.5 DISCUSSION

When comparing the results from the stochastic two-dimensional model with the deterministic model, the stochastic model allows for a larger separation between active fibres and the target fibre. The addition of a noise term to the neural model seems to sensitize the target neuron for ephaptic excitation. This is in correspondence with literature which reports that noise enhances both detection (Zeng et al., 2000) and discrimination (Behnam et al., 2003) of sound. Sensitization of the target neuron could be a result of stochastic resonance. Since internal noise exists in normal auditory nerve fibres (Zeng et al., 2000) and there is a significant difference between the results of the deterministic and the stochastic two-dimensional models, it is concluded that noise should be included in models of auditory nerve fibres dealing with thresholds.

According to the results presented in this chapter, the influence of ephaptic contribution depends to a great degree on the pulse shape. The ephaptic effect was significant for both pulses used in this study, but the effect was the largest for the monophasic pulse. This pulse also seemed to decrease the effect of the noise in that ephaptic effect was large in both the deterministic and stochastic model. An explanation for the larger ephaptic effect is that monophasic pulses decrease threshold compared to biphasic pulses, since the second phase of a pulse can reduce the strength of the first phase due to membrane integration of the externally applied current (van Wieringen et al., 2005). The ephaptic contribution will then constitute a larger part of the total stimulus. Furthermore, the spread of excitation is wider so more fibres contribute to the ephaptic excitation. Reducing the threshold is good for two reasons: it reduces power consumption and increases spatial selectivity (van Wieringen et al., 2005). For this reason could pulse shapes that reduce thresholds lead to better current steering strategies. Monophasic current pulses are more desirable since they reduce the threshold, but since they are not charge-balanced they are for safety reasons not used with human subjects (van Wieringen et al., 2005). Pseudomonophasic pulses, i.e. biphasic

pulses of which one of the two phases has a different duration and amplitude, have been suggested as a possible solution (van Wieringen et al., 2005) which would make the ephaptic contribution a significant factor.

Ephaptic contribution has an effect on latency at threshold. The results in Figure 4.10 show that the difference in latency is at most 1.3 ms for the biphasic pulse and -0.36 ms for the monophasic pulse. Latency decreases with increasing stimulus (Rubinstein, 1995; Miller et al., 1999). Rubinstein (1995) showed an 84 μs decrease in latency for a 1.6 pA increase in stimulus. That is a ratio of 5.25×10^7 s/A. In comparison, the width of excitation at threshold for the biphasic pulse is 28 clusters resulting in a maximum total ephaptic nodal current of approximately 0.19 μA. That yields an increase in latency of 6482 s/A. The corresponding measurement for the monophasic pulse yields a maximum total ephaptic nodal current of approximately 0.35 μA caused by 53 excited clusters which render a decrease in latency of 2400 s/A. So even though it is surprising that the result for the biphasic pulse is positive, implying a larger latency when ephaptic influence is included, the shifts in latency for both pulses are very small and occur only at threshold. However, since latency is a temporal characteristic of a pulse it should be included in neural models to accurately describe the excitation behaviour of a neuron when dealing with intensities close to threshold.

The three-dimensional geometry of the cochlear volume provides a suitable environment for ephaptic excitation to occur among nerve fibres innervating different turns of the cochlea. Ectopic excitation will therefore affect pitch perception of cochlear implant subjects. Although no direct experimental assessment of ectopic excitation is found in literature, a number of reports can be interpreted as evidence for the ephaptic effect. Several studies show that one or more electrodes are frequently indiscriminable with regard to pitch (Henry, McKay et al., 2000; Throckmorton and Collins, 1999; Busby, Whitford et al., 1994), that reversals in place-pitch ordering on some electrodes in some subjects occur (Shannon, 1983; Busby, Whitford et al., 1994; Nelson, Van Tasell et al., 1995) and that instances were seen of better electrode ranking in the apical half of the electrode array than in the basal half and vice-versa (Nelson, Van Tasell et al., 1995). Mens, Brokx et al. (1995) reported that one of their subjects experienced complex pitch sensations on three of his apical electrodes.

Di Nardo, Scorpecci et al. (2010) performed a study on mismatch between electrode assigned frequencies and perceived pitch. In this study subjects with adequate residual

hearing in one ear was asked to match acoustic pitch to pitch elicited by anyone of their cochlear implant electrodes. All subjects presented some degree of mismatch between the acoustic frequencies assigned to their implant electrodes and the pitch elicited by stimulation of the same electrode, with high between-individual variability. The authors found that array insertion depth could not account for the highly irregular, subject-dependent mismatch observed for middle and high frequencies, which patients allocate to electrodes. They speculated that some of their findings could be explained if a single electrode could activate different sites of the modiolar portion of the acoustic nerve at the same time. As was shown in this chapter, ephaptic excitation facilitates activation of neural populations transmitting pitch information in different tonotopic regions and could therefore provide an explanation for the variability in the data.

When evaluating spread of excitation using ECAPs, Goffi-Gomez, Abdala et al. (2010) found a large neural overlap for most electrodes. It was speculated that a possible explanation could be excitation of remote neurons or few viable local neurons. This speculation fits the ephaptic excitation model in that it seems that excitation is not limited to a localized population in the vicinity of the electrode, i.e. there is evidence for ectopic excitation. Furthermore, the perception that is elicited could be influenced by the neural survival pattern, i.e. the ectopically excited region could dominate the perception if neural survival at the target site is poor.

McKay, McDermott et al. (1996) reported that at least two to three dimensions are required in a multidimensional scaling analysis of their pitch ranking experimental results to describe the perceptual space of single electrode stimuli. The first dimension was arbitrarily aligned to correspond with the apical-to-basal position of the electrodes, i.e. along the tonotopic axis while the interpretation of the second and third (where applicable) dimensions were not directly associated with physical quantities. The authors remarked that subjects definitely perceived two qualities in the stimuli that could be mapped to a two-dimensional space. In this context, ephaptic excitation of an ectopic neural population could provide a second percept that might have lead to the two-dimensional manifestation of the data in the scaling analyses.

4.6 CONCLUSION

The simple model presented in Chapter 3 showed the presence of an ephaptic effect and the amendments made to it in this chapter, to provide a more comprehensive computational and physiological description of the phenomenon, have verified the existence and importance thereof. Chapter 3 showed that spatial separation of source neurons result in significant ephaptic effect close to threshold but negligible effect at higher stimulus intensities. However, a deterministic model of an auditory neuron in an infinite, homogeneous, isotropic and resistive medium was utilized. This chapter expanded the neural model to include membrane noise and the volume conduction model to represent the morphology and morphometry of a mammalian cochlea. The inclusion of membrane noise in the neural model sensitized the target neurons for ephaptic excitation and it could be as a result of stochastic resonance. It was shown that the magnitude of the effect is dependent on pulse shape and pulse shapes designed to mimic monophasic stimulation would thus be more prone to ephaptic effects than biphasic pulse shapes. Since this chapter has shown that the ephaptic effect is more pronounced for monophasic pulses, it will have an even more significant effect when accurate current steering strategies resulting in accurate targeting of neural populations are employed in future cochlear implant technologies.

Chapter 5

COMPARISON OF POTENTIAL DISTRIBUTION IN HOMOGENEOUS AND HETEROGENEOUS MEDIA

Jönsson, R., Hanekom T., Hanekom J.J., 2010. Homogeneous versus heterogeneous representation of the neural volume in conduction models of the implanted cochlea, *submitted for publication*

5.1 OBJECTIVE

The models of field interactions thus far in the study have focused on the ephaptic effect alone. The neural models have been based on the cable equation and Hodgkin-Huxley membrane kinetics. This chapter presents a finite element method (FEM) approach to investigating field interactions in a bundle of central axons. The objective is to assess how the structure of the nerve, including the volumes and locations of individual fibres within the nerve bundle affects the potential field distribution and ephaptic interaction. The models are based on the neural morphology used for the single fibre model in Chapters 3 and 4. An excited node of Ranvier is simulated by applying ionic currents based on the HH system of equations. A finite element (FE) model is coupled with an active neuron model by using an FE model to calculate the

distribution of the extracellular potential and inserting this potential into a single fibre model to investigate the neural response. The direction of propagation, i.e. whether conduction is orthodromic or antidromic, is also investigated.

5.2 BACKGROUND

Several studies show how distributions of electrical fields vary in homogeneous and heterogeneous media. A modelling study used for molecular surgery presented by Daniels and Rubinsky (2009) show that heterogeneities have a substantial impact on the electrical field distribution and should not be neglected. A study on heterogeneous tissue conductivity in human brain modelling, presented by Wen and Li (2006), concludes that conductive heterogeneity within tissues has significant influence on the potential distribution in a human head model and should be included for accurate models of the brain's electrical activities. A modelling study of brain inhomogeneities including a boundary element method model presented by Huang et al. (1990) demonstrated significant effects on the magnitude of the electric potentials. Haueisen et al. (1997) presented a FEM study of the head and concluded that accurate knowledge of tissue resisitivities is required for accurate modelling of electric potential.

On a neural level, Miranda et al. (2007) showed that tissue heterogeneity can function as a mechanism for localized neural stimulation via applied electric fields for axons crossing internal boundaries. The potential distribution is dependent on the conductivity of the medium in which it appears and the compound model in the previous chapter took the anatomy of the cochlea into account and included a heterogeneous medium in that it implemented different conductivities in different materials. For a bundle of fibres, the homogeneity of the extracellular medium is also altered by the presence of the fibres. This chapter investigates to what extent the inclusion of the electrical properties of individual nerve fibres in a medium (instead of assuming a homogeneous neural volume) affects the potential distribution and the ephaptic interaction in a bundle of central axons.

The approach that was taken is the following: a 3D FE model of segments of central axons based on the morphology presented by Rattay et al. (2001) was implemented to investigate the effect of heterogeneity on the potential distribution. The FE model was

then coupled with a single fibre active neuron model to predict the neural response. The neural model uses the extracellular electrical potential distribution output from the FE model as input to investigate the neural response. Simulations were carried out with an anodic monophasic pulse. For comparison, the effects of biphasic pulses were also determined and, finally, the effect of a homogeneous medium on ephaptic excitation was investigated for a monophasic pulse.

5.3 METHODS

5.3.1 Description of axonal model

Models of a bundle of central axons, based on Rattay's neural model described in Chapter 3 and 4, were implemented in Comsol Multiphysics 3.5a. An axonal density of 10 fibres per 500 μm^2 was chosen, which is within the density interval from 122 to 233 nerve fibres per 0.01 mm^2 reported by Spoendlin and Schrott (1989). The modelled central bundle consisting of ten axons was implemented with the chosen density, i.e. all ten axons were placed in a circle with a radius of 12.6 μm. To increase computational efficiency only segments of complete fibres were implemented. For the model investigating how the presence of fibres affects the field distribution, the objective is to measure potential distributions in a cross-sectional plane perpendicular to the axons, so the implemented axonal segments can be kept short, thereby approaching a two-dimensional model. Each axonal segment consists therefore of one node and two internodes. Simulations of the decay of the potential caused by ionic nodal currents show that at the distance of an axonal internode (500 μm), the potential is only 2% of its initial magnitude. It is thereby concluded that implementing only segments of fibres is permitted. For the model investigating the ephaptic effect, the objective is to measure distributions along the axons so longer segments are needed. Each axonal segment in this model consists of five nodes and four internodes.

The standard human neuron presented by Rattay et al. (2001) and utilized in chapter 4 consists of six peripheral and 15 central nodes, one postsomatic and three presomatic compartments, soma and 21 internodes. The axonal model implemented in Comsol simulates the middle section of the central axon in Rattay's model, i.e. the third node in the axonal model investigating the ephaptic effect, represents the eighth central

node in Rattay's model.

The length of a node of Ranvier is 2.5 μm and the diameter of the unmyelinated segments of the central axon is 2 μm. The internodes in the central axon have the length 500 μm and are covered by 80 myelin layers. Setting the thickness of a myelin layer to 8.5 nm, the total internodal diameter becomes $2 \times 80 \times 8.5 \times 10^{-3}$ μm + 2 μm = 3.360 μm. The axonal segments are implemented as cylinders of different lengths and diameters. A segment consisting of one node and two internodes has the total length of 1002.5 μm and the segment consisting of five nodes and four internodes has the total length of 2012.5 μm. The long axonal segment is shown in Figure 5.1. The unmyelinated part of the axon is modelled as a homogeneous cylinder and four hollow cylinders, with inner diameter 2 μm, outer diameter 3.360 μm and length 500 μm, are added as the myelin sheaths at the location of the internodes. The nodes of Ranvier are then modelled as the resulting gaps between the internodes. The dimensions of the nodes and internodes are summarised in Table 5.1.

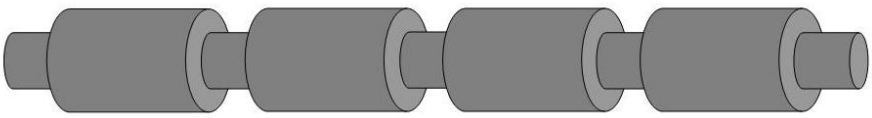

Figure 5.1: Long axonal segment consisting of five nodes and four internodes. The compartments are not drawn to scale.

Table 5.1: Lengths and diameters.

	Length (μm)	Diameter (μm)
Node of Ranvier	2.5	2
Internode	500	3.36

The infinite medium function in Comsol Multiphysics was used when applying boundary conditions for the model, simulating ground infinitely far away. The values for the

extracellular (σ_E) and intracellular conductivity (σ_I) were taken from Rattay et al. (2001) and set to $\sigma_E = \frac{1}{3}$ S/m and $\sigma_I = 2$ S/m.

5.3.2 Capacitive current

The maximum amplitude of the excited membrane potential is chosen for calculation of the membrane currents (see Figure 5.2). The capacitive current is given by

$$I_C = V_m \cdot \frac{dV_m}{dt} \tag{5.1}$$

Since $V_m = V_{m,max} \Rightarrow \frac{dV_m}{dt} = 0$, there is not a capacitive contribution to the membrane current.

5.3.3 Calculation of the membrane currents

Since the capacitive current is zero for the chosen membrane potential, the total ionic currents for an excited compartment is given by

$$I_{ion,HH} = D_C \cdot [I_{Na} + I_K + I_L] \cdot A \tag{5.2}$$

where A the area of the of the compartment and D_C is the channel density factor which is 1 for the soma and 10 for all other compartments to better represent human morphology (Rattay et al., 2001). The three ionic current densities in brackets are given by the standard HH equations

$$I_{Na} = g_{Na,max} \cdot m^3 \cdot h \, (V - V_{Na}) \tag{5.3}$$

$$I_K = g_{K,max} \cdot n^4 \, (V - V_K) \tag{5.4}$$

$$I_L = g_L \cdot (V_m - V_L) \tag{5.5}$$

The standard HH parameters are used, i.e.:

$$\begin{aligned} g_{Na} &= 120\ \text{k}\Omega^{-1}\text{cm}^{-2} \\ V_{Na} &= 115\ \text{mV} \\ g_K &= 36\ \text{k}\Omega^{-1}\text{cm}^{-2} \\ V_K &= -12\ \text{mV} \\ g_L &= 0.3\ \text{k}\Omega^{-1}\text{cm}^{-2} \\ V_L &= 10.6\ \text{mV} \end{aligned} \tag{5.6}$$

For a detailed overview of the HH model, see Addendum A. The currents are calculated for the maximal amplitude of the action potential. MATLAB is used to find the gating variables at V_{max} (see Figure 1) and the values are

$$\begin{aligned} m_{V_{max}} &= 0.9703 \\ n_{V_{max}} &= 0.5900 \\ h_{V_{max}} &= 0.2230 \end{aligned} \tag{5.7}$$

Transmembrane potential is measured to $V_m = 100$ mV and when inserting all the values the current densities becomes

$$\begin{aligned} I_{Na} &= -366.6870\ \mu\text{A cm}^{-2} \\ I_K &= 488.5720\ \mu\text{A cm}^{-2} \\ I_L &= 26.8200\ \mu\text{A cm}^{-2} \end{aligned} \tag{5.8}$$

5.3.4 Field investigation for axonal model

Point sources were applied to the axonal model to investigate how the location of the axons affected the potential field distribution. Eight point sources were inserted in a cross-sectional plane according to Figure 5.3. Since the locations of the fibres

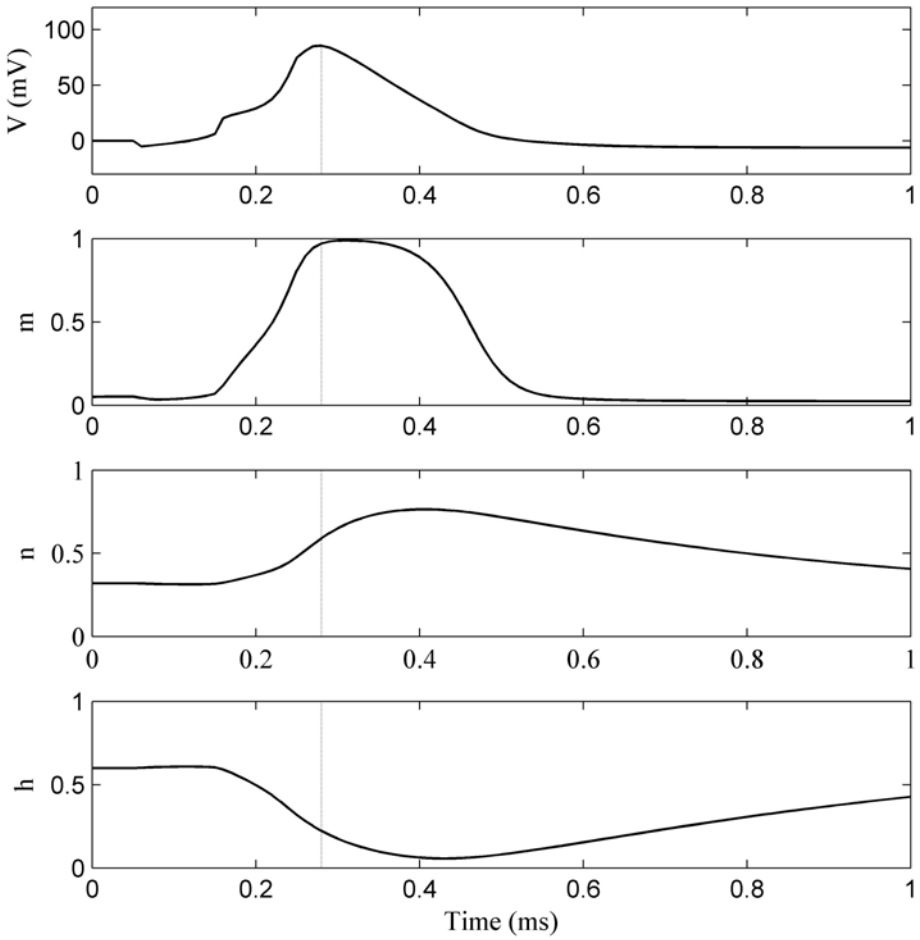

Figure 5.2: An action potential (top) and the three gating variables for the second peripheral node calculated for a heated Hodgkin-Huxley system. The vertical dotted lines indicate the time for the maximum potential and what the values for m, n and h are at this time.

were random within the volume, using eight point sources allowed for eight times more variation of the fibre positions relative to the source without regenerating the model. The potential distributions were then measured at the centre points in each fibre. Only one point source was simulated at a time. Simulations were carried out for both a homogeneous medium (providing a reference potential distribution) and for a heterogeneous medium containing a bundle of axons to investigate the influence of the axons on the potential field. For each simulation the active point source defined the centre of the model with a radius of 60 μm. The outer boundaries were implemented as infinite boundaries. An arbitrary current of 400 μA was applied to each point source. The results were then compared to the analytical distribution, which is calculated by

$$V_e = \frac{\rho I}{4\pi r} \tag{5.9}$$

where $\rho = 3$ Ωm and $I = 400$ μA.

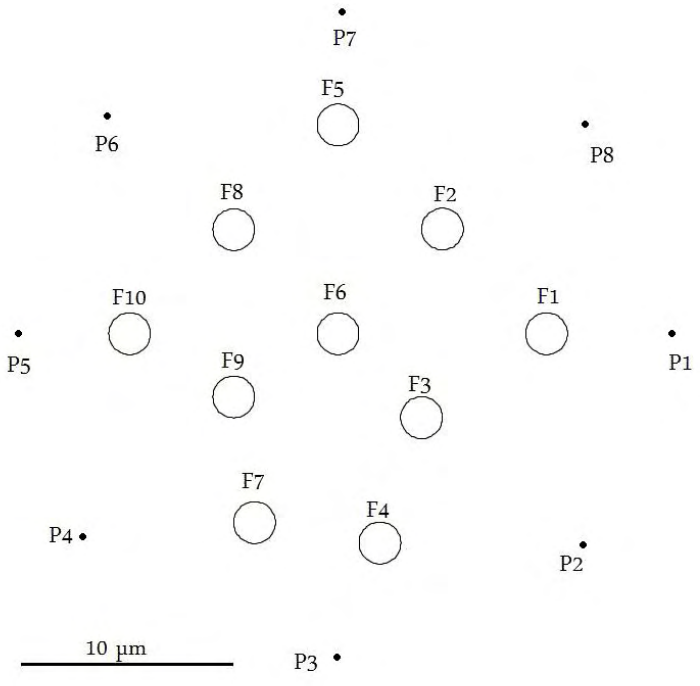

Figure 5.3: Overview of the model. The figure shows a cross section of a bundle of 10 fibres and 8 point sources. The point sources are marked P_i ,with $i \in [1;8]$ and fibres F_j with $j \in [1;10]$.

5.3.5 Investigation of the ephaptic effect in the heterogeneous axonal model

The potential distribution along each fibre as a result of stimulation with stimulus pulse applied to point source p1 was simulated in Comsol. The location and labelling of the 10 fibre sections were set up as shown in 5.4. Each fibre was a part of the central axon and consisted of 5 nodes and 4 internodes. The point source was located in the plane intersecting the central nodes of the axonal sections. An infinite medium condition was applied to the outer cylinder representing the boundary of the model domain. The potential was predicted at the centre points of each node and internode

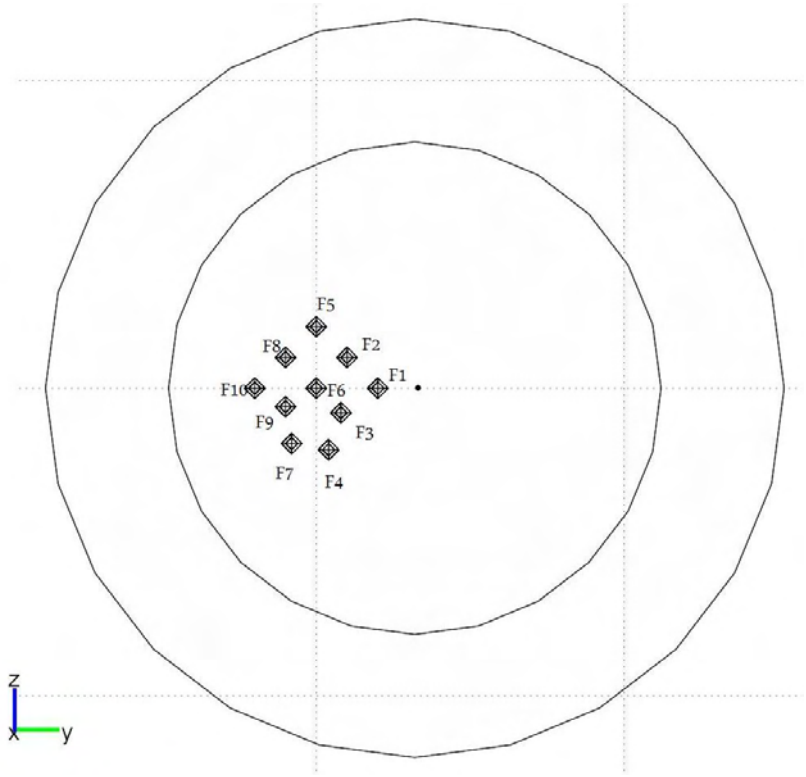

Figure 5.4: Location of fibres and point source.

and the results for a monophasic pulse are shown in Figure 5.5. The fibre segments were placed in the full fibre model and the node closest to the point source was located at central node 8 in the full model. This node was chosen since there are 15 central nodes and node number 8 is therefore in the middle of the axon. The measured data was then fitted to exponential curves in order to extrapolate the potential for the whole fibre (Figure 5.6). The extrapolated potential distributions were subsequently scaled

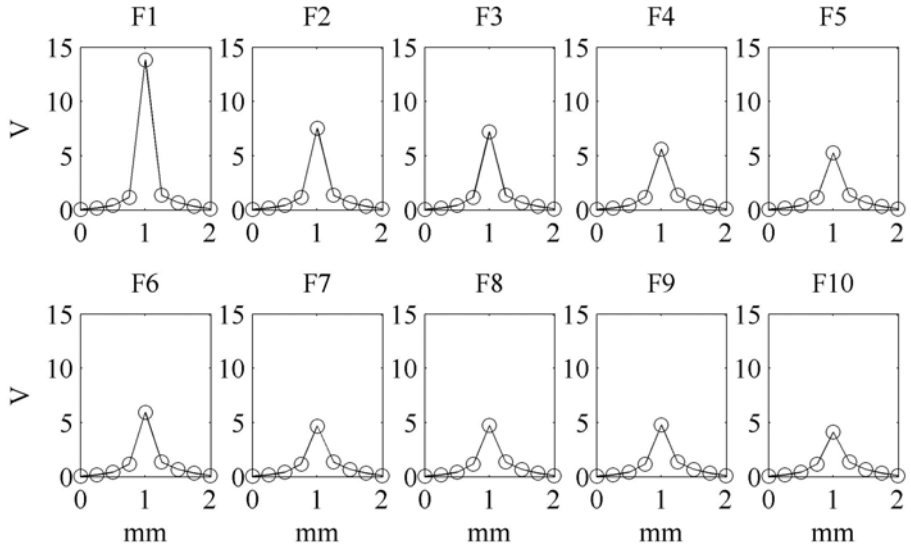

Figure 5.5: Measured distribution from point source along each fibre.

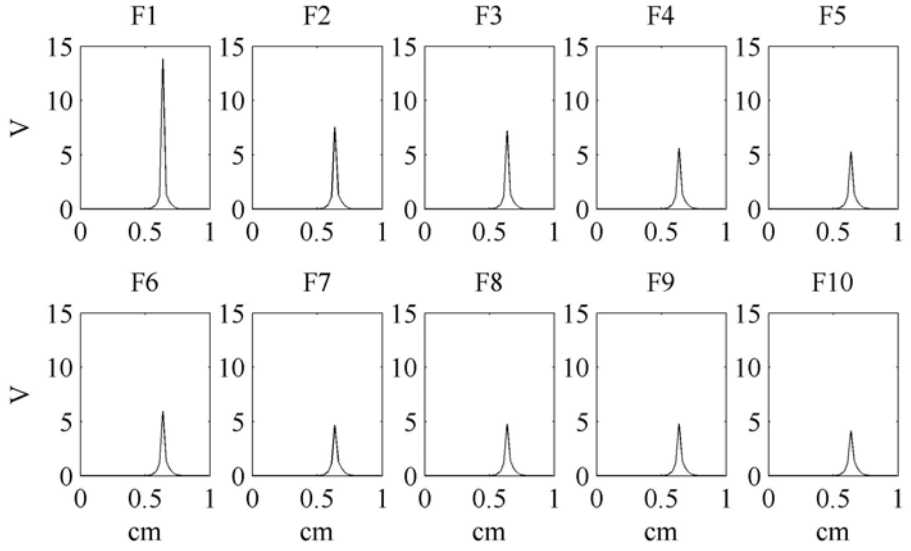

Figure 5.6: Measured and extrapolated potential distributions for whole fibres.

Table 5.2: Thresholds.

Fibre	Threshold (μA)
F1	4.5332
F2	7.2764
F3	7.5096
F4	8.7588
F5	9.0712
F6	8.4684
F7	9.6668
F8	9.6044
F9	9.5500
F10	10.2732

and used as input to the neural model in MATLAB to find the threshold currents iteratively. Scaling of the potential distribution to predict threshold currents was allowed since the volume conduction model was purely resistive.

5.3.5.1 Monophasic pulse

The potential distribution along each fibre as a result of stimulation with a 400 μA, 600 μs monophasic pulse applied to point source p1 was simulated. The results are listed in 5.2.

The arrangement of the fibres according to threshold (from low to high) becomes: F1, F2, F3, F6, F4, F5, F9, F8, F7 and F10. For each fibre that is to be investigated, the point source is set just below the threshold stated above. Then for each fibre in the region of excitation, an excited node is implemented by applying the current density J=14.8702 A/m^2. Table 5.3 shows the point sources and excited fibres.

5.3.5.2 Biphasic pulse

To investigate the effect of biphasic pulses on field interactions and their resulting excitation characteristics in heterogeneous and homogeneous media, fibre F8 was chosen since it displayed the largest ephaptic effect (approximately 55.9 μV at the compartment closest to the point source). The effect of both cathodic/anodic (C/A) and

Table 5.3: Currents and excited fibres.

Fibre to investigate	Point source (μA)	Excited fibres
F2	7.2760	F1
F3	7.2760	F1, F2
F6	8.4680	F1, F2, F3
F4	8.7584	F1, F2, F3, F6
F5	9.0708	F1, F2, F3, F6, F4
F8	9.5496	F1, F2, F3, F6, F4, F5
F9	9.6040	F1, F2, F3, F6, F4, F5, F9
F7	9.6664	F1, F2, F3, F6, F4, F5, F9, F8
F10	10.2728	F1, F2, F3, F6, F4, F5, F9, F8, F7

anodic/cathodic (A/C) pulses were investigated.

Two potential distributions were needed since the pulse now was biphasic. The anodic phase is the same as the monophasic simulation. The cathodic phase is just a mirroring of the anodic phase since the model is purely resistive and thus without any memory of the previous phase. Figure 5.7 shows the extrapolated potential distributions along F8 for the unscaled point source for both the anodic and cathodic phase.

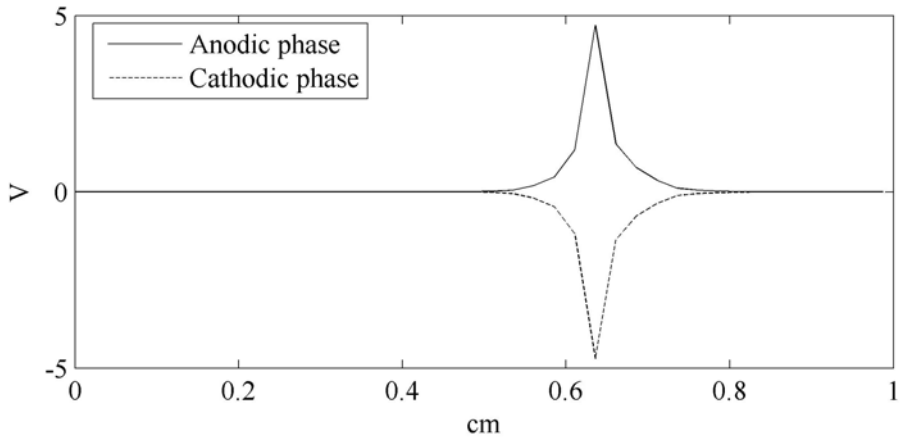

Figure 5.7: The anodic phase and the cathodic phase.

When investigating the ephaptic effect, nodal currents from seven fibres (i.e. F1, F2, F3, F6, F4, F5 and F9) were added. Furthermore, the excitation of the nodes constituting the ephaptic effect was assumed to occur during the second phase. This means that the ephaptic currents were added during the cathodic phase for an A/C pulse and during the anodic phase for a C/A pulse.

Table 5.4: Biphasic pulses.

Pulse	Phase duration (μs)	Threshold (μA)
C/A	100	1.888652
C/A	200	1.289368
A/C	100	1.784256
A/C	200	1.187756

Table 5.5: Threshold for F8.

Fibre	Threshold (μA)
F8	9.3632

Simulations for both short and long biphasic pulses with phase durations of 100 μs and 200 μs respectively, were carried out. In all cases the thresholds were determined by scaling the 400 μA point source and the result is shown in table 5.4.

5.3.5.3 Investigation of the ephaptic effect in the homogeneous axonal model

To provide a reference for the ephaptic effect in models that ignore heterogeneity, the effect of a homogeneous medium on ephaptic excitation was investigated. In the homogeneous medium the conductivity is 0.33 S/m. The threshold was found the same way as for the heterogeneous medium, i.e. with a test source of 400 μA to get the potential distribution along the fibre and a scaling factor to find the threshold. Simulations were performed for all fibres and fibre F8 was chosen for an in depth investigation. The result is shown in Table 5.5.

5.4 RESULTS

5.4.1 Field distribution

To evaluate the effect of homogeneity of the neural volume on the potential distribution throughout the model domain, Figures 5.8 and 5.9 show the simulated potential

distributions throughout the model domain from the eight individual point sources for both a homogeneous and heterogeneous medium. Using all eight sources instead of one (i.e. 80 data points instead of 10) provided sufficient data to present a good estimation of the potential decay as a function of distance and homogeneity. Figure 5.10 shows all the results for the two media as well as the analytical solutions for a homogeneous medium as reference. There is a notable difference between the homogeneous and heterogeneous cases for short distances. The result of the homogeneous medium corresponds with the analytical solution, whereas the potential in the heterogeneous medium is lower. For the measured distance closest to the source, the heterogeneous potential is about 84.6% of the homogeneous potential and for the largest measured distance they have almost converged and the heterogeneous potential is about 98.8% of the homogenous one.

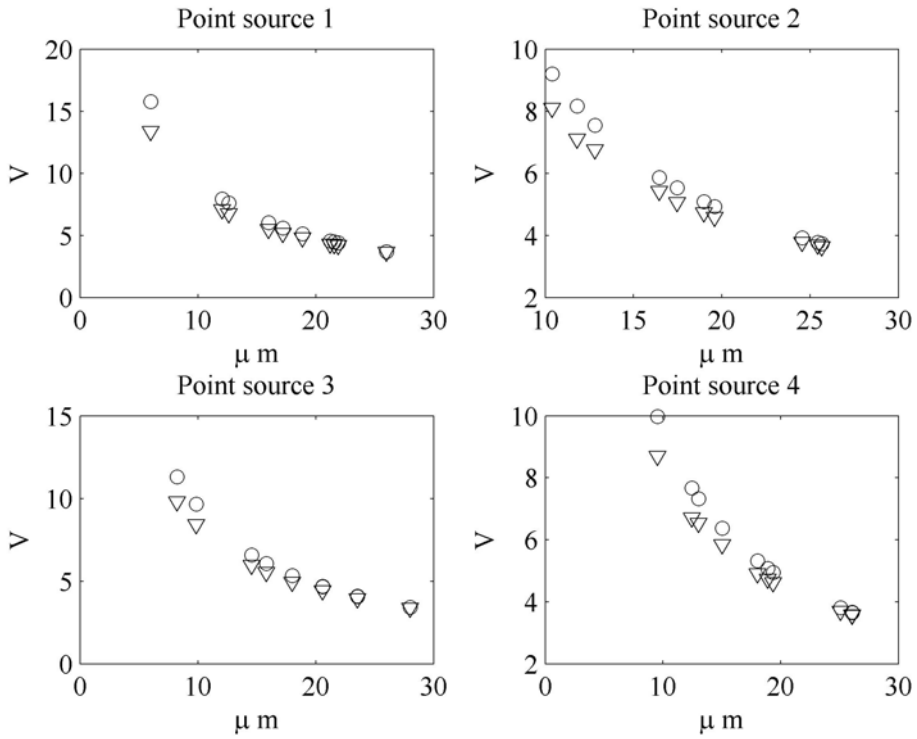

Figure 5.8: Simulated extracellular potential distribution for the first four point sources as a function of distance. The circles indicate simulations of a homogeneous medium and the triangles show the results for when axons are included.

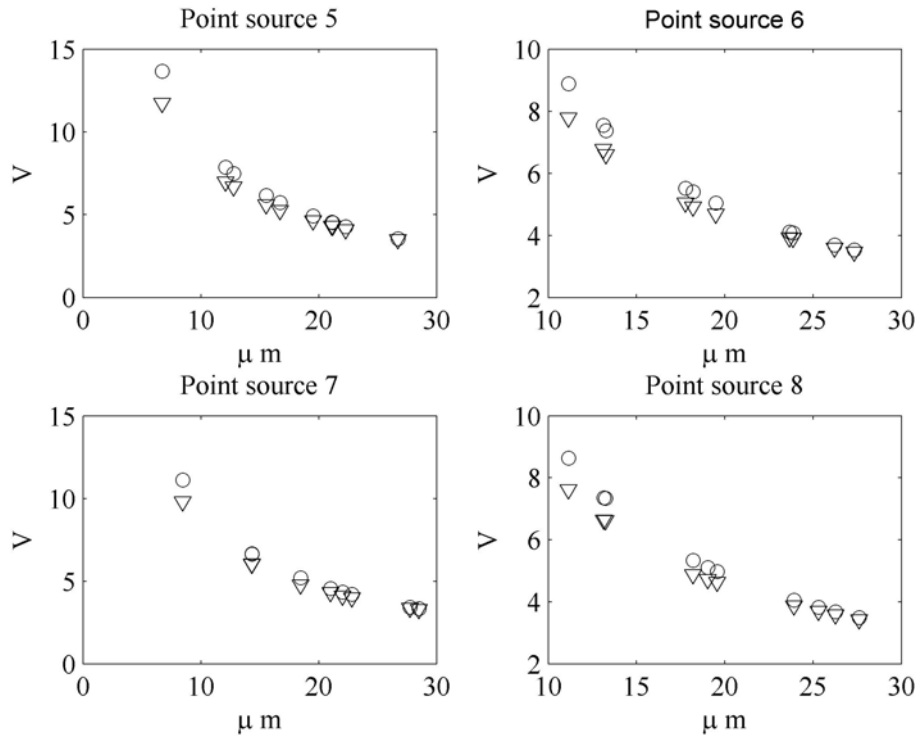

Figure 5.9: Simulated extracellular potential distribution for the last four point sources as a function of distance. The circles indicate simulations of a homogeneous medium and the triangles show the results for when axons are included.

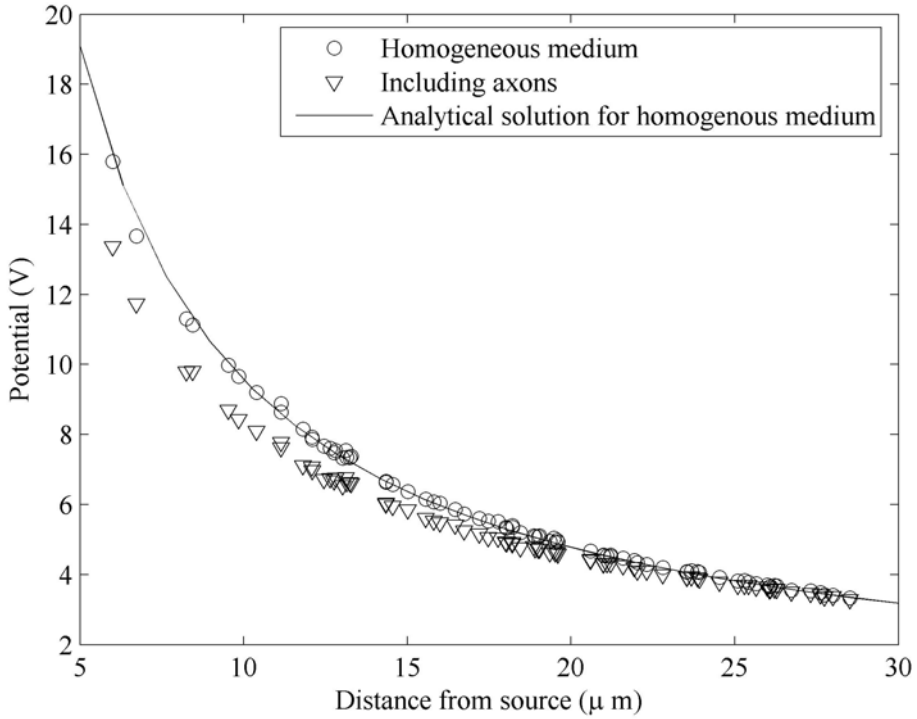

Figure 5.10: Potential distributions as a function of distance for both including and excluding the axons for all point sources as well as the analytical solution for a homogeneous medium. The result for the homogeneous medium coincides with the analytical solution.

5.4.2 Ephaptic effect

5.4.2.1 Monophasic pulse

Figure 5.11 shows the difference between the extracellular potential distribution when the stimulus contribution of the all the excited nodes is included in the stimulus (refer to Table 5.3) and the extracellular potential distribution as a result of the stimulus alone, i.e. the graphs show the ephaptic contribution to the potential distribution along each fibre. The effect varies notably with fibres F2, F3 and F6 at the low end and F7, F8 and F10 at the high end. The increase in ephaptic effect is expected since the number of excited nodes constituting the ephaptic effect increases. The effect is lowest at F2 with 6.4 μV and highest at F8 with 55.9 μV.

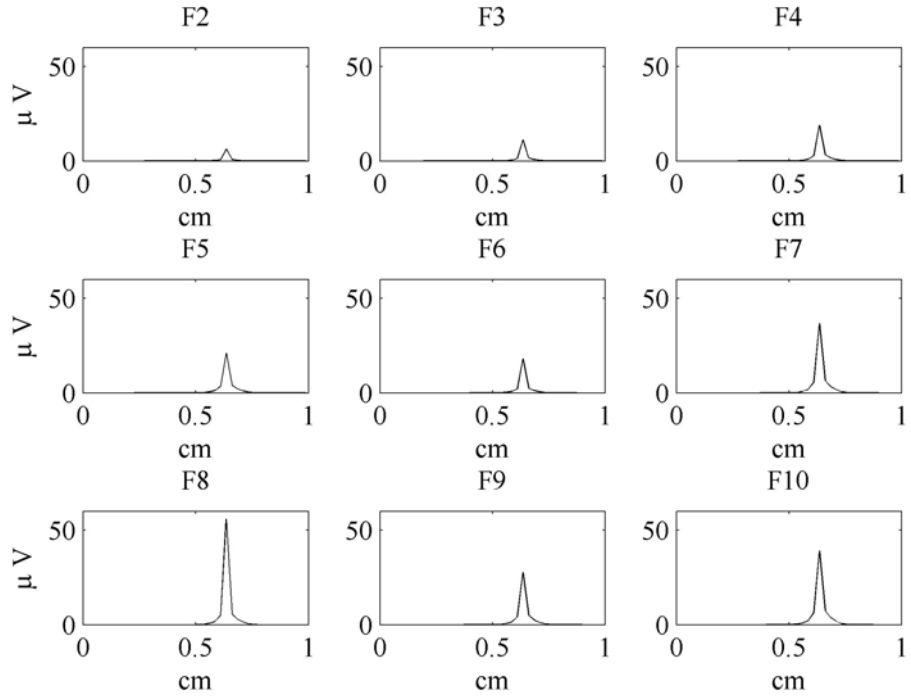

Figure 5.11: Differences between the extracellular potential distributions for including and excluding the ephaptic effect.

The MATLAB model was solved with the imported extracellular potential distributions for both excluding and including the ephaptic effect for each fibre (i.e. F2-F10).

The results are shown in Figures 5.12 to 5.14. It is shown that the ephaptic influence is sufficient to evoke an AP along every fibre. Furthermore, it is observed that only an antidromic AP is fired in fibres F2, F3, F4 and F6, whereas both antidromic and orthodromic APs are evoked in the rest of the fibres.

5.4.3 Biphasic pulses in heterogeneous medium

5.4.3.1 C/A pulse with phase duration 100 μs

Figure 5.15 shows the stimulation of fibre F8 for a short (100 μs) C/A pulse at threshold for both excluding and including EE.

At threshold an antidromic AP is evoked, but when the ephaptic effect is included the fibre does not fire. The result is counterintuitive since the ephaptic currents are added to the anodic phase and should therefore increase the stimulus effect. Also, the threshold for a biphasic pulse is lower than for a monophasic pulse, which means that the ephaptic currents constitute a larger part of the total stimulus. Figure 5.16 shows the difference between the potential including EE and the one excluding EE, i.e. the figure shows the effect of only the ephaptic currents. Although there is a large positive effect on the part of the fibre closest to the source, a closer look (see the small inserted figures) reveals that there sections along the fibre where the difference is negative and where the propagation of an action potential could thus be inhibited.

This last observation was investigated using the activating function, which is the direct stimulating influence on the n-th compartment and is given by

$$f_n = \left[\frac{V_{e,n-1} - V_{e,n}}{R_{n-1}/2 + R_n/2} + \frac{V_{e,n+1} - V_{e,n}}{R_{n+1}/2 + R_n/2} \right] / C_{m,n} \tag{5.10}$$

where V_e is the extracellular potential, R_n is the axoplasmatic resistance and $C_{m,n}$ is the membrane conductance (see Chapter 3). The activating function is a useful tool that provides information of possible sites of excitation. Positive regions in the activating function indicate regions of possible excitation while negative regions indicate inhibitory regions (Rattay and Aberham, 1993; Rattay et al., 2001a).

To investigate the ephaptic influence on excitation in this way, the activating function

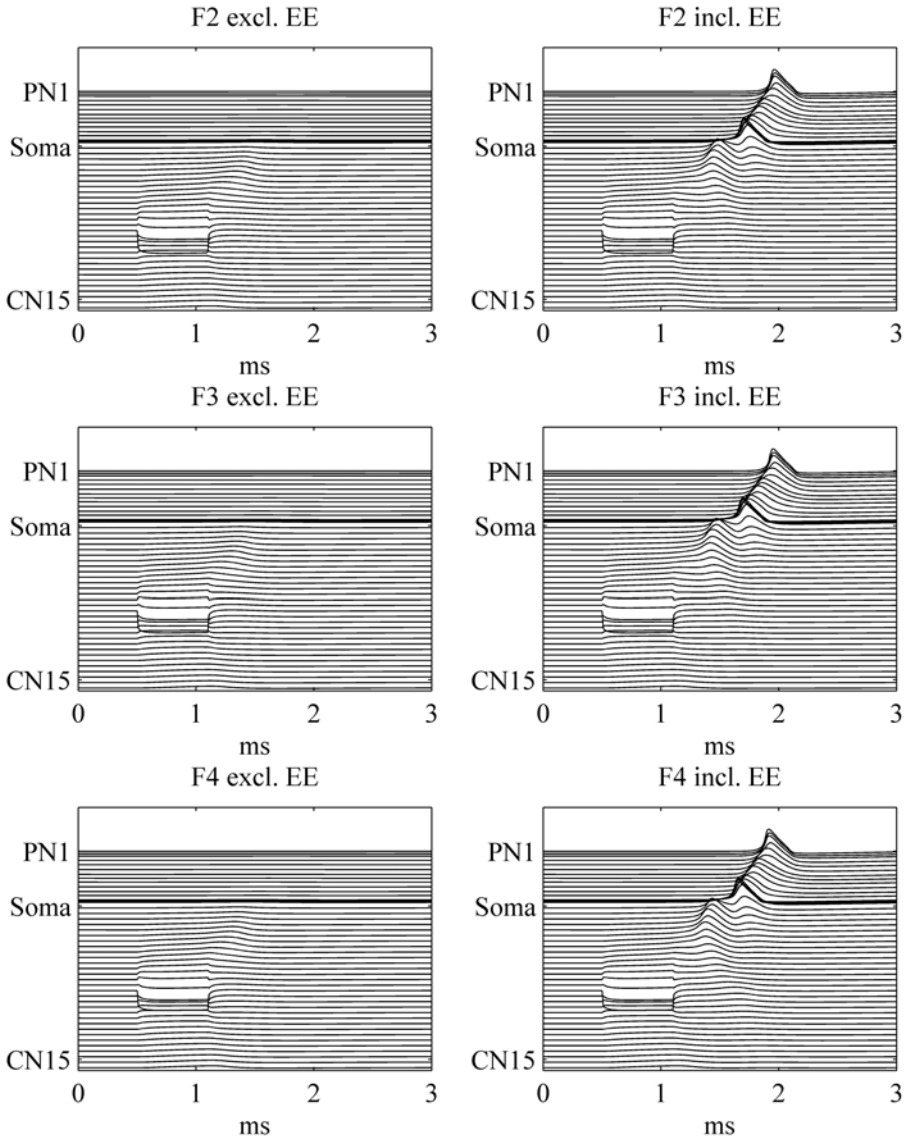

Figure 5.12: Fibres F2 to F4. Only antidromic APs are evoked when the ephaptic effect (EE) is included.

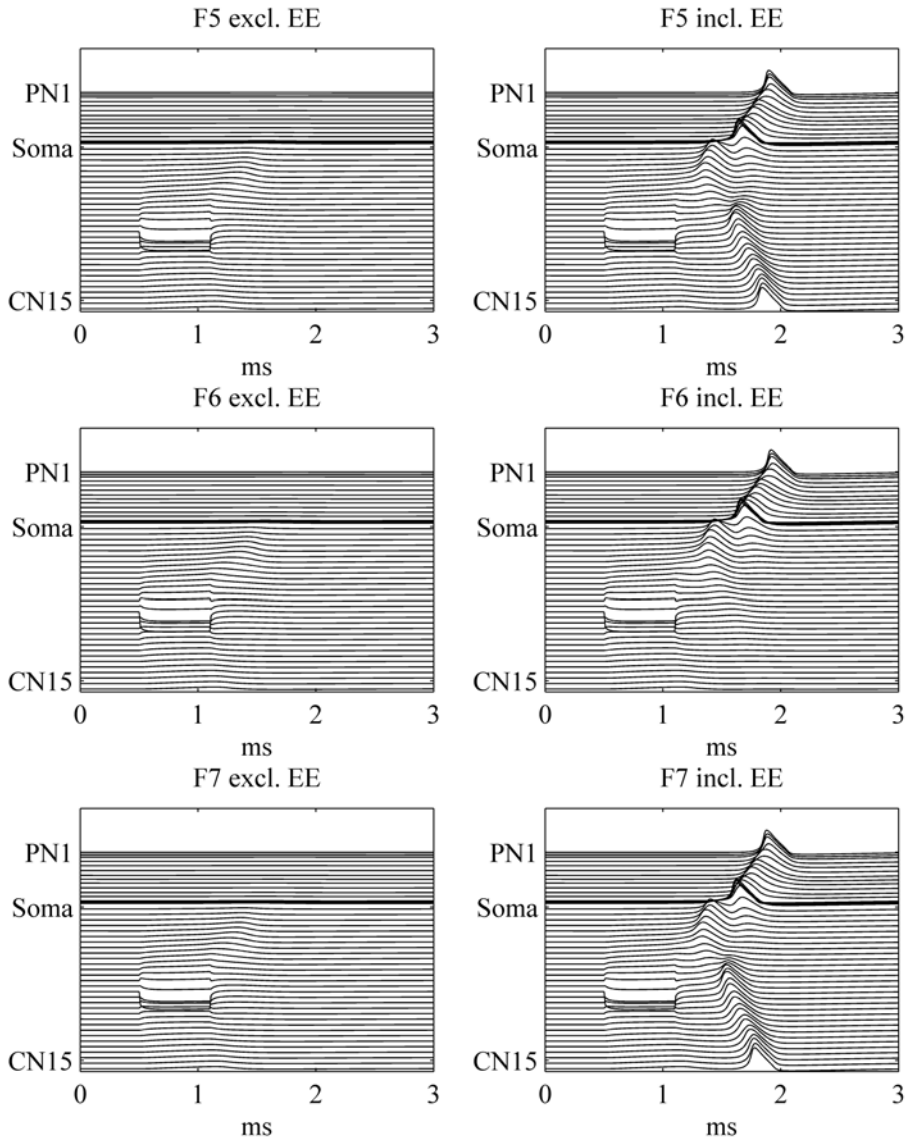

Figure 5.13: Fibres F5 to F7. In F6 only an antidromic AP is evoked when EE is included and the other fibres trigger both antidromic and orthodromic APs.

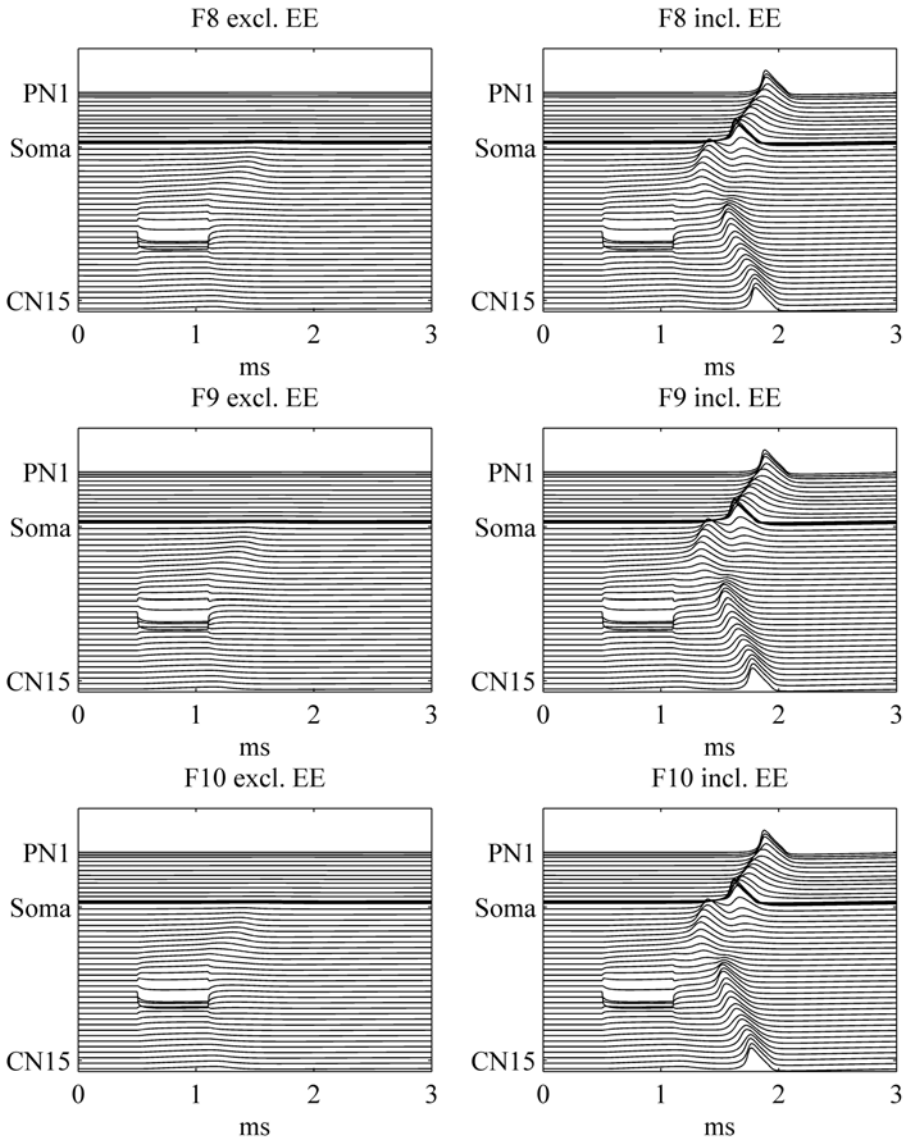

Figure 5.14: Fibres F8 to F10. Both antidromic and orthodromic APs are evoked.

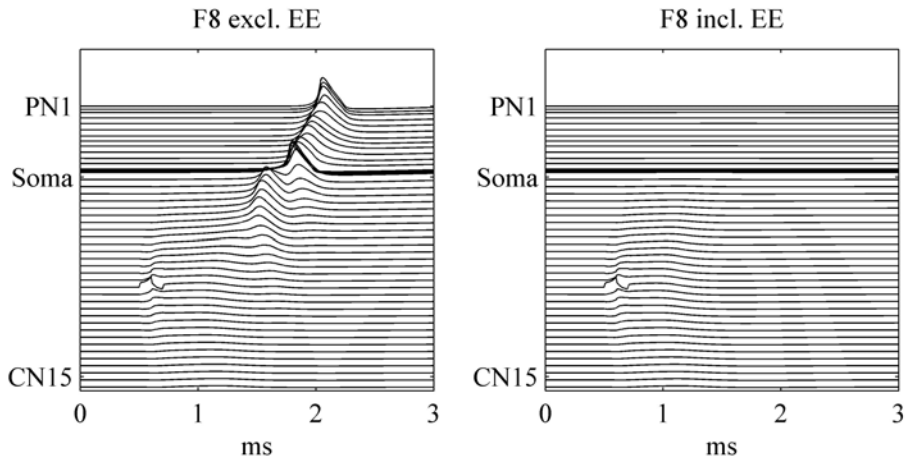

Figure 5.15: The left figure shows stimulation at threshold without ephaptic influence. The right figure shows the result of the same stimulus but including the ephaptic effect. The ephaptic influence has an inhibitory effect on the firing mechanism.

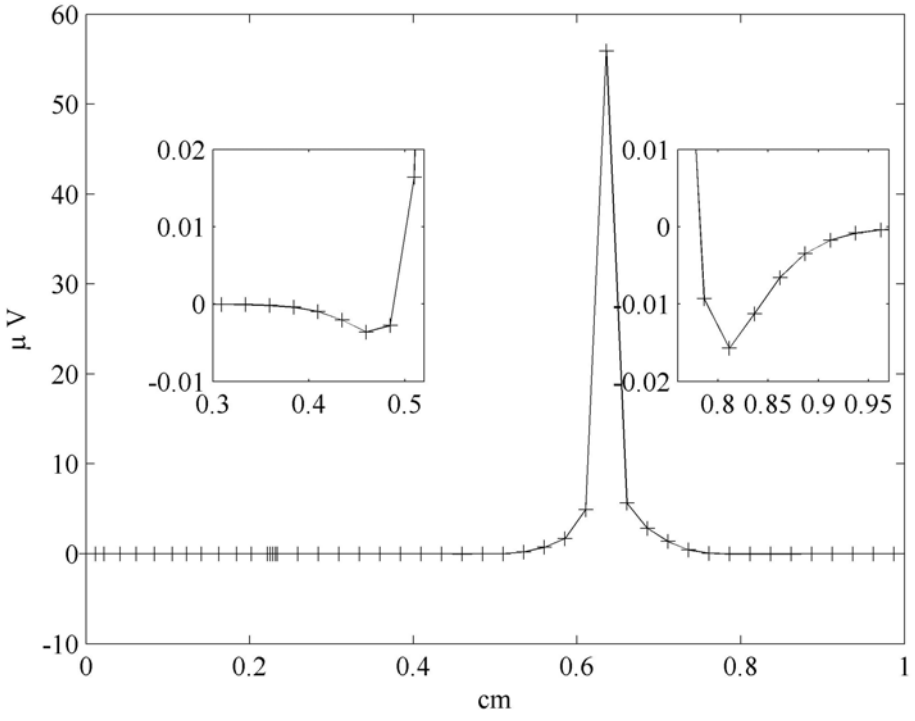

Figure 5.16: The potential along the fibre including EE minus the potential excluding EE. The part of the fibre that is closest to the point source shows a positive difference, but there are also negative differences. This could explain the inhibitory effect.

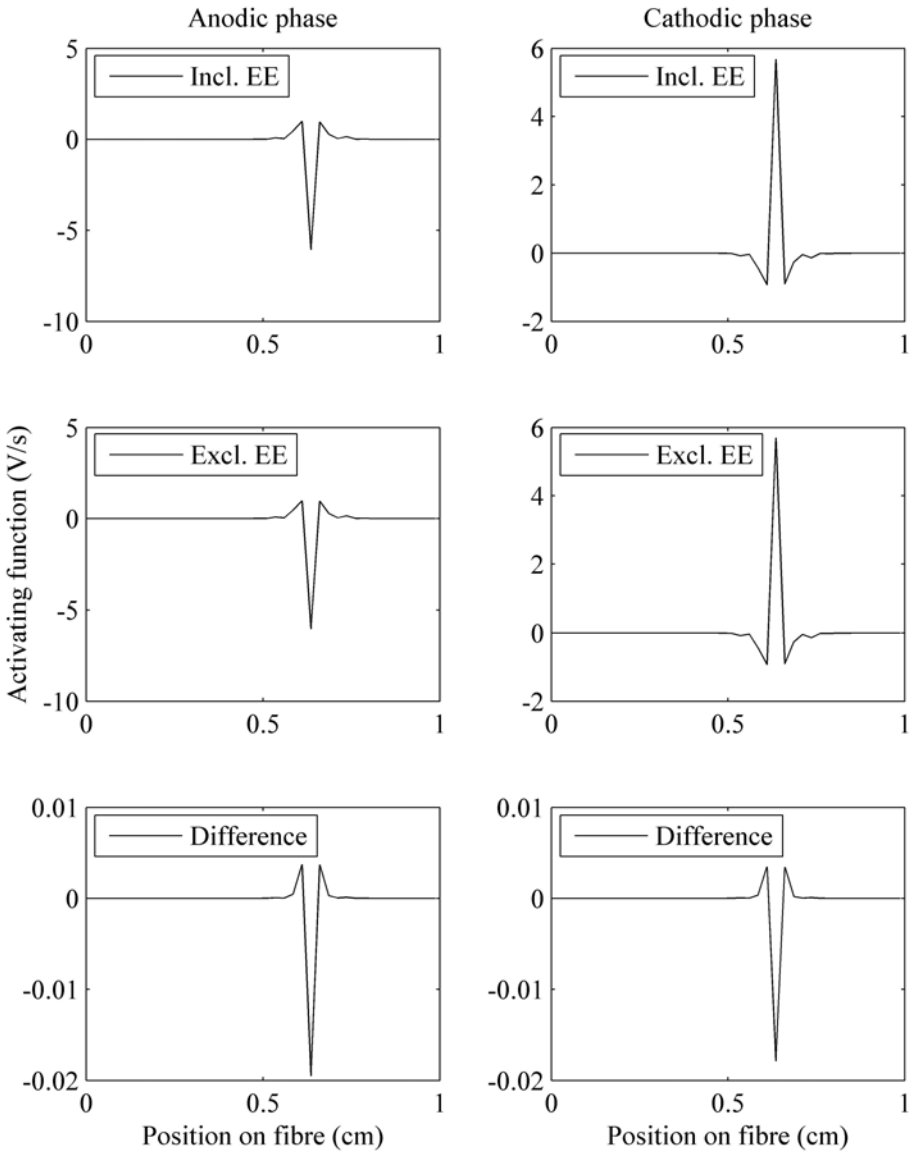

Figure 5.17: Activating function on F8 for anodic phase (left column) and cathodic phase (right column) with phase duration 100 μs. The top figures show the function including the ephaptic effect. The middle figure show the function of the stimulus alone and the bottom figures show the difference between including and excluding the ephaptic effect.

for both stimulus alone and when the ephaptic effect is included for both the anodic phase and cathodic phase were calculated (Figure 5.17). The ephaptic influence on the activating function is small but the bottom figures in Figure 5.17 show that the ephaptic effect decreases the excitatory region, i.e. the part of the fibre that is closest to the point source for the cathodic phase. Thus the inhibitory effect by the ephaptic influence on the firing mechanism for the C/A pulse occurs during the cathodic phase.

5.4.3.2 C/A pulse with phase duration 200 μs

Figure 5.18 shows the result for a long (200 μs) C/A pulse for both excluding and including EE. The simulations are performed with a stimulus at threshold.

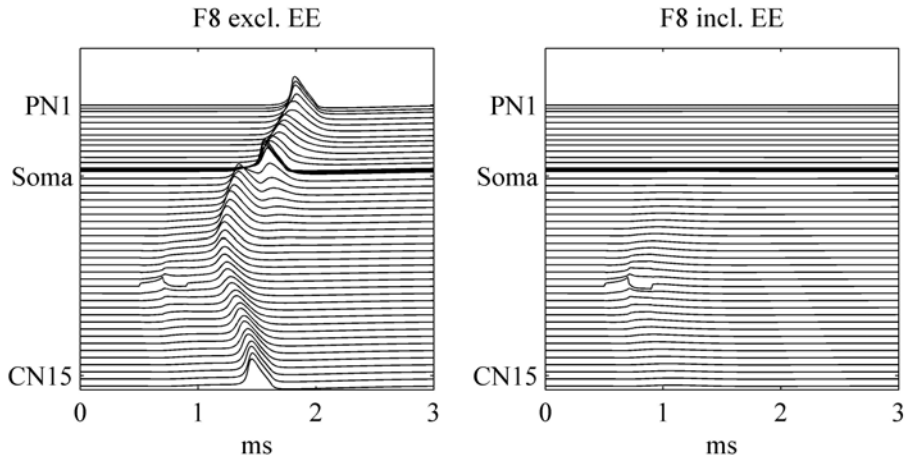

Figure 5.18: The left figure shows stimulation at threshold without ephaptic influence. The right figure shows the result of the same stimulus but including the ephaptic effect. The ephaptic influence has an inhibitory effect on the firing mechanism.

Figure 5.19 shows the activating function for anodic and cathodic phases with duration 200 μs. The ephaptic currents decrease the amplitude of the function in the depolarizing region which may explain why no excitation occurs.

5.4.3.3 A/C pulse with phase duration 100 μs

Figure 5.20 shows the stimulation of fibre F8 for a short A/C pulse at threshold for both excluding and including EE.

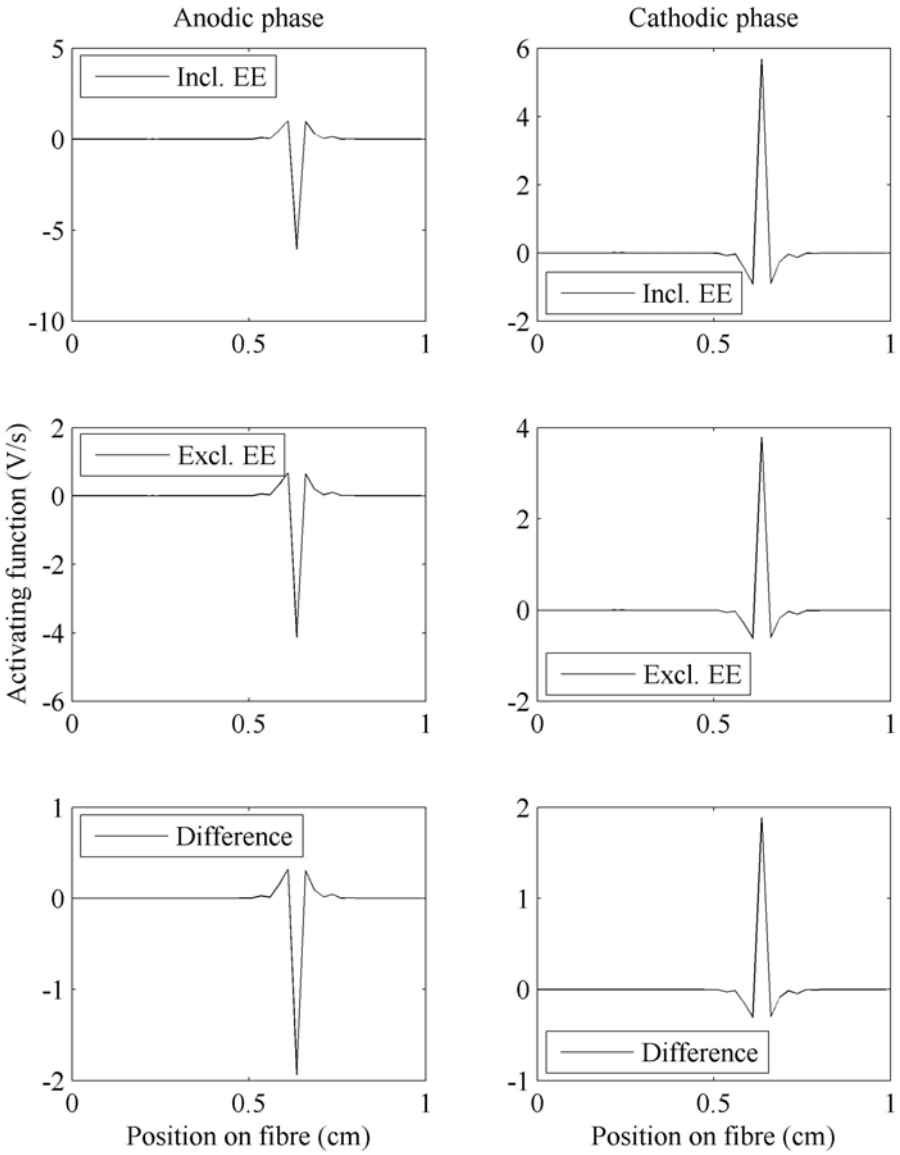

Figure 5.19: Activating function on F8 for anodic phase (left column) and cathodic phase (right column). The top figures show the function including the ephaptic effect. The middle figure show the function of the stimulus alone and the bottom figures show the difference between including and excluding the ephaptic effect.

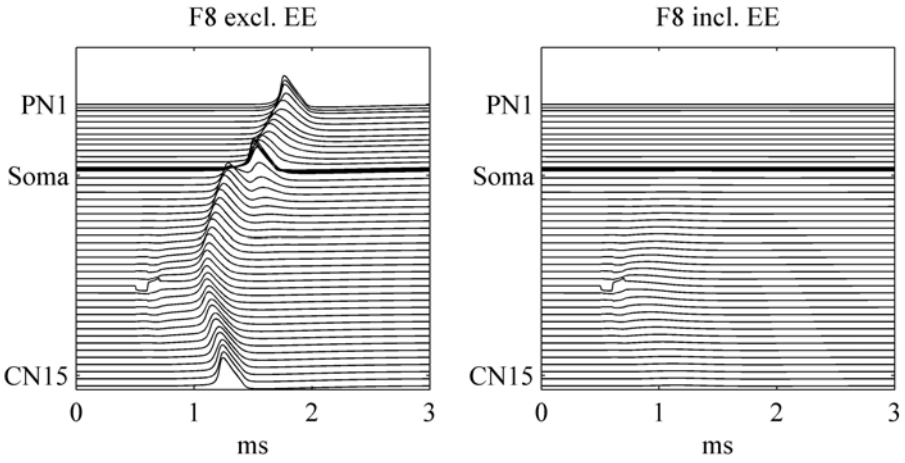

Figure 5.20: Stimulus at threshold (1.784256 μA). When the ephaptic currents are included, there is no excitation.

When the ephaptic currents are included, no excitation occurs. Again the activating function in Figure 5.17 might provide an explanation for the inhibitory effect of the ephaptic influence in the cathodic phase.

5.4.3.4 A/C pulse with phase duration 200 μs

Figure 5.21 shows the stimulation of fibre F8 for a long A/C pulse just below threshold for both excluding and including EE. For the long A/C pulse the ephaptic currents

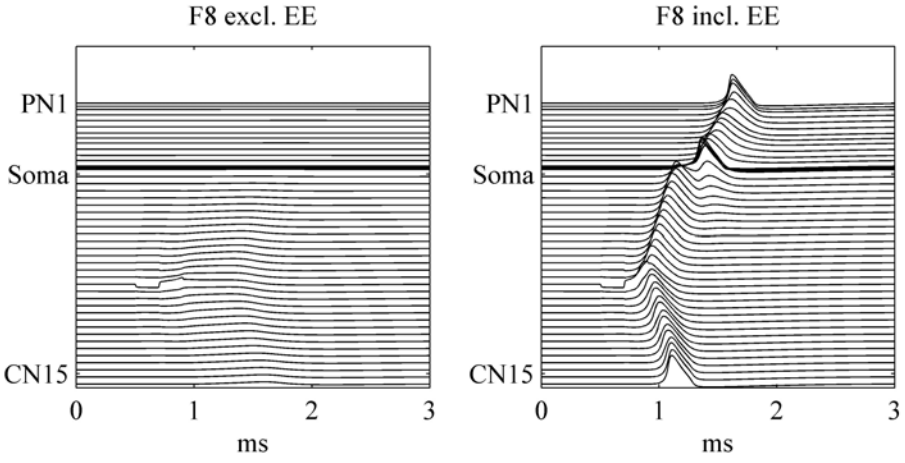

Figure 5.21: Stimulus just below threshold (1.187756 μA). The ephaptic currents are sufficient to elicit excitation.

are sufficient to elicit excitation. This corresponds with the activating function for the cathodic phase in Figure 5.19 which shows that the ephaptic influence increases the amplitude of the depolarizing region.

5.4.4 Monophasic pulse in homogeneous medium

The ephaptic effect in the homogeneous medium is shown in Figure 5.22. It has a maximum value of 80.65 μV, which is larger than the ephaptic effect in the heterogeneous medium, in which the maximum value is 55.9 μV.

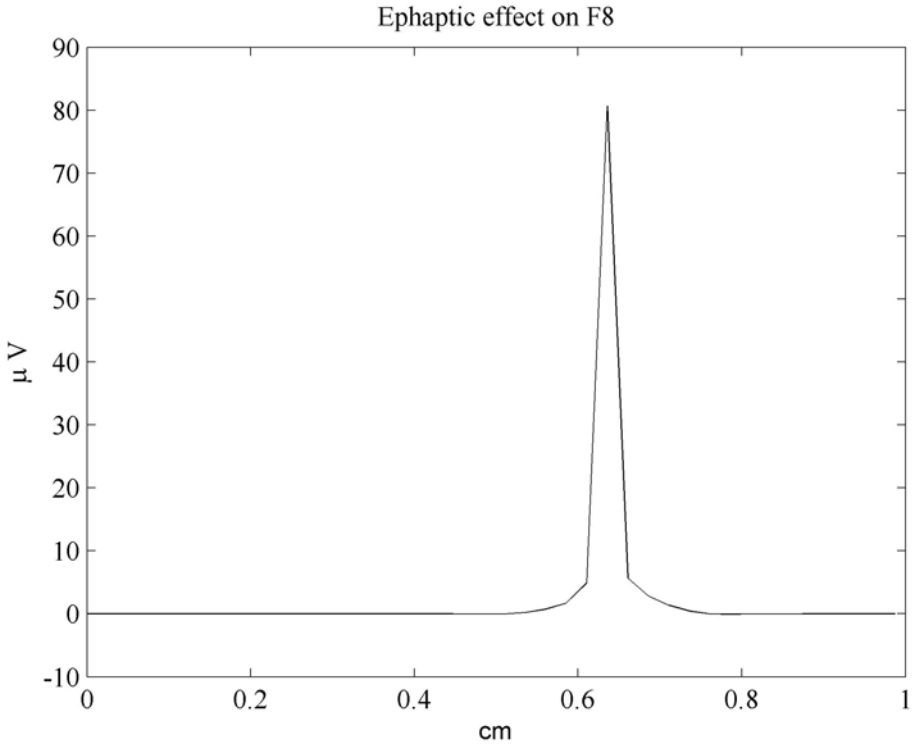

Figure 5.22: The ephaptic effect on fibre F8 in a homogeneous medium. The effect is larger than in the heterogeneous medium.

Simulations where ephaptic currents are included were carried out with the current I=9.3628 μA, i.e. just below threshold. The resulting potential distribution elicits an AP, which is shown in Figure 5.23. The same kind of excitation, i.e. both an antidromic and orthodromic AP, occurred for all fibres in the homogeneous medium except F2 and F3, which only fired antidromically. In the heterogeneous medium F2,

F3, F4 and F6 only fired antidromically. This shows that the ephaptic effect is larger in a homogeneous medium.

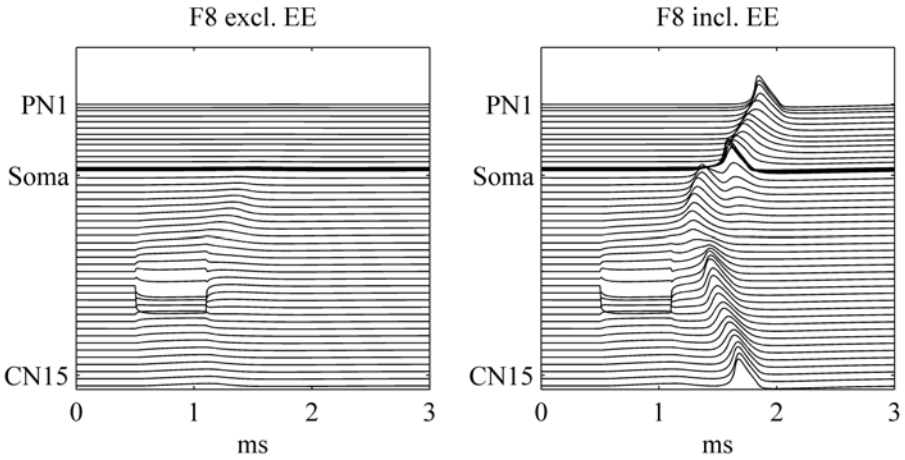

Figure 5.23: Stimulus is 9.3628 μA, which is just below threshold for the non-ephaptic case. As can be seen in the right figure, the EE has a large enough effect to evoke an AP.

5.5 DISCUSSION

This chapter has demonstrated the effect of ephaptic interaction and the influence of heterogeneity in a medium with realistic fibre density on neural excitation with an FE model. In the investigation of the field distribution, the simulations of a homogeneous medium fit well to the analytical solution, validating the model. The presence of fibres in the medium has a significant effect on the extracellular potential distribution at small distances from the point sources in that it decreases the potential. The difference between the homogeneous and heterogeneous case then decreases as the distance from the point sources increases and at large distances the distribution for the heterogeneous medium converges to that of the homogeneous medium.

For monophasic stimulation the ephaptic influence is sufficient to evoke an AP close to threshold. The highest ephaptic influence predicted was 55.9 μV (F8) which is 0.05% of the maximum extracellular potential at that fibre provided by the stimulus alone. The lowest stimulating current to elicit an AP in this fibre when the ephaptic effect was included was 9.6012 μA, which is a decrease of 0.03% of the threshold without any ephaptic influence. The ephaptic effect on F8 increased the intensity of the potential

by 0.004 dB, which is about 0.6% of the average dynamic range for cochlear implant patients. The ephaptic effect is cumulative over the number of excited fibres, but since the electric potential is also inversely proportional to the distance from the source, the magnitude of the ephaptic effect depends both on the number of excited neurons and the neural density. Only a small bundle of fibres was implemented in this study. The cumulative ephaptic effect has been shown in the previous chapters to be significant. Thus, the relatively small effect demonstrated in this chapter is expected to be significant if a complete neural population is involved.

It was observed that only an antidromic AP is fired in fibres F2, F3, F4 and F6, whereas both antidromic and orthodromic APs are evoked in the rest of the fibres. This is an interesting result since F2, F3, F4 and F6 have the lowest thresholds, indicating that antidromic APs fire first and only when the stimulus is further increased are orthodromic APs evoked as well. For fibres F5, F7, F8, F9 and F10 there are more excited nodes than for the others fibres and therefore the total stimulus (i.e. including the ephaptic effect) is larger, which could explain the orthodromic AP.

For the biphasic pulses the ephaptic influence evoked an excitation only for a long A/C pulse. For the other biphasic pulses the ephaptic currents had an inhibitory effect on the firing mechanism. This is in correspondence with the activating functions in Figures 5.17 and 5.19, which show that the ephaptic effect increases the amplitude of the function in the depolarizing region for the long cathodic phase and decreases the function for the other phases.

The ephaptic effect is larger in the homogeneous medium, with a maximum value of 80.65 μV, compared to the heterogeneous medium, in which the maximum value is 55.9 μV. The thresholds in this chapter are low because the electrode is located very close to the fibres. However, electrode locations very close to the fibres are relevant for electrodes that penetrate the nerve volume, i.e. mid-modiolar or intramodiolar electrodes. The threshold in the homogeneous medium is $I_{th,hom} = 9.3632$ μA and is lower than in the heterogeneous case, which has a threshold $I_{th,het} = 9.6044$ μA. This is of importance since many cochlear and neural models assume a homogeneous medium which will affect the predicted thresholds. This effect could also alter the results of the previous two chapters. Chapter 3 assumed an infinite homogeneous medium with single neuron resolution and Chapter 4 performed simulations with a cluster resolution at neural level and also a homogeneous representation of the neural volume. The results

of this chapter could mean a decrease of the ephaptic effect presented in the Chapters 3 and 4 when heterogeneity of the neural volume is included. A crude estimate based on the threshold currents mentioned above would indicate a decrease in ephaptic effect of approximately 3% in dB level when heterogeneity is included. Although a decrease occurs, the ephaptic effect is still significant.

In conclusion, this chapter has shown that field interactions in neural tissue are affected by the heterogeneity caused by the volumes and locations of individual fibres within the nerve bundle. The heterogeneity has a notable effect on the potential distribution in the neural volume at small distances from the stimulus and should therefore be taken into account in models containing neural tissue. The ephaptic effect was shown to evoke an AP for a monophasic pulse and a long A/C biphasic pulse when the stimulus is close to threshold. Furthermore, the ephaptic excitation could contribute to randomised firing patterns and could therefore be a useful element in models of neural populations.

Chapter 6

GENERAL DISCUSSION AND CONCLUSION

6.1 RESEARCH OVERVIEWS

The objective of this study was to investigate the effect of variation in electrical potential field interactions in general - and more specifically the phenomenon of ephaptic excitation - caused by the morphology of the auditory nerve and its constituting neurons, on neural excitation profiles in cochlear implants. The study aimed to quantify the amount of morphological and physiological detail that is required to make accurate predictions of spread of neural excitation to advance existing models and provide insights for the development of future cochlear implants. The study consists of different implemented models with increasing level of detail.

6.2 RESULTS AND DISCUSSION

In Chapter 3 a simplified version of the neural model presented by Rattay et al. (2001), where the fibres were placed in an infinite, homogeneous, isotropic and resistive medium, was used to quantify the influence of the ephaptic effect. The influence of the spatial location of the active neurons relative to the target neuron, stimulus intensity

and neural density on ephaptic excitation was investigated. The results from this model suggest that the contribution of ephaptic excitation seems to be important up to at least 6 to 7 dB above threshold (Research topic 1). Cochlear implant patients normally have a small dynamic range (average of 7 dB), indicating that the ephaptic effect might be important in models of the implanted cochlea.

The ephaptic excitation was also applied to modelled neural excitation profiles (Hanekom, 2001) and then compared to translated neural excitation profiles measured in cat (Moore et al., 2002). Measured data have a larger spread of excitation than modelled data when the stimulus is close to threshold and it was shown that the spread of excitation for the modelled data was increased close to threshold when the ephaptic effect was added, suggesting that the ephaptic influence should not be neglected in neuromodelling.

Amendments to the model were made in Chapter 4 to provide a more comprehensive computational and physiological description of the phenomenon. The study on ephaptic excitation was thereby expanded by increasing the level of details of the model by including membrane noise, three-dimensional geometry and conductive properties of the cochlear volume to represent the morphology and morphometry of a mammalian cochlea (Research topic 2). Moreover, the effect of variation of pulse shapes was also investigated.

The addition of a noise term to the neural model sensitized the target neuron for ephaptic excitation. This is in correspondence with literature which reports that noise could enhance both detection (Zeng et al., 2000) and discrimination (Behnam et al., 2003) of sound. Sensitization of the target neuron could be a result of stochastic resonance. Since internal noise exists in normal auditory nerve fibres (Zeng et al., 2000) and the stochasticity affected the model predictions, it is concluded that noise should be included in models of auditory nerve fibres dealing with thresholds.

Furthermore, the pulse shape was shown to affect ephaptic contribution to a great degree. The ephaptic effect was significant for both pulses used in Chapter 4, but the effect was the largest for the monophasic pulse. This pulse also seemed to decrease the effect of the noise in that ephaptic effect was large in both the deterministic and stochastic model. An explanation for the larger ephaptic effect is that monophasic pulses decrease threshold compared to biphasic pulses, since the second phase of a

pulse can reduce the strength of the first phase due to membrane integration of the externally applied current (van Wieringen et al., 2005). The ephaptic contribution will then constitute a larger part of the total stimulus. Furthermore, the spread of excitation is wider so more fibres contribute to the ephaptic excitation.

The implementation of a three-dimensional geometry of the cochlear volume allowed for an investigation of ephaptic excitation in nerve fibres innervating different turns of the cochlea. Because of this cross-turn stimulation, ectopic excitation could affect pitch perception of cochlear implant subjects. Although no direct experimental assessment of ectopic excitation is found in literature, a large number of studies that report on pitch confusion indirectly suggests the existence of the ephaptic effect (Henry, McKay et al., 2000; Throckmorton and Collins, 1999; Busby, Whitford et al., 1994; Shannon, 1983; Nelson, Van Tasell et al., 1995; Mens, Brokx et al., 1995; Di Nardo, Scorpecci et al., 2010).

Chapter 5 investigated the effect of heterogeneity, caused by the structure of the neural tissue, on potential distributions within the nerve fibre population by means of FE modelling (Research topic 3). Furthermore, by coupling the FE model to a single fibre model, the neural responsiveness was also investigated. It was demonstrated that the presence of fibres in the medium has a significant effect on the extracellular potential distribution at small distances from the point sources in that it decreased the potential. The difference between the homogeneous and heterogeneous case then decreased as the distance from the point sources increased and at large distances the distribution for the heterogeneous medium converged to the homogeneous distribution.

As in Chapter 4, pulse shape was shown to have a large influence on neural responsiveness. The results in Chapter 5 showed that monophasic pulses facilitated ephaptic excitation whereas the only biphasic pulse to evoke an AP was a C/A pulse with phase duration 200 μs. The activating function was used to explain why no excitation occurred for the other biphasic pulses used.

It was observed that only antidromic APs were evoked when the ephaptic influence was low and when the effect increased an orthodromic AP fired as well. The latencies could be increased as a consequence, since the fibre then is in a refractory state and cannot fire until it has recovered. This implies that the firing efficiency, i.e. the ratio of the number of spikes evoked and the stimuli presented, could be decreased. Thus more

randomised excitation such as that observed in naturally occurring firing patterns could be a consequence of ephaptic interaction and should therefore be included in models of neural populations.

6.3 CONCLUSION AND FUTURE RESEARCH DIRECTIVES

When implementing models of physiological systems, the level of detail included in the model is always balanced against how much computational effort is needed to achieve results. A model containing much details might produce good results, but at the cost of a longer simulation time. It is therefore desired to know how much detail is needed to get sufficiently accurate predictions. This study has demonstrated that a very simple deterministic model shows that the ephaptic effect could be significant at stimulus intensities close to threshold. However, further quantification of the effect showed that anatomical, morphological and morphometrical details, e.g. three dimensional geometry and membrane noise should not be excluded when modelling the responsiveness of auditory nerve fibres close to threshold.

The antidromic firing for low ephaptic influence in Chapter 5 was an interesting observation in that it implies an increased latency since the fibre will be in a refractory state and cannot fire until it has recovered. Thus, the ephaptic effect could contribute to more randomised excitation similar to that observed in naturally occurring firing patterns. This could be especially significant at lower stimulus intensities where the ephaptic effect has been shown to be significant and where phase locking in cochlear implants occurs to a lesser extent. However, more research is needed to determine whether a randomised effect would be noticeable in cochlear implants. Furthermore, propagation of antidromic spikes throughout a whole fibre requires intact peripheral processes and cochlear implantees with a long duration of deafness typically suffer from degeneration of the peripheral processes (Miller et al., 2004; Macherey et al., 2008).

One limitation of the FE model in Chapter 5 is the assumption of when the ephaptic contribution is added to the stimulus. The ephaptic contribution is more realistic in the neural and volume conduction models in Chapters 3 and 4 because proper

time-dependent excitation profiles are simulated in the single fibre model. However, without these profiles the FE model showed the importance of homogeneity in the neural tissue, which is lacking in the volume conduction model. Future research could be directed to add heterogeneity to the neural volume in the volume conduction model and thereby replace the cluster resolution with single fibre resolution. However, this would imply the implementation of a realistic number of neurons (in the order of 30 000 neurons) into the volume conduction model to achieve the desired neural density. The computational effort to achieve this, especially in a complete model of the cochlear volume, is detrimental at this stage, but such a model might become viable with the development of computer technology.

This study has showed that the ephaptic effect is larger for longer pulse durations. Intraneural arrays for stimulation of the auditory nerve use shorter pulses and it would be of interest to find out whether the ephaptic effect would still be noticeable. For an ephaptic effect to occur there must be an overlap between all contributing stimuli and for short pulses there is a lower chance of overlap. On the other hand, intraneural arrays are close to the nerve which would decrease the latency. Future research about the ephaptic effect in intraneural arrays would be of interest.

As discussed in Chapter 4, reducing threshold currents required for excitation is advantageous for two reasons: it reduces power consumption and increases spatial selectivity (van Wieringen et al., 2005). For this reason pulse shapes that reduce thresholds could lead to improved current excitation strategies in future cochlear implants. However, investigating new ways to lower thresholds is also of interest for the research of ephaptic interaction, since lower stimuli make the ephaptic contribution constitute a larger part of the total extracellular potential. This could be undesirable since it is speculated that the ephaptic effect could be harmful to frequency discrimination tasks. This study has showed that monophasic current pulses are more desirable since they reduce the threshold, but since they are not charge-balanced they are for safety reasons not used with human subjects (van Wieringen et al., 2005). Therefore, biphasic pulses are used even though the effective strength of the first phase can be reduced by the second one since the neural membrane integrates the externally applied current. Pseudomonophasic pulses, i.e. biphasic pulses of which one of the two phases has a different duration and amplitude, have been suggested as a possible solution (van Wieringen et al., 2005) and then ephaptic contribution should be taken into account. Pseudomonophasic pulses were not covered by this study and future research of this

type of pulses, as well as other means to lower threshold, and its impact on ephaptic interaction would be of interest.

One challenge with investigating the ephaptic effect by means of computational modelling is that the phenomenon has not yet been directly assessed experimentally, making the modelling results difficult to verify. Future research could include masking experiments using a long electrode array of which the contacts span more than 360 degrees along the cochlear turns. The magnitude of the cross-turn stimulation could potentially be assessed if the masker and probe electrodes are aligned in different cochlear turns.

In conclusion, this study provides evidence that the ephaptic effect could be a significant contributor to the determination of neural excitation profiles in cochlear implant subjects. It is suggested that the ephaptic effect could be a significant parameter in pitch perception and in the interpretation of pitch-related psychoacoustic data. Finally, the results of this study suggest that field interactions among neurons and the heterogeneity of the neural volume affect ephaptic excitation. Both should thus be included in neuromodelling where an accurate description of neural excitation behaviour is required.

References

Behnam, S.E., Zeng, F.G. 2003, "Noise improves suprathreshold discrimination in cochlear-implant listeners", *Hearing Research* 186, pp. 91-93.

Briaire, J.J. and Frijns, J.H.M. 2005, "Unraveling the electrically evoked compound action potential", *Hearing Research* 205, pp. 143-156.

Briaire, J.J. and Frijns, J.H.M. 2006, "The consequences of neural degeneration regarding optimal cochlear implant position in scala tympani: a model appproach", *Hearing Research* 214, pp. 17-27.

Brown, M., Webster, W.R., Martin, R.L. 1997, "Intensity and frequency functions of [^{14}C]2-deoxyglucose labelling in the central nucleus of the inferior colliculus in the cat", *Hearing Research* 104 (1–2), pp. 73–89.

Bruce, I.C., White, M.W., Irlicht, L.S., O'Leary, S.J. and Clark, G.M. 1999, "The effects of stochastic neural activity in a model predicting intensity perception with cochlear implants: low-rate stimulation", *IEEE Transactions on Biomedical Engineering* 46(12), pp. 1393-1404.

Busby, P.A., Whitford, L.A., Blamey, P.J., Richardson, L.M., Clark, G.M. 1994, "Pitch perception for different modes of stimulation using the Cochlear multiple-electrode prosthesis", *J. Acoust. Soc. Am.* 95, pp. 2658-69.

Cartee, L.A., vad den Honert, C., Finley, C.C. and Miller, R.L. 2000, "Evaluation of a model of the cochlear neural membrane. I. Physiological measurement of membrane characteristics in response to intrameatal electrical stimulation", *Hearing Research* 146, pp. 143-152.

Cartee, L.A. 2000, "Evaluation of a model of the cochlear neural membrane. II: Comparison of model and physiological measures of membrane properties measured

in response to intrameatal electrical stimulation", *Hearing Research* 146 (1-2), pp. 153-166.

Cartee, L.A., Miller, C.A., van den Honert, C. 2006, "Spiral ganglion cell site of excitation I: Comparison of scala tympani and intrameatal electrode responses", *Hearing Research* 215, pp. 10–21.

Cartee, L.A. 2006, "Spiral ganglion cell site of excitation II: Numerical model analysis", *Hearing Research* 215, pp. 22–30.

Chiu, S.Y., Ritchie, J.M., Rogart, R.B. and Stagg, D. 1979, "A quantitative description of membrane currents in rabbit myelinated nerve", *Journal of Physiology* 292, pp. 149-166.

Dalkara, T., Krnjevic, K., Ropert, N., Yim, C.Y. 1986, "Chemical modulation of ephaptic activation of CA3 hippocampal pyramids", *Neuroscience* 17 (2), pp. 361-370.

Daniels, C., Rubinsky, B. 2009, "Electrical field and temperature model of nonthermal irreversible electroporation in heterogeneous tissues", *Journal of Biomechanical Engineering* 131 (7), art. no. 710061.

Di Nardo, W., Scorpecci, A., Giannantonio, S., Cianfrone, F., Parrilla, C., Paludetti, G. 2010, "Cochlear implant patients' speech understanding in background noise: effect of mismatch between electrode assigned frequencies and perceived pitch", *J. Laryngol. Otol.* 124 (8), pp. 828-34.

Dynes, S.C.B. and Delgutte, B. 1992, "Phase-locking of auditory-nerve discharges to sinusoidal electric stimulation of the cochlea", *Hearing Research* 58, pp. 79-90.

Faber, D.S., Korn, H. 1989, "Electrical field effects: Their relevance in central neural networks", *Physiol. Rev.* 69, pp. 821-863.

Finley, C.C., Wilson, B.S., White, M.W. 1990, "Models of neural responsiveness to electrical stimulation. In: Miller, J.M., Spelman, F.A., (eds), Cochlear Implants. Models of the Electrically Stimulated Ear, *Springer-Verlag Inc.*, New York, pp. 55-96.

Frankenhæuser, B. and Huxley, A.F. 1964, "The action potential in the myelinated nerve fibre of Xenopus laevis as computed on the basis of voltage clamp data, *Journal of Physiology* 171, pp. 302-315.

Frijns, J.H.M., Mooij, J. and ten Kate, J.H. 1994, "A quantitative approach to modeling mammalian myelinated nerve fibers for electrical prosthesis design", *IEEE Transactions on Biomedical Engineering* 41(6), pp. 556-566.

Frijns, J.H.M. and ten Kate, J.H. 1994, "A model of myelinated nerve fibers for electrical prosthesis design", *Medical and Biological Engineering and Computing* 32(4), pp. 391-398.

Frijns, J.H.M., de Snoo, S.L., Schoonhoven, R. 1995, "Potential distributions and neural excitation patterns in a rotationally symmetric model of the electrically stimulated cochlea", *Hearing Research* 87, pp. 170-186.

Frijns, J.H.M., de Snoo, S.L., ten Kate, J.H. 1996, "Spatial selectivity in a rotationally symmetric model of the electrically stimulated cochlea", *Hearing Research* 95, pp. 33-48.

Frijns, J.H.M., Briaire, J.J., Grote, J.J. 2001, "The Importance of Human Cochlear Anatomy for the Results of Modiolus-Hugging Multichannel Cochlear Implants", *Otology & Neurotology* 22, pp. 340–349.

Frijns J.H.M., Briaire J.J., Schoonhoven R. 2000, "Integrated use of volume conduction and neural models to simulate the response to cochlear implants", *Simulation Practice and Theory* 8, pp. 75-97.

Gleich, O., Wilson, S. 1993, "The diameters of guinea pig auditory nerve fibres: Distribution and correlation with spontaneous rate", *Hearing Research* 71, pp. 69-79.

Glueckert, R., Pfaller, K., Kinnefors, A., Rask-Andersen, H. and Schrott-Fischer, A. 2005, "Ultrastructure of the normal human organ of Corti. New anatomical findings in surgical specimens", *Acta Oto-Laryngologica* 125 (5), pp. 534-539.

Glueckert, R., Pfaller, K., Kinnefors, A., Schrott-Fischer, A. and Rask-Andersen, H. 2005, "High resolution scanning electron microscopy of the human organ of Corti. A study using freshly fixed surgical specimens", *Hearing Research* 199, pp. 40–56.

Goffi-Gomez, M.V., Abdala, C.F., Peralta, C.G., Tsuji, R.K., de Brito Neto, R.V., Bento, R.F. 2010, "Neural response telemetry in patients with the double-array cochlear implant", *Eur Arch Otorhinolaryngol* 267, pp. 515-522.

Hanekom, T. 2001, "Three-dimensional spiraling finite element model of the electrically stimulated cochlea", *Ear and Hearing* 22 (4), pp. 300-315.

Hanekom, T. 2005, "Modelling encapsulation tissue around cochlear implant electrodes", *Medical and Biological Engineering and Computing* 43 (1), pp. 47-55.

Haueisen, J., Ramon, C., Eiselt, M., Brauer, H., Nowak, H. 1997, "Influence of Tissue Resistivities on Neuromagnetic Fields and Electric Potentials Studied with a Finite Element Model of the Head", *IEEE Transactions on Biomedical Engineering* 44 (8), pp. 727-735.

Henry, B.A., McKay, C.M., McDermott, H.J., Clark, G.M. 2000, "The relationship between speech perception and electrode discrimination in cochlear implantees", *J. Acoust. Soc. Am.* 108, pp. 1269-80.

Hinojosa, R. and Marion, M. 1983, "Histopathology of profound sensorineural deafness, *Ann. New York Acad. Of Sci.*, 405, pp. 459-484.

Hodgkin, A.L., Huxley, A.F. 1952, "A quantitative description of membrane current and its application to conduction and excitation in nerve", *Journal of Physiology* 117, pp. 500-544.

Holt, G.R., Koch, C. 1999, "Electrical Interactions via the Extracellular Potential Near Cell Bodies", *Journal of Computational Neuroscience* 6, pp. 169-184.

Hormuzdi, S.G., Filippov, M.A., Mitropoulou, G., Monyer, H., Bruzzone, R. 2004, "Electrical synapses: A dynamic signaling system that shapes the activity of neuronal networks", *Biochimica et Biophysica Acta* 1662, pp. 113-137.

Huang, J.C., Nicholson, C., Okada, Y.C. 1990, "Distortion of magnetic evoked fields and surface potentials by conductivity differences at boundaries in brain tissue", *Biophysical Journal* 57 (6), pp. 1155-1166.

Javel, E., Tong, Y.C., Shepherd, R.K., Clark, G.M. 1987, "Responses of cat auditory nerve fibers to biphasic electrical current pulses. Annals of Otology, *Rhinology and Laryngology* 96 (Suppl. 128), pp. 26-30

Javel, E. 1990, "Acoustic and electrical encoding of temporal information. In: Miller, J.M., Spelman, F.A. (Eds.), Cochlear Implants: Models of the Electrically Stimulated Ear", *Springer*, New York, pp. 247-295.

Javel, E., Shepherd, R.K. 2000, "Electrical stimulation of the auditory nerve. III. Response initiation sites and temporal fine structure", *Hearing Research* 140 (1-2), pp. 45-76.

Jönsson, R., Hanekom T., Hanekom J.J. 2008, "Initial results from a model of ephaptic excitation in the electrically excited peripheral auditory nervous system, *Hearing Research*, 237, pp. 49-56.

Keithley, E.M., Schreiber, R.C. 1987, "Frequency map of the spiral ganglion in the cat", *Journal of the Acoustical Society of America* 81 (4), pp. 1036–1042.

Kellerhals, B., EngstrSm, H. and Ades, H.W. 1967, "Die Morphologie des Ganglion spirale cochleae", *Acta Otolaryngol.* (Stockh.) Suppl. 226, pp. 1-78.

Kiang, N.Y.S., Liberman, M.C., Gage, J.S., Northrop, C.C., Dodds, L.W.and Oliver, M.E. 1984, "Afferent innervation of the mammalian cochlea. In: L. Bolis, R.D. Keynes and S.H.P. Maddrell (Eds.), *Comparative Physiology Sensory Systems*, Cambridge University Press. pp. 143-161.

Kimura, R.S., Bongiorno, C.L., Iverson, N.A. 1987, "Synapses and ephapses in the spiral ganglion", *Acta Oto-Laryngologica* 104 (SUPPL. 438), pp. 1-18.

Koop, G., Graf, M. 2006, "Ocular neuromyotonia", *Klinische Monatsblatter fur Augenheilkunde* 223 (3), pp. 247-251.

Korn, H., Axelrad, H. 1980, "Electrical inhibition of Purkinje cells in the cerebellum of the rat", *Proc. Natl. Acad. Sci. USA* 77, pp. 6244-6247.

Korn, H., Faber, D.S. 1980, "Electrical field effect interactions in the vertebrate brain", *Trends Neurosci.* 3, pp. 6-9.

Kral, A., Hartmann, R., Mortazavi, D., Klinke, R. 1998, "Spatial resolution of cochlear implants: the electrical field and excitation of auditory afferents", *Hearing Research* 121, pp. 11-28.

Liberman, M.C., Oliver, M.E. 1984, "Morphometry of intracellularly labeled neurons of the auditory nerve: correlations with functional properties", *J. Comp. Neurol.* 223, pp. 163-176.

Loizou, P.C. 1998, "Mimicking the human ear", *IEEE Signal Processing Magazine*, 15(5), pp. 101-120.

Macherey, O., Carlyon, R.P., van Wieringen, A., Deeks, J.M., Wouters, J. 2008, "Higher sensitivity of human auditory nerve fibers to positive electrical currents", *J. Assoc. Res. Otolaryngol.* 9 (2), pp. 241-251.

Mainen, Z.F., Sejnowski, T.J. 1996, "Influence of dendritic structure on firing pattern in model neocortical neurons", *Nature* 382, pp. 363-366.

McCormick, D.A., Contreras, D. 2001, "On the cellular and network bases of epileptic seizures", *Annual Review of Physiology* 63, pp. 815-846.

McKay, C.M., McDermott, H.J., Clark, G.M. 1996, "The perceptual dimensions of single-electrode and nonsimultaneous dual-electrode stimuli in cochlear implantees", *J. Acoust. Soc. Am.* 99, pp. 1079-90.

Mens, L.H.M., Brokx, J.P., Van den Broek, P. 1995, "Averaged electrode voltages: Management of electrode failures in children, fluctuating threshold and comfort levels, and otosclerosis", *Annals of Otology, Rhinology and Laryngology Supplement* 166, pp. 169-72.

Middlebrooks, J.C. and Snyder, R.L. 2008, "Intraneural stimulation for auditory prosthesis: Modiolar trunk and intracranial stimulation sites", *Hearing Research* 242, pp. 52-63.

Miller, C.A., Woodruff, K.E. and Pfingst, B.E. 1995, "Functional responses from guinea pigs with cochlear implants. I. Electrophysiological and phychophysical measures", *Hearing Research* 92, pp. 85-99.

Miller, C.A., Abbas, P.J., Rubinstein, J.T. 1999a, "An empirically based model of the electrically evoked compound action potential", *Hearing Research* 135, pp. 1-18.

Miller, C.A., Abbas, P.J., Rubinstein, J.T., Robinson, B.K., Matsuoka, A.J. and Woodworth, G. 1998, "Electrically evoked compound action potentials of guinea pig and cat: responses to monopolar, monophasic stimulation, *Hearing Research* 119, pp. 142-154.

Miller, C.A., Abbas, P.J., Robinson, B.K., Rubinstein, J.T. and Matsuoka, A.J. 1999b, "Electrically evoked single fiber action potentials from cat: responses to monopolar, monophasic stimulation", *Hearing Research* 130, pp. 197-218.

Miller, C.A., Abbas, P.J., Robinson, B.K. 2001a, "Response properties of the refractory auditory nerve fibre", *Journal of the Association for Research in Otolaryngology* 2(3), pp. 216-232.

Miller, C.A., Robinson, B.K., Rubinstein, J.T., Abbas, P.J. and Runge-Samuelson, C.L. 2001b, "Auditory nerve responses to monophasic and biphasic electric stimuli, *Hearing Research* 151, pp. 79-94.

Miller, C.A., Abbas, P.J., Hay-McCutcheon, M.J., Robinson, B.K., Nourski, K.V., Jeng, F.C. 2004, "Intracochlear and extracochlear ECAPs suggest antidromic action potentials", *Hearing Research* 198, pp. 75–86.

Miranda, P.C., Correia, L., Salvador, R., Basser, P.J. 2007, "Tissue heterogeneity as a mechanism for localized neural stimulation by applied electric fields", *Physics in Medicine and Biology* 52 (18), pp. 5603-5617.

Moore, C.M., Vollmer, M., Leake, P.A., Snyder, R.L., Rebscher, S.J. 2002, "The effects of chronic intracochlear electrical stimulation on inferior colliculus spatial representation in adult deafened cats", *Hearing Research* 164 (1–2), pp. 82–96.

Nadol Jr, J.B. 1988, "Comparative anatomy of the cochlea and auditory nerve in mammals", *Hearing Research* 34, pp. 253-266.

Nelson, D.A., Van Tasell, D.J., Schroder, A.C., Soli, S., Levine, S. 1995, "Electrode ranking of 'place pitch' and speech recognition in electrical hearing", *J. Acoust. Soc. Am.* 98, pp. 1987-99.

Ota, C.Y., Kimura, R.S. 1980, "Ultrastructural study of the human spiral ganglion", *Acta Otolaryngol.* 89, pp. 53-62.

Parkins, C.W., Colombo, J. 1987, "Auditory-nerve single-neuron thresholds to electrical stimulation from scala tympani electrodes", *Hearing Research* 31, pp. 267-286.

Ranck Jr, J.B. 1975, "Which elements are excited in electrical stimulation of mammalian central nervous system: a review", *Brain Research* 98(3), pp. 417-440.

Rattay, F. 1989, "Analysis of models for extracellular fiber stimulation", *IEEE Transaction on Biomedical Engineering* Vol. 36, Issue 7, pp. 676-682.

Rattay, F. and Aberham, M. 1993, "Modeling Axon Memebranes for Functional Electrical Stimulation", *IEEE Transactions on Biomedical Engineering* 40 (12), pp. 1201-1209.

Rattay, F., Lutter, P., Felix, H. 2001, "A model of the electrically excited human cochlear neuron. I. Contribution of neural substructures to the generation and propagation of spikes", *Hearing Research* 153, pp. 43-63.

Rattay, F. 2008, "Current distance relations for fiber stimulation with pointsources", *IEEE Transactions on Biomedical Engineering* 55 (3), pp. 1122-1127.

Reilly, J.P., Freeman, V.T., Larkin, W.D. 1985, "Sensory effects of transient electrical stimulation. Evaluation with a neuroelectric model", *IEEE Transactions on Biomedical Engineering* 32 (12), pp. 1001–1011.

Rosbe, K.W., Burgess, B.J., Glynn, R.J., Nadol Jr., J.B. 1996, "Morphologic evidence for three cell types in the human spiral ganglion", *Hearing Research*, 93 (1-2), pp. 120-127.

Rubinstein, J.T. 1991, "Analytical theory for extracellular electrical stimulation of nerve with focal electrodes: II. Passive myelinated axon", *Biophysical Journal* 60 (3), pp. 538-555.

Rubinstein, J.T. 1993, "Axon termination conditions for electrical stimulation", *IEEE Transactions on Biomedical Engineering* 40(7), pp. 654-663.

Rubinstein, J.T. 1995, "Threshold Fluctuations in an N Sodium Channel Model of the Node of Ranvier", *Biophysical Journal* Vol 68, pp. 779-785.

Rusznák, Z. and Szücs, G. 2009, "Spiral ganglion neurones: an overview of morphology, firing behaviour, ionic channels and function", *Pflügers Archiv: European Journal of Physiology* 457(6), pp. 1303-1325.

Schwarz, J.R., Eikhof, G. 1987, "Na currents and action potentials in rat myelinated nerve fibres at 20 and 37 °C", *Pflügers Archiv: European Journal of Physiology* 409, pp. 569-577.

Shannon, R.V. 1983, "Multichannel electrical stimulation of the auditory nerve in man. I. Basic psychophysics", *Hearing Research* 11, pp. 157-89.

Shannon, R.V. 1985, "Threshold and loudness functions for pulsatile stimulation of cochlear implants, *Hearing Research* 18, pp. 135-143.

Shepherd, R.K., Javel, E. 1997, "Electrical stimulation of the auditory nerve. I. Correlation of physiological responses with cochlear status", *Hearing Research* 108, pp. 112-144.

Shepherd, R.K., Javel, E. 1999, "Electrical stimulation of the auditory nerve: II. Effect of stimulus waveshape on single fibre response properties", *Hearing Research* 130, pp. 171-188.

Shin-ichi, H., Shepherd, R.K., Tong, Y.C., Clark, G.M., Funasaka, S. 1990, "Dimensions of the scala tympani in the human and cat with reference to cochlear implants", *Annals of Otology, Rhinology and Laryngology* 99 (11), pp. 871-876.

Smit, J.E. 2008, "Modelled response of the electrically stimulated human auditory nerve fibre", *University of Pretoria*.

Spelman, F.A., Clopton, B.M. and Pfingst, B.E. 1982, "Tissue impedance and current flow in the implanted ear. Implications for the cochlear prosthesis", *The Annals of Otology, Rhinology & Laryngology*. Supplement 98, pp. 3-8.

Spoendlin, H. 1972, "Innervation densities of the cochlea", *Acta Otolaryngol.* (Stockh.) 73, pp. 235-248.

Spoendlin, H. 1978, "The afferent innervation of the cochlea. In: R.F. Naunton and P. Fernandez (Eds.), Evoked Electrical Activity in the Auditory Nervous System, *Academic Press*, New York, pp. 21-41.

Spoendlin, H., Schrott, A. 1988, "The spiral ganglion and the innervation of the human organ of Corti", *Acta Oto-Laryngologica* 105 (5-6), pp. 403-410.

Spoendlin, H., Schrott, A. 1989, "Analysis of the human auditory nerve", *Hearing Research* 43 (1), pp. 25-38.

Stickney, G.S., Loizou, P.C., Mishra, L.N., Assmann, P.F., Shannon, R.V., Opie, J.M. 2006, "Effects of electrode design and configuration on channel interactions", *Hearing Research* 211, pp. 33-45.

Taylor, C.P., Krnjevic, K., Ropert, N. 1984, "Facilitation of hippocampal CA3 pyramidal cell firing by electrical fields generated antidromically", *Neuroscience* 11, pp. 101-109.

Tehovnik, E.J. 1996, "Electrical stimulation of neural tissue to evoke behavioral responses", *Journal of Neuroscience Methods* 65, pp. 1-17.

Throckmorton, C.S., Collins, L.M. 1999, "Investigation of the effects of temporal and spatial interactions on speech-recognition skills in cochlear-implant subjects", *J. Acoust. Soc. Am.* 105, pp. 861-73.

Turner, R.W., Richardson, T.L. 1991, "Apical dendritic depolarizations and field interactions evoked by stimulation of afferent inputs to rat hippocampal CA1 pyramidal cells", *Neuroscience* 42 (1), pp. 125-135.

Tylstedt, S. 2003, "The human spiral ganglion. Ultrastructural and Immunohistochemical Observations", *Umeå University.*

Tylstedt, S., Rask-Andersen, H. 2001, "A 3-D model of membrane specializations between human auditory spiral ganglion cells", *Journal of Neurocytology* (30), pp. 465-473.

Van den Honert, C., Stypulkowski, P.H. 1984, "Physiological properties of the electrically stimulated auditory nerve. II. Single fiber recordings", *Hearing Research* 14, pp. 225-243.

Van den Honert, C., Stypulkowski, P.H. 1987a, "Single fiber mapping of spatial excitation patterns in the electrically stimulated auditory nerve", *Hearing Research* 29, pp. 195-206.

Van den Honert, C., Stypulkowski, P.H. 1987b, "Temporal response patterns of single auditory nerve fibers elicited by periodic electrical stimuli", *Hearing Research* 29, pp. 207-222.

van Wieringen, A., Carlyon, R.P., Laneau, J., Wouters, J. 2005, "Effects of waveform shape on human sensitivity to electrical stimulation of the inner ear", *Hearing Research* 200, pp. 73-86.

Wardrop, P., Whinney, D., Rebscher, S.J., Roland Jr., J.T., Luxford W., Leake, A.L. 2005, "A temporal bone study of insertion trauma and intracochlear position of cochlear implant electrodes. I: comparison of Nucleus banded and Nucleus Contour electrodes", *Hearing Research* 203, pp. 54-67.

Wei, X., Wang, J., Deng, B. 2009, "Introducing internal model to robust output synchronization of FitzHugh-Nagumo neurons in external electrical stimulation",

Communications in Nonlinear Science and Numerical Simulation 14 (7), pp. 3108-3119.

Wen, P., Li, Y. 2006, "EEG human head modelling based on heterogeneous tissue conductivity", *Australasian Physical & Engineering Sciences in Medicine* 29 (3), pp. 235-240.

Wilson, B.S., Dorman, M.F. 2008, "Cochlear implants: A remarkable past and a brilliant future", *Hearing Research* 242, pp. 3-21.

Yim C.C., Krnjevic K., Dalkara T. 1986, "Ephaptically generated potentials in CA1 neurons of rat's hippocampus in situ", *Journal of Neurophysiology 56* (1), pp. 99-122.

Zeng, F.G., Fu, Q.J., Morse, R. 2000, "Human hearing enhanced by noise", *Brain Research* 869, pp. 251-255.

Addendum A

HODGKIN-HUXLEY MODEL OVERVIEW

A.1 THE BASIC MODEL

The Hodgkin-Huxley model is an empirical model published in 1952. It consists of a set of non-linear differential equations that describe changes in the membrane potential in the squid giant axon. The current across the cell membrane depends on the membrane capacitance and the resistance of the ionic channels. The ionic current consists of the sum of the sodium current, potassium current and a term labelled leakage current which accounts for all other ions such as chloride and bicarbonate. The total current can then be written as

$$I = I_C + I_{Na} + I_K + I_L \tag{A.1}$$

where I_C is the capacitive current, I_{Na} is the sodium current, I_K is the potassium current and I_L is the leakage. The capacitive current is written as

$$I_C = C_m \cdot \frac{\mathrm{d}V_m}{\mathrm{d}t} \tag{A.2}$$

where C_m is the capacitance and V_m is the transmembrane voltage.

A.1.1 Sodium ionic current I_{Na}

The ionic currents are dependent on the transmembrane voltage and the resting or equilibrium potentials of each type of ion. Applying Ohm's law, the sodium ionic current can be written as

$$I_{Na} = g_{Na} \cdot (V_m - V_{Na}) \tag{A.3}$$

where g_{Na} is the conductance of sodium ions. The conductance is not constant and there are two state variables that control the opening and closing of the sodium ion channel: m controls the opening and h controls the closing. The conductance is then expressed by

$$g_{Na} = g_{Na,max} \cdot m^3 \cdot h \tag{A.4}$$

where $g_{Na,max}$ is the maximum sodium conductance and the state variables are governed by the differential equations

$$\frac{\mathrm{d}m}{\mathrm{d}t} = [-(\alpha_m + \beta_m) \cdot m + \alpha_m] \cdot \kappa \tag{A.5}$$

and

$$\frac{\mathrm{d}h}{\mathrm{d}t} = [-(\alpha_h + \beta_h) \cdot h + \alpha_h] \cdot \kappa \tag{A.6}$$

where the coefficients α_i and β_i are voltage dependent and given by

$$\begin{aligned} \alpha_m &= \frac{0.1 \cdot (25 - V_m)}{\exp\left[(25 - V_m)/10\right] - 1} \\ \beta_m &= 4 \cdot \exp\left(-V_m/18\right) \\ \alpha_h &= 0.07 \cdot \exp\left(-V_m/20\right) \\ \beta_h &= \frac{1}{\exp\left[(30 - V_m)/10\right] + 1} \end{aligned} \tag{A.7}$$

The original model data in the Hodgkin-Huxley system were based on low temperature experiments at a temperature of 6.3 °C. At other temperatures the gating processes must be multiplied with the thermic coefficient κ, where

$$\kappa = 3^{(T-6.3)/10} \tag{A.8}$$

where T is the temperature in °C. For all simulations performed in this study a temperature of 29°C was assumed, resulting in the value $\kappa \approx 12$. An additional alteration of the model utilized in this study was a change of ion channel density. For all com-

partments, except for the soma, the sodium, potassium, and leakage conductances were multiplied by the factor 10 to simulate 10-fold channel density (see Chapter 3).

The final expression for I_{Na} then becomes

$$I_{Na} = g_{Na,max} \cdot m^3 \cdot h \, (V - V_{Na}) \tag{A.9}$$

A.1.2 Potassium ionic current I_K

The model for the potassium current is similar. Applying Ohm's law the potassium ionic current can be written as

$$I_K = g_K \cdot (V_m - V_K) \tag{A.10}$$

where g_K is the conductance of potassium ions. For the potassium conductance there is only one state variable, n, which activates the channel and the conductance is then expressed by

$$g_K = g_{K,max} \cdot n^4 \tag{A.11}$$

where $g_{K,max}$ is the maximum potassium conductance and the state variable is governed by the differential equation

$$\frac{\mathrm{d}n}{\mathrm{d}t} = [-(\alpha_n + \beta_n) \cdot n + \alpha_n] \cdot \kappa \tag{A.12}$$

where

$$\alpha_n = \frac{0.01 \cdot (10 - V_m)}{\exp\left[(10 - V_m)/10\right] - 1}$$
$$\beta_n = 0.125 \cdot \exp\left(-V_m/80\right)$$

The total expression for the potassium current then becomes

$$I_K = g_{K,max} \cdot n^4 \, (V - V_K) \tag{A.13}$$

A.1.3 Leakage ionic current I_L

The leakage current is given by

$$I_L = g_L \cdot (V_m - V_L) \tag{A.14}$$

where g_L is the conductance. The leakage channels are always open and the conductance is therefore constant.

A.1.4 Excitation

When depolarization occurs, the sodium channels open and sodium ions flow into the cell. As sodium ions flood in, the membrane potential reverses such that the interior becomes positive relative to the outside. The positive potential then causes potassium channels to open resulting in an outflow of potassium ions. When the potential falls the sodium channels close. Figure A.1 shows the dynamics of the gating variables during an AP.

At the resting potential V_R, i.e. $V_m = 0$, a quick look at the steady state (i.e. $dm/dt = dh/dt = dn/dt = 0$) shows that

$$\begin{aligned} m_{V_R} &= \frac{\alpha_{m,V_R}}{\alpha_{m,V_R} + \beta_{m,V_R}} \approx 0.0529 \\ n_{V_R} &= \frac{\alpha_{n,V_R}}{\alpha_{n,V_R} + \beta_{n,V_R}} \approx 0.3177 \\ h_{V_R} &= \frac{\alpha_{h,V_R}}{\alpha_{h,V_R} + \beta_{h,V_R}} \approx 0.5961 \end{aligned}$$

See also Figure A.1. This results in the following conductances

$$\begin{aligned} g_{Na} &= m_{V_R}^3 \cdot h_{V_R} \cdot g_{Na,max} = 8.8244 \times 10^{-5} \cdot g_{Na,max} \\ g_K &= n_{V_R}^4 \cdot g_{K,max} = 0.01019 \cdot g_{K,max} \end{aligned}$$

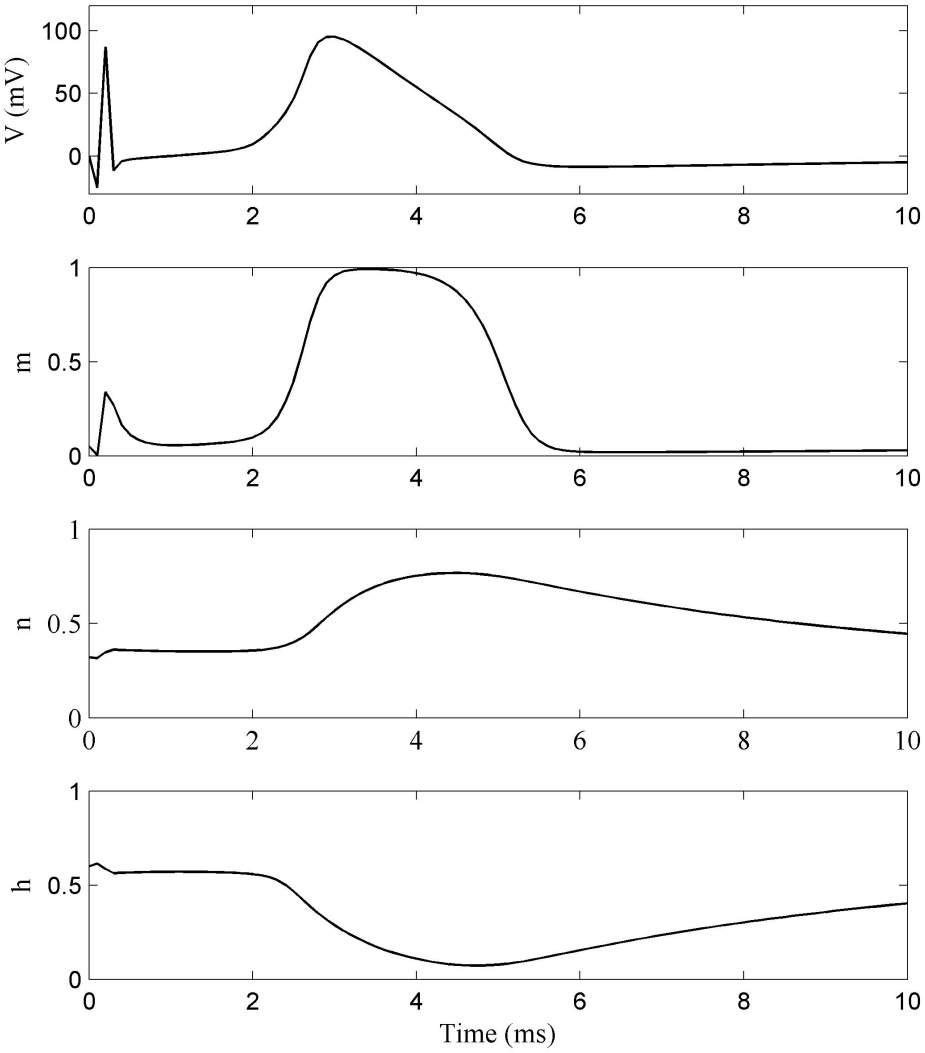

Figure A.1: Original HH system used in a Rattay fibre.